View metadata, citation and similar papers at core.ac.uk

brought to you by CORE

provided by Clemson University: TigerPrints

Clemson University
TigerPrints

All Dissertations | Dissertations

8-2008

FRAMEWORK FOR THE FULLY PROBABILISTIC ANALYSIS OF EXCAVATION-INDUCED SERVICEABILITY DAMAGE TO BUILDINGS IN SOFT CLAYS

Matt Schuster
Clemson University, mschust@clemson.edu

Follow this and additional works at: https://tigerprints.clemson.edu/all_dissertations

 Part of the Civil Engineering Commons

Recommended Citation
Schuster, Matt, "FRAMEWORK FOR THE FULLY PROBABILISTIC ANALYSIS OF EXCAVATION-INDUCED SERVICEABILITY DAMAGE TO BUILDINGS IN SOFT CLAYS" (2008). *All Dissertations*. 257.
https://tigerprints.clemson.edu/all_dissertations/257

This Dissertation is brought to you for free and open access by the Dissertations at TigerPrints. It has been accepted for inclusion in All Dissertations by an authorized administrator of TigerPrints. For more information, please contact kokeefe@clemson.edu.

FRAMEWORK FOR THE FULLY PROBABILISTIC ANALYSIS OF EXCAVATION-INDUCED SERVICEABILITY DAMAGE TO BUILDINGS IN SOFT CLAYS

A Dissertation
Presented to
the Graduate School of
Clemson University

In Partial Fulfillment
of the Requirements for the Degree
Doctor of Philosophy
Civil Engineering

---

by
Matt John Schuster
August 2008

Accepted by:
Dr. C.H. Juang, Committee Chair
Dr. Mary J.S. Roth
Dr. Ronald D. Andrus
Dr. Hoke S. Hill, Jr.

ABSTRACT

In this dissertation, a framework for a fully-probabilistic analysis of the potential for building serviceability damage induced by an excavation in soft clays is established. This analysis framework is established based on the concept of a serviceability limit state where the *resistance* is represented by the capacity of a building to resist serviceability damage, and the *loading* is represented by the demand on a building due to excavation-induced ground movements. In this study, both the resistance and the loading are treated as a random variable; the resistance is characterized empirically based on a database of the observed building performance while the loading is estimated for a specific case using semi-empirical models that were created with the results of finite element analysis and field observations.

A simplified procedure is developed for estimating the loading on a building induced by an excavation. In this simplified procedure, the loading is expressed in terms of damage potential index (*DPI*) that is based on the concept of principal strain. On the other hand, the resistance as a random variable is characterized based on observed building performance, also in terms of the *DPI*. The uncertainties of both the resistance and the loading are fully characterized in this dissertation study to enable a fully probabilistic analysis. The developed framework for the fully-probabilistic assessment of the potential for excavation-induced building damage is demonstrated with the well-known TNEC case history.

Finally, since the observational method is commonly applied to the design and construction of excavation systems, a simplified scheme for updating the soil parameters

(and consequently *DPI*) based on the observations of the maximum wall deflection and ground settlement is developed. This updating scheme is demonstrated with an excavation case history and shown to be an effective technique for monitoring the damage potential of buildings adjacent to an excavation.

The developed framework allows for fully-probabilistic assessment of the potential of building damage induced by an excavation, and thusly, provides engineers with a more transparent assessment of the risk associated with a particular excavation design and construction. Furthermore, with the observational method, the potential for excavation-induced serviceability damage can be reassessed as the excavation proceeds. With this approach, the excavation system can be monitored as the excavation proceeds and necessary measures can be taken to prevent damage to buildings adjacent to the excavation.

DEDICATION

This dissertation is dedicated to my family and fiancée, Ms. Jessica Moore.

ACKNOWLEDGMENTS

I would like to express my sincere appreciation to Dr. C.H. Juang, my advisor, for all of his guidance and encouragement during my studies here at Clemson University. Without his help, I would not have been able to complete my dissertation studies.

I wish to also thank my other committee members, Dr. Mary J.S. Roth, Dr. Ronald D. Andrus, and Dr. Hoke S. Hill, Jr., for their assistance and review of my dissertation.

I wish to acknowledge my fellow graduate students, Evan Hsiao, Sunny Fang, David Li, Yuting Su, Hossein Hayati, Raul Flores Peñalva, Jesse Chen, and David Powell, for many helpful discussions on my research.

Finally, I would like to thank Clemson University and the National Science Foundation for their financial support during my studies. The studies on which this dissertation is based were supported by the National Science Foundation through Grant No. CMS-0300198 under program director Dr. Richard J. Fragaszy. This financial support is greatly appreciated. The results and opinions expressed in this paper are those of the writer and do not necessarily represent the view of the National Science Foundation.

TABLE OF CONTENTS

Table of Contents (Continued)

Page

LIST OF TABLES

LIST OF FIGURES

List of Figures (Continued)

Figure Page

List of Figures (Continued)

CHAPTER ONE

INTRODUCTION

Background- Purpose of research

In urban areas, the design of high rise buildings and other infrastructure often necessitates the construction of braced excavations. However, it is well-known that construction utilizing braced excavations induces vertical and lateral ground movements. Consequently, in urban areas where buildings are frequently in close proximity to the construction, there is a potential for *damage*, defined herein as violation of serviceability requirements, to these structures due to excessive vertical and lateral ground movements.

The possible effects of an excavation are illustrated in Figure 1.1. As the excavation proceeds, the retaining wall deflects as a result of stress relief. The wall deflection at a given excavation stage, shown in Figure 1.1 in a profile, causes the vertical

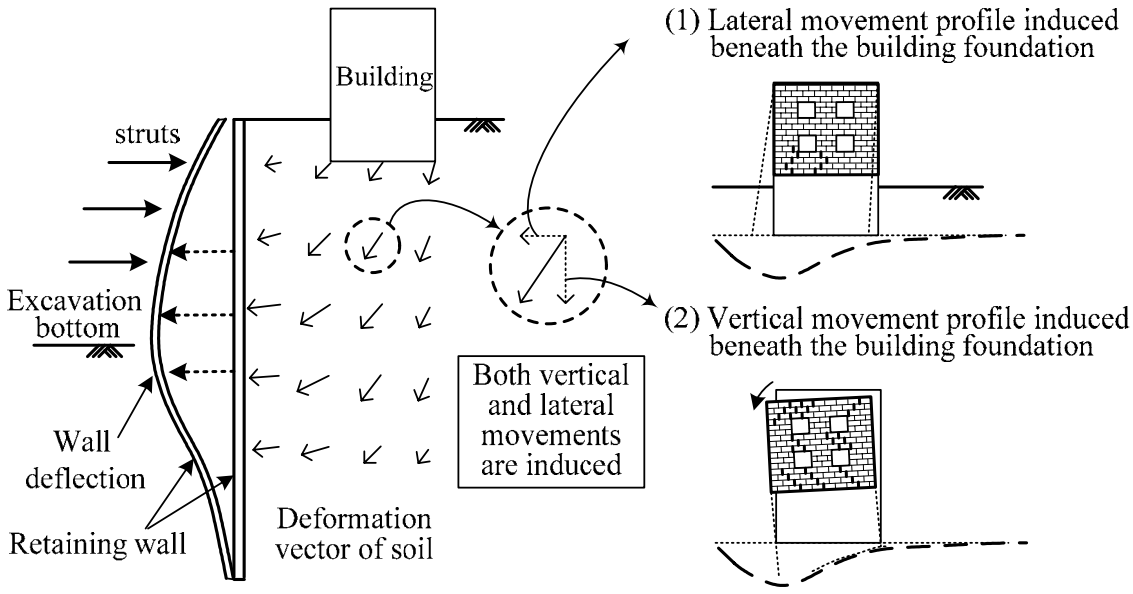

Figure 1.1 Schematic diagram of excavation effects

and lateral ground movements, which are shown in their respective profiles. The vertical and lateral ground movements then induce building distortion and as the building distorts, strains develop in the building. As the building distorts and larger strains develop, increased damage starts to occur in the building.

With the application of reliability analysis in geotechnical engineering becoming more common (Christian 2004), it is desirable to establish a framework for a rigorous fully-probabilistic assessment of excavation-induced building damage. The framework for such a fully-probabilistic assessment requires the formulation of a serviceability limit state and the subsequent reliability analysis considering both the *resistance* part and the *loading* part of the limit state "equation." In the context of reliability analysis, the *resistance* and the *loading* can both be expressed in terms of damage potential index (*DPI*), which is a "derived" parameter used for damage potential evaluation. The *resisting DPI* represents the threshold (limiting) value of the *DPI* beyond which damage begins to occur and the *loading DPI* represents the "applied" *DPI* for a particular case. In order to facilitate a fully-probabilistic analysis, both the *resistance* part and the *loading* part of the serviceability limit state equation, as well as the uncertainty associated with each of them, must be defined.

A number of evaluation criteria have been developed for estimating the potential for building damage (Skempton and MacDonald 1956, Polshin and Tokar 1957, Bjerrum 1963, O'Rourke et al. 1976, Boscardin and Cording 1989, Boone 1996, Finno et al. 2005, Son and Cording 2005) and can be used in the formulation of a serviceability limit state. Although relationships between the evaluation criteria and damage levels have been

established for a deterministic analysis, little effort has been made to define the *resistance* term for a probabilistic analysis using any of these evaluation criteria. Therefore, to facilitate the probabilistic analysis, the evaluation criterion of principal strain presented by Son and Cording (2005) is adopted and Chapter 2 of this dissertation is devoted to characterizing the *resistance* term and its associated uncertainty with the application of Bayesian mapping techniques.

In addition to the *resistanc*e term, the *loading* term also needs to be evaluated to facilitate a probabilistic assessment of the potential for excavation-induced building damage. The estimation of the *loading* first requires the determination of the excavation-induced wall deflection and ground movements. Since the design of a deep excavation is a soil-structure interaction problem, the finite element method (FEM) is often utilized to predict the wall deflection and ground movement caused by the excavation (Whittle et al. 1993, Hsieh and Ou 1997, Calvello and Finno 2004, Finno and Calvello 2005, Kung et al. 2007a). Alternatively, the wall deflection and ground movements can also be predicted using an empirical and semi-empirical method (Peck 1969, Bowles 1988, Clough and O'Rourke 1990, Ou et al. 1993, Hsieh and Ou 1998, Finno and Roboski 2005, Kung et al. 2007a, Kung et al. 2007b). However, a fully-probabilistic analysis is difficult to implement under the previously developed approaches as the uncertainty of the *loading* is difficult to characterize. Thus, Chapter 3 of the dissertation is devoted to developing a simplified procedure with semi-empirical models for assessing the damage potential of buildings adjacent to an excavation from which the *loading* on a building induced by an excavation can be estimated and its associated uncertainties can be characterized. Within

the framework of this procedure, both a deterministic and probabilistic assessment can be performed.

It should be noted that the *loading* developed within Chapter 3 is in terms of the damage potential index (*DPI*), and not the principal strain, which is used to define the *resistance*. However, for a fully-probabilistic analysis, both the *loading* and *resistance* have to be defined in terms of a consistent evaluation criterion. Therefore, Chapter 4 of this dissertation is devoted to combining the efforts of Chapters 2 and 3 in order to establish a fully-probabilistic analysis.

The observational method (Peck 1969) is often utilized to improve the design and execution of deep excavations, particularly in regards to predictions of the wall deflection, ground settlement, and damage potential of buildings adjacent to an excavation. Peck recognized the importance of the observational method as he "emphasized the need to first compute the various quantities that can be measured in the field and then close the gaps in knowledge on the basis of such measurements" (Wu 2008). To improve the design of a deep excavation with the simplified procedure presented in Chapter 3, an observational method-based procedure that can be applied in conjunction with the simplified procedure is developed in Chapter 5 of the dissertation.

Objectives and Scope of the Research

The scope of the research presented in this dissertation is limited to the development of a simplified, yet comprehensive probabilistic procedure for evaluating

the potential for excavation-induced building damage. To this end, the specific objectives of this dissertation are:

1. Characterize the limiting principal strain and its associated model uncertainty for the probabilistic assessment of excavation-induced building damage.
2. Develop a comprehensive evaluation procedure with simplified models for the deterministic and probabilistic assessment of the damage potential of buildings adjacent to an excavation.
3. Develop a fully-probabilistic procedure for evaluating excavation-induced building damage.
4. Establish an observational method-based procedure for updating the assessment of the damage potential of a building adjacent to an excavation.

Significance of Research

Concerns often arise from excavations when the resulting ground movements are excessive. When buildings are in close proximity to an excavation, there is a potential for damage to these structures. The current design procedures, however, are less than adequate for the evaluation of excavation-induced building damage and often lead to the over-design or under-design of braced excavations, which subsequently results in additional costs in the construction of braced excavations (Boone 2001). Therefore, the major contribution of this dissertation is the development of a fully-probabilistic procedure, which enables a more accurate assessment of the potential for excavation-induced building damage. Additionally, to enable updating of an excavation design

during construction, a simplified observational method-based procedure for updating the potential for excavation-induced building damage is also developed.

The establishment of a fully-probabilistic procedure provides engineers with an invaluable tool for assessing the risk associated with an excavation. With the developed procedure, the uncertainty associated with a given design is completely characterized and there is less confusion in regard to the potential for excavation-induced building damage. In turn, the risk associated with a particular excavation design becomes more transparent to the practicing engineer as well as the general public. Furthermore, with the availability of information on the costs and risks associated with excavation-induced building damage, the most economical excavation design can be selected based on a cost/benefit analysis. Finally, with the observational method-based procedure presented, engineers can ensure that the selected excavation design is performing appropriately and the risk can be monitored as the excavation proceeds.

The Structure of the Dissertation

This dissertation is divided into six chapters. The Introduction is presented in current chapter, Chapter 1, to organize the entire dissertation. Chapters 2 through 5 consist of major aspects of the dissertation work and Chapter 6 presents the conclusions of this dissertation. In Chapter 2, the major part of the paper titled "Reliability Analysis of Serviceability Problems Caused by Excavation" is presented. The major contribution of Chapter 2 is the characterization of the *resistance* term of the serviceability limit state model for a fully-probabilistic analysis. In Chapter 3, the major part of the paper titled "Simplified Model for Evaluating Damage Potential of Buildings Adjacent to a Braced

Excavation in Clays" is presented and a simplified procedure is developed for assessing the potential for excavation-induced building damage and the uncertainty associated with this procedure is evaluated. The results of the analysis in Chapter 3 allow for the characterization of the *loading* term of the serviceability limit state model for a fully-probabilistic analysis. In Chapter 4, the major part of a paper titled "Fully-Probabilistic Framework for Excavation-Induced Building Damage Potential" is presented. In Chapter 4, the developments of Chapter 2 and 3 are combined in an effort to produce a comprehensive fully-probabilistic procedure for evaluating the potential for excavation-induced building damage. In Chapter 5, the major part of the paper titled "Updating Soil Parameters for Excavation-Induced Building Damage Potential Assessment" is presented. The major contribution of Chapter 5 is the development of a simplified observational method-based procedure for updating the assessment of excavation-induced building damage, as shown in Figure 1.2. In the observational method-based procedure, the initial design is based on initial estimates of the input parameters before construction. Subsequently, as an excavation proceeds, the soil parameters are updated based on observations made during the excavation. The updated soil parameters are then used to reassess the potential for excavation-induced building damage for future stages of excavation. Finally, in Chapter 6, the major conclusions of this dissertation are summarized and detailed.

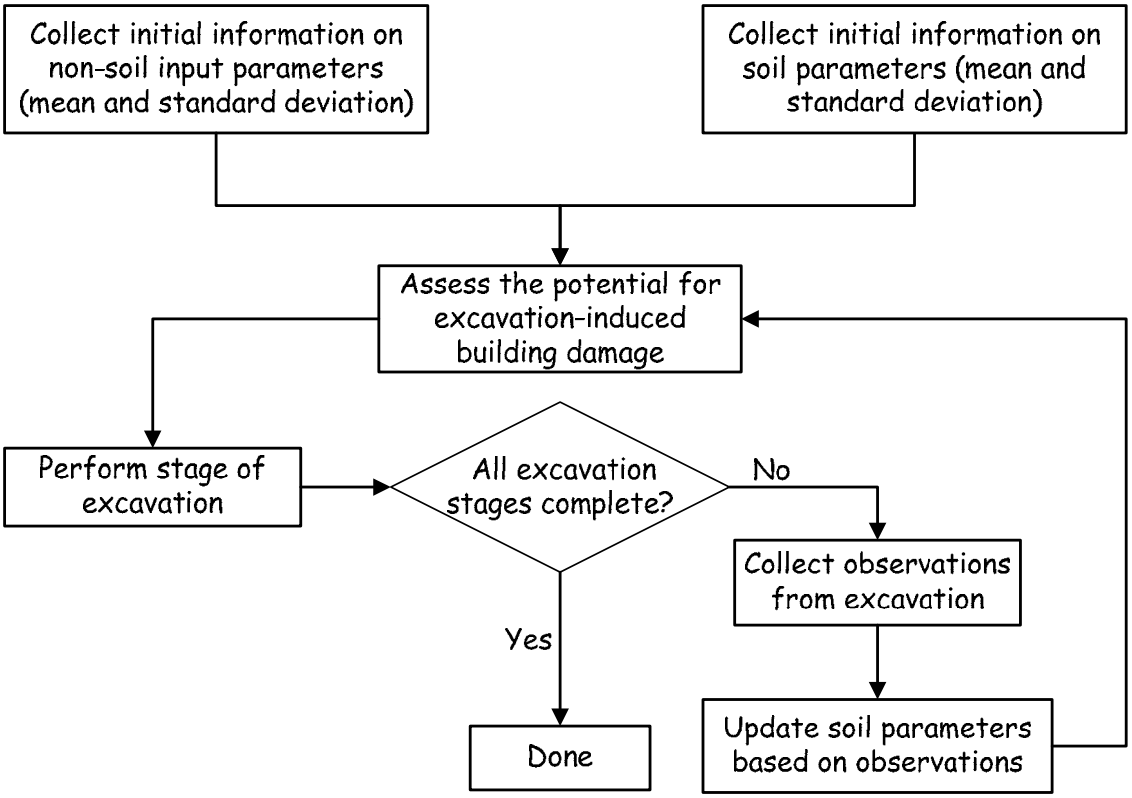

Figure 1.2 Observational-based procedure for updating the assessment of excavation-induced building damage

CHAPTER TWO

CHARACTERIZATION OF LIMITING PRINCIPAL STRAIN FOR RELIABILITY ANALYSIS OF BUILDING SERVICEABILITY PROBLEMS CAUSED BY EXCAVATION*

Introduction

Building damage due to excavation-induced settlement in urban construction has increasingly received greater attention than in the past. However, the damage to buildings from ground settlement is a result of a complex soil-structure interaction, which is not easily evaluated and thus difficult to predict. Previous research has concluded that damage to buildings caused by excavation is generally a result of both settlement and lateral movement of the ground (Skempton and MacDonald 1956, Polshin and Tokar 1957, Bjerrum 1963, O'Rourke et al. 1976, Boscardin and Cording 1989, Boone 1996, Finno et al. 2005, Son and Cording 2005). Accordingly, Son and Cording (2005) developed a phased procedure to estimate the potential for building damage based on angular distortion (β) and lateral strain (ε_l), two commonly used parameters to express the strains induced in a building by the settlement and lateral movement of ground; these two parameters can be combined into a single parameter termed principal strain, which represents the tensile principal strain in the building.

Although probabilistic analysis is becoming more common in geotechnical engineering (Christian 2004), its application within excavations has been limited. Excluding studies by Zhang and Ng (2005) and Hsiao et al. (2008), the assessment of

* A similar form of this chapter has been accepted for publication by *Geotechnique* at the time of writing; Schuster, M.J., Juang, C.H., Roth, M.J.S., and Rosowsky, D.V., "Reliability Analysis of Serviceability Problems Caused by Excavation."

excavation-induced building damage has focused mainly on a deterministic approach. In the study by Zhang and Ng (2005), the limiting angular distortion was determined based on the assessment of case histories of buildings undergoing excavation-induced settlement. The limiting angular distortion was analyzed with fragility curves, which facilitates reliability analysis with the formulation of a limit state based on the limiting angular distortion. In the study by Hsiao et al. (2008), the simplified criterion of maximum settlement was adopted for reliability analysis. However, a more thorough analysis based on principal strain is necessary to fully develop a rigorous probabilistic analysis for excavation-induced building damage.

In this chapter, a framework for the simplified probabilistic assessment of excavation-induced building damage based on principal strain is developed. It should be emphasized that the focus of this chapter is on establishing a serviceability limit state for assessing the potential for excavation-induced building damage, and fully characterizing the resistance (in terms of principal strain) of the serviceability limit state equation. To this end, the data set compiled by Son and Cording (2005) is first used to develop a serviceability limit state. Next, the Bayesian mapping approach developed by Juang et al. (2000) is used to interpret the distributions of the principal strains assessed for all cases in the database. The established Bayesian mapping function is then used to *calibrate* (or back-calculate) the uncertainty of the developed limit state model. The limiting principal strain is recalibrated to produce an unbiased limit state and the model uncertainty or model bias of the modified limit state is reassessed. Subsequently, the effect of prior

probability on the model bias is explored and an iterative procedure to reduce the dependency of the knowledge of prior probability is developed.

Serviceability Limit State for Building Damage Evaluation

A rigorous probabilistic assessment of excavation-induced building damage requires a collection of a large number of quality case histories and formulation of an appropriate serviceability limit state. Therefore, the characteristics of the database of excavation-induced building damage cases will be described, and a serviceability limit state will be established to facilitate the application of reliability analysis.

Database of Excavation-Induced Building Responses

The database of the responses of buildings adjacent to excavations compiled and assessed by Son (2003) and Son and Cording (2005) is employed in this study. Son (2003) collected and summarized 142 building responses from a variety of sources including 18 field observations (full scale), 2 physical model tests (1/10 model scale), and 122 numerical experimentation cases (1/10 model scale). The validity of the numerical model results were confirmed through comparison with the field observations and physical models. The majority of the buildings in the database were brick-bearing structures, which tend to be the most sensitive to the excavation-induced ground movements (Boone 1996). Similar values of lateral strain and angular distortion were observed in these buildings. The principal strain values in the buildings, which are derived from the lateral strains and angular distortions in the buildings, generally were less than 4.00×10^{-3}.

Establishment of Serviceability Limit State

The damage levels for the cases in the database were determined based on the observed damage for field tests and on the observed and calculated crack width criteria as recommended by Burland et al. (1977) for the model tests and numerical experimentation

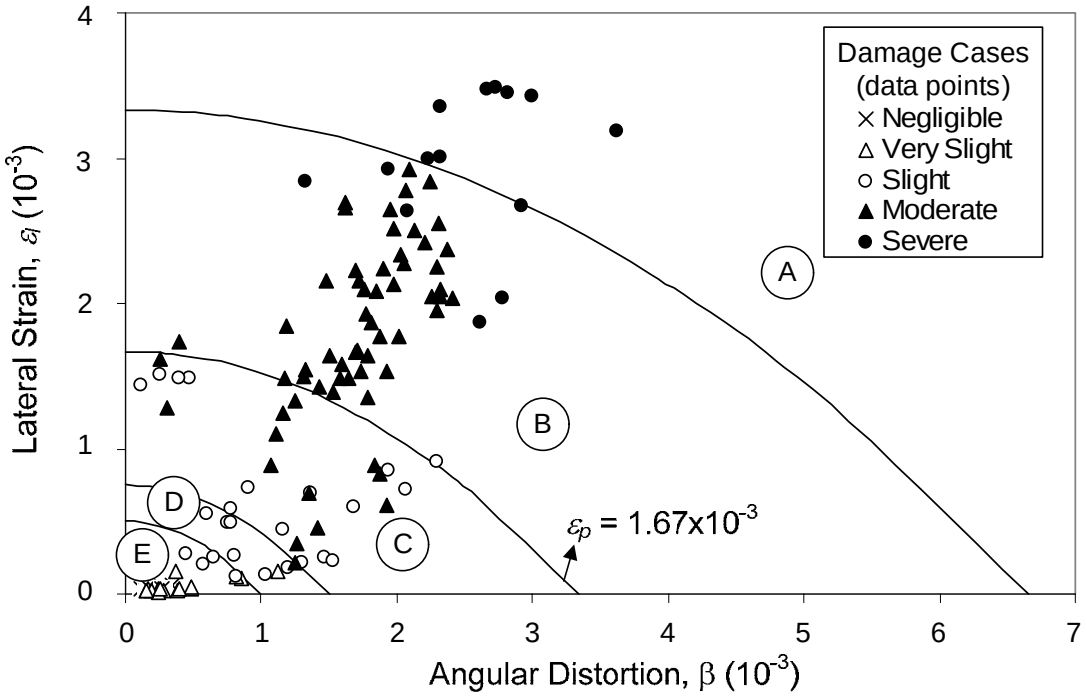

**Boundaries Established by Son and Cording*
A – *Severe to Very Severe Damage*
B – *Moderate to Severe Damage*
C – *Slight Damage*
D – *Very Slight Damage*
E – *Negligible Damage*

Figure 2.1 Characteristics of excavation-induced building damage data compiled by Son and Cording (2005)

cases. Based on the damage classification of these cases, which ranged from "Very Severe" (highest) to "Negligible" (lowest), Son and Cording (2005) established the boundaries of these classes in terms of principal strain as shown in Figure 2.1. Son and

Cording (2005) provided the following equations for the calculation of principal strain, ε_p at a point in a building:

$$\varepsilon_p = \varepsilon_l \times (\cos\theta_{\max})^2 + \beta \sin\theta_{\max} \cos\theta_{\max} \quad (2.1a)$$

$$\tan(2\theta_{\max}) = \beta / \varepsilon_l \quad (2.1b)$$

where β = angular distortion as defined with Figure 2.2a, ε_l = lateral strain (i.e. horizontal strain) as defined with Figure 2.2b, and $\theta_{\max}$ = direction of crack formation measured from the vertical plane (i.e., the angle of the plane on which the principal strain ε_p acts). For example, if $\beta = 0$, then $\theta_{\max} = 0$, and ε_p (which is equal to ε_l in this case) acts on the vertical plane and a crack forms along the vertical plane (Figure 2.2b); if $\varepsilon_l = 0$, then $\theta_{\max} = 45^\circ$, and ε_p acts on the plane at $\theta_{\max} = 45°$ (Figure 2.2a).

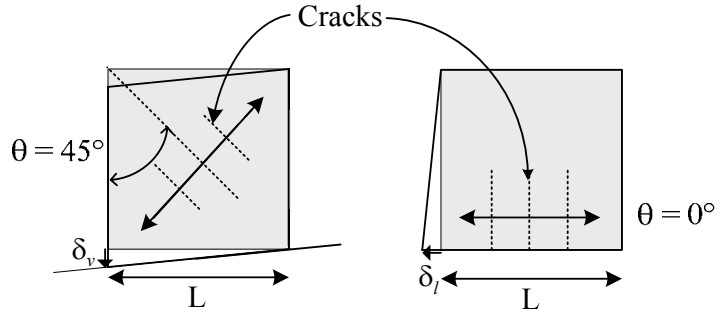

Figure 2.2 State of strain at the distorted portion of a structure (modified from Son and Cording 2005)

Symbolically, a limit state for building damage potential evaluation may be expressed as (assuming that the degree of building damage could be divided into binary classes, either tolerable or intolerable):

$$g(x) = \varepsilon_{p,R} - \varepsilon_{p,L} \tag{2.2}$$

where $\boldsymbol{x}$ is the vector of basic variables leading to the *resisting* principal strain ($\varepsilon_{p,R}$) and the *loading* principal strain ($\varepsilon_{p,L}$). Notice that the loading principal strain is the principal strain calculated for a given building subject only to loading from the adjacent excavation, and the resisting principal strain is the *limiting* principal strain that may be specified *empirically* based on the building damage observations. For example, a limiting principal strain for the evaluation of building damage potential may be chosen as the boundary between slight damage and moderate damage defined in the classification chart by Son and Cording (2005) as shown previously in Figure 2.1. The selection of this limiting principal strain ($\varepsilon_{p,R} = 1.67\times10^{-3}$) appears to be reasonable, since buildings with a principal strain less than 1.67×10^{-3} would suffer only slight damage. Nevertheless, selection of this limiting principal strain (and thus the limit state model) is quite *arbitrary* and should be calibrated with field observations. With $\varepsilon_{p,R} = 1.67\times10^{-3}$, the serviceability limit state model can simply be expressed as:

$$g(x) = h(\varepsilon_{p,L}) = 1.67\times10^{-3} - \varepsilon_{p,L} = 0 \tag{2.3}$$

In a deterministic analysis, $g(\boldsymbol{x}) < 0$ would indicate "failure" (meaning that the building would suffer *intolerable* damage).

Development of Bayesian Mapping Functions

Calibration of the serviceability limit state model expressed in Equation 2.3 requires a data set of binary observations. In the current study, the cases compiled by Son (2003) are grouped into only two classes, damaged (*intolerable*) and undamaged (*tolerable*), for the purpose of calibrating the limit state model. Here, a case with damage level more severe than "slight damage" (crack width >5 mm) as defined by Burland et al. (1977) is considered intolerable and requires remediation. On the other hand, any damage equal to or less severe than slight damage as defined by Burland et al. (1977) is considered tolerable. Of the 142 cases compiled by Son (2003), 124 had sufficient data to be classified into tolerable or intolerable. Of the total of 124 cases, 75 were classified as intolerable and 49 were classified as tolerable.

Figure 2.3 shows histograms displaying the relative frequencies of intolerable and tolerable cases with respect to the principal strains and the cumulative distribution functions for intolerable and tolerable cases. Based on the cumulative distribution functions of tolerable and intolerable cases, the limiting principal strain should fall in the range of 1.00×10^{-3} to 1.50×10^{-3}. This observation is inconsistent with the limiting principal strain of 1.67×10^{-3} selected previously based on data shown in Figure 2.1, which highlights the importance and the need for calibrating the *chosen* limiting principal strain (and thus the limit state model) with field observations. The distributions of the principal strains of the groups of intolerable and tolerable cases can be used to interpret

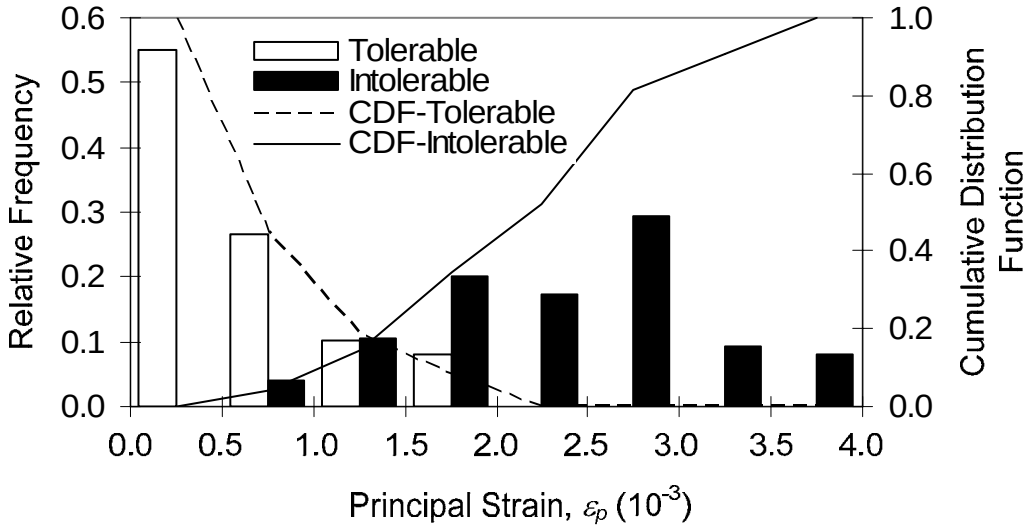

Figure 2.3 Histogram and cumulative distribution of the group of intolerable cases and the group of tolerable cases

the probability of building damage (implying intolerable damage) using Bayes' Theorem. Following the procedure developed by Juang et al. (2000), the following mapping function that relates the principal strain ε_p to the probability of intolerable damage, or simply the probability of damage (P_D) hereinafter, can be established:

$$P_D = P(D \mid \varepsilon_p) = \frac{P(\varepsilon_p \mid D)P(D)}{P(\varepsilon_p \mid D)P(D) + P(\varepsilon_p \mid ND)P(ND)} \tag{2.4}$$

where $P(D|\varepsilon_p)$ = conditional probability of building damage for a given ε_p; $P(\varepsilon_p|D)$ = probability of ε_p given that building damage did occur; $P(\varepsilon_p|ND)$ = probability of ε_p given that building damage did not occur; $P(D)$ = prior probability of building damage for a given ε_p; $P(ND)$ = prior probability of no building damage for a given ε_p.

To evaluate Equation 2.4, it is noted that the terms $P(\varepsilon_p|D)$ and $P(\varepsilon_p|ND)$ are the probability (or relative frequency) of ε_p in the group of intolerable cases and the group of

tolerable cases, respectively, as shown in Figure 2.3. Thus, for a known prior probability, $P(D)$, the prior probability of no damage $P(ND) = 1 - P(D)$, and the conditional probability of damage, $P(D|\varepsilon_p)$, can be evaluated. The knowledge of prior probability, $P(D)$, for a future case, however, is generally unknown. Based on the principle of maximum entropy (Jaynes 1978, Harr 1987), for a case with no information available other than that used for the calculation of ε_p, $P(D)$ can reasonably be assumed to be equal to $P(ND)$, and thus, $P(D) = P(ND) = 0.50$. Alternatively, the characteristics of the database may be used to estimate the prior probability. Although the accuracy of such estimate may depend on how well the database (a sample) represents the "population," it is considered an improvement over the assumption of "no prior knowledge."

For convenience, the knowledge of prior probability is expressed hereinafter in terms of "prior probability ratio," defined as r =P(D)/P(ND). If the characteristics of the database of 124 cases (including 75 damaged cases and 49 undamaged cases) are used as a guide, $r = 1.53$ is obtained. Based on this prior probability ratio, a mapping function that relates the principal strain (ε_p) to the probability of damage (P_D) is established:

$$P_D = \frac{1}{1 + \left(\frac{\varepsilon_p \times 10^3}{a}\right)^b} \tag{2.5}$$

where the coefficients a =1.14 and b = –5.35 are obtained based on curve-fitting of the data pairs (P_D, ε_p) obtained from Equation 2.4 with data shown in Figure 2.3.

To estimate the possible variation of the obtained mapping function, a number of samples of the database of 124 cases are further analyzed. Approximately, 40 samples are required to obtain an estimate of the variation of the obtained mapping function. For each sample, cases are randomly selected from the database of 124 cases with the exceptions that the number of cases in the sample falls in the range of 80 to 124 and the characteristics (i.e. prior probability) of the database are maintained. The derived samples yield a mean prior probability ratio of 1.53 and a standard deviation of 0.26, indicating that the characteristics of the database are maintained. A range of mapping functions are obtained by repeating the procedure for establishing the P_D–ε_p mapping function as described previously with these randomly selected samples. Figure 2.4 shows the mean P_D–ε_p mapping function and its range defined by the maximum (upper bound) and the minimum (lower bound) mapping functions. It is noted that at a given ε_p, the maximum

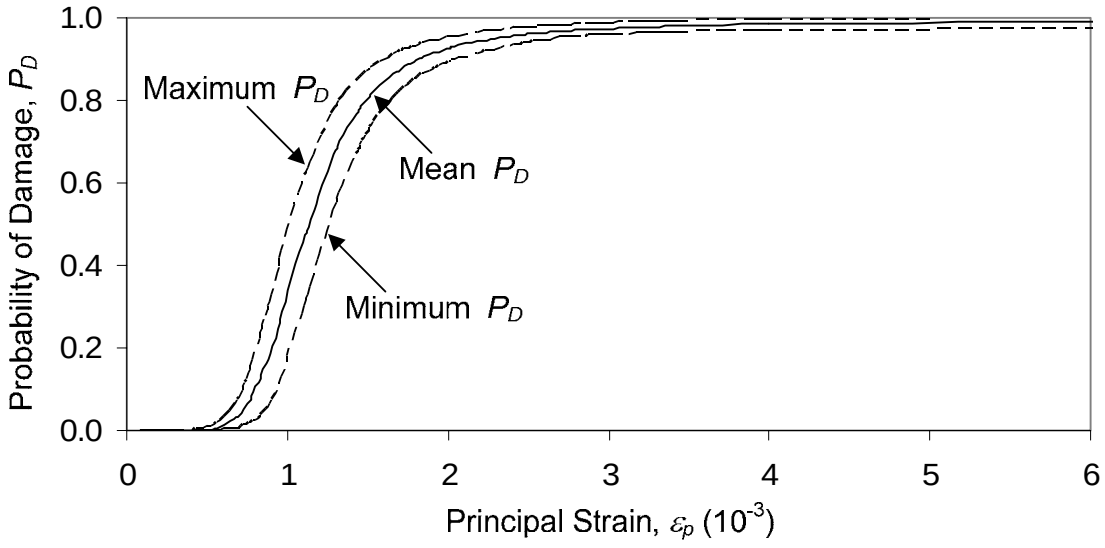

Figure 2.4 Bayesian mapping function curves

and the minimum P_D values are found to be approximately equal to the mean P_D plus and minus three times the standard deviations, respectively, which indicates the estimated range of the mapping functions is approximately correct. Table 2.1 summarizes the results of the curve-fitting coefficients for the minimum, maximum, and mean curves.

Table 2.1 Coefficients of the P_D- ε_p mapping functions (Equation 2.5)

Mapping Function	**Coefficients in Equation (2.5)**	
	a	***b***
Maximum P_D Curve*	1.03	-5.35
Mean P_D Curve*	1.14	-5.35
Minimum P_D Curve*	1.24	-5.35

*Referring to Figure 2.4.

Estimation of Uncertainty of Limit State Model

The primary purpose for developing the P_D–ε_p mapping function (Equation 2.5 and Figure 2.4) is to provide a basis to estimate the probability of damage for a given ε_p, which in turn, provides a reference for back-figuring the uncertainty (or model bias) of the limit state model (Equation 2.3). The concept of using the "observed" binary data (tolerable and intolerable cases and their distributions) to calibrate model bias of an empirical model was proposed by Juang et al. (2004, 2006).

As noted previously, the limit state model (Equation 2.3) was established based on the classification of building damage in the database (Figure 2.1). To account for model uncertainty in the limit state equation, a model bias factor, c_1, is introduced so that the limit state model becomes:

$$g(x) = h(c_1, \varepsilon_{p,L}) = c_1(1.67 \times 10^{-3}) - \varepsilon_{p,L} = 0 \quad (2.6)$$

In the present study, the model bias factor c_1 is assumed to follow a lognormal distribution, a common assumption in the literature (e.g., Juang et al. 2006; Phoon and Kulhawy 2005). A lognormal distribution avoids the situation of having a negative model bias factor and still has the flexibility of modeling the "true" distribution of the model bias factor. Using this assumption, the model bias factor can be characterized by its mean and standard deviation (in terms of a coefficient of variation, *COV*). The model bias factor is also assumed to be uncorrelated to the input variable ($\varepsilon_{p,L}$) in the current study. Whereas these assumptions may need to be examined further, the focus of the paper is to present an approximate method by which the bias of a limit state model can be estimated so that the probability of failure (or intolerable building damage in this case) can be determined through a reliability analysis. In the end, what matters most is the probability of damage (P_D).

Based on the limit state model expressed in Equation 2.6, the reliability index can be determined with a closed-form solution. In Equation 2.6, if the term $c_1(1.67 \times 10^{-3})$ is treated as the resistance (R) and the term $\varepsilon_{p,L}$ is treated as the load (L), and both R and L follow lognormal distribution, then the reliability index β_L can be calculated as (Ang and Tang, 2006):

$$\beta_L = \frac{\ln\left[\frac{\mu_R}{\mu_L}\sqrt{\frac{1+COV_L^{\,2}}{1+COV_R^{\,2}}}\right]}{\sqrt{\ln[(1+COV_L^{\,2})(1+COV_R^{\,2})]}} \tag{2.7}$$

where μ_R and μ_L are the mean values of R and L, respectively, and COV_R and COV_L are the coefficients of variation of R and L, respectively. It should be noted that R and L are assumed to be uncorrelated. The effect of this assumption is trivial since in all cases analyzed, $COV_L = 0$. The probability of damage P_D is then obtained as follows:

$$P_D = 1 - \Phi(\beta_L) \tag{2.8}$$

where Φ is the standard normal cumulative distribution function.

The procedure to back-calculate the model bias factor using the Bayesian mapping function that was calibrated with "observed data" was developed by Juang et al. (2004, 2006). The model bias factor c_1, with a mean, μ_{c1}, and coefficient of variation, COV_{c1}, can be back-calculated with the aid of the previously developed Bayesian mapping function (mean P_D curve, for example). The back-calculation is performed by varying μ_{c1} and COV_{c1} until the P_D from reliability analysis (Equation 2.7 and 2.8) best matches the P_D from the Bayesian mapping function. The latter serves as a reference since it has been calibrated with observations. The μ_{c1} and COV_{c1} values are determined by minimizing the root mean squared error (RMSE) between the P_D determined from the Bayesian mapping function and the corresponding value obtained from the reliability analysis, defined as (Juang et al. 2006):

$$RMSE = \sqrt{\frac{\sum_{i=1}^{N} (P_{D2} - P_{D1})^2}{N}} \tag{2.9}$$

where P_{D1} is the P_D obtained from the Bayesian mapping function for a particular case, P_{D2} is the P_D obtained from the reliability analysis that incorporates the model bias factor, and N is the number of cases.

To calculate the P_D with a particular set of μ_{c1} and COV_{c1}, the closed-form solution (Equations 2.7 and 2.8) presented previously can be applied. The essential approach originated from Juang et al. (2004, 2006) to find the optimum μ_{c1} and COV_{c1} values involves initially assuming a value for COV_{c1} and varying μ_{c1} values until the *RMSE* is minimized. Then the optimum μ_{c1} value is held constant and the COV_{c1} value is determined by varying COV_{c1} until the *RMSE* is minimized. This process is repeated until μ_{c1} and COV_{c1} converge to their optimum values. However, since the P_D can be found with closed-form equations, μ_{c1} and COV_{c1} can be determined simultaneously using Excel Solver by minimizing the *RMSE*. Although the comparison is not shown here, this latter approach gives the same results as those obtained using the approach developed by Juang et al. (2004, 2006), but is much less time consuming. Using the mean P_D curve (Equation 2.5 with a =1.14 and b = –5.35) as the reference, the following statistics of the model bias factor are obtained: μ_{c1} = 0.71 and COV_{c1} = 0.33.

To investigate possible variation in the resulting μ_{c1} and COV_{c1} due to the variation in the Bayesian mapping function, the calibration process is repeated using all other mapping functions developed previously. Based on the calibration with each of

these mapping functions, the mean values and standard deviations of μ_{c1} and COV_{c1} respectively are determined: $\mu_{c1} = 0.71$ with $\sigma_{\mu c1} = 0.03$ and $COV_{c1} = 0.33$ with $\sigma_{COVc1} = 0.02$. This result suggests that σ_{COVc1} is quite negligible and COV_{c1} could be treated as a constant for the selected limit state model (Equation 2.6). If the effects of $\sigma_{\mu c1} = 0.03$ and $COV_{c1} = 0.33$ (or standard deviation = 0.71x0.33 = 0.234) are combined, a standard deviation of c_1 of 0.236 (assuming the two effects are uncorrelated) or 0.264 (assuming perfect correlation) is obtained. Thus, a conservative estimate (by taking the larger of the two values) would yield the combined standard deviation of 0.264, which yields a final $COV_{c1} = 0.37$ at the mean of $\mu_{c1} = 0.71$.

Calibration of the Limiting Principal Strain

Previously, the limiting principal strain ($\varepsilon_{p,R} = 1.67\times10^{-3}$) was established quite *arbitrarily* based on the building damage classification by Son and Cording (2005). However, it would be useful to examine the relationship between the limiting principal strain and the model uncertainty, and to calibrate the limiting principal strain so that the serviceability limit state becomes unbiased ($\mu_{c1} = 1.00$).

Effect of Assumed Limiting Principal Strain

To examine the effect of the assumed limiting principal strain on model uncertainty, the limiting principal strain is redefined so that any damage more severe than "Very Slight" (in reference to Figure 2.1) is considered intolerable. Thus, the limiting principal strain is now assumed to be 0.75×10^{-3}, and the new limit state with consideration of model bias is expressed as:

$$g(x) = h(\varepsilon_{p,L}) = c_1(0.75\times10^{-3}) - \varepsilon_{p,L} = 0 \tag{2.10}$$

As demonstrated previously with the original limit state model, the model bias factor (μ_{c1} and COV_{c1}) can be back-figured. Repeating the previous calibration process with the new limit state model (Equation 2.10), the following results are obtained: μ_{c1} = 1.59 with $\sigma_{\mu c1}$ = 0.07 and COV_{c1} = 0.33 with $\sigma_{COVc1} \approx 0$. As can be seen from the results, both the mean and standard deviation of the mean model bias factor (μ_{c1}) increase significantly when the limiting principal strain is lowered, but the mean and standard deviation of the *COV* values remain approximately the same. As calculated previously, a conservative combination of the effects of $\sigma_{\mu c1}$ and COV_{c1} yields the final statistics, μ_{c1} = 1.59 and COV_{c1} = 0.37 for this limit state model (Equation 2.10).

It should be noted that the product of the mean model bias factor and the limiting principal strain is equal to 1.19×10^{-3}, regardless of whether the original limit state (Equation 2.6) or the new limit state (Equation 2.10) is adopted in the analysis. This suggests that the limiting principal strain should be equal to 1.19×10^{-3} for the unbiased limit state.

Calibration of Unbiased Limit State

Based on the previous analyses, it is observed that the model uncertainty varies with the limiting principal strain employed in the limit state model. Using a trial-and-error procedure to search for the limiting principal strain until the mean model bias factor

(μ_{c1}) is equal to 1.00, the limiting principal strain is determined to be 1.19×10^{-3}. Thus, an unbiased serviceability limit state may be expressed as:

$$g(x) = h(c_1, \varepsilon_{p,L}) = c_1(1.19\times10^{-3}) - \varepsilon_{p,L} = 0 \tag{2.11}$$

Repeating the calibration procedure as described previously, the following final statistics of the model bias factor were determined: μ_{c1} = 1.00 and COV_{c1} = 0.37.

In summary, reliability analysis (Equations 2.7 and 2.8) based on the developed unbiased limit state model (Equation 2.11 with the back-calculated model bias factor) can produce an estimate of the probability of building damage that is as accurate as those obtained from the Bayesian mapping function that was calibrated with "observed" data compiled and assessed by Son and Cording (2005). The results of this study confirm the concept proposed by Juang et al. (2006) that the bias of a limit state model may be estimated from the "observed" binary data. With a calibrated model bias factor, a routine reliability analysis can be performed to determine the probability of building damage caused by an excavation.

Effect of the Assumed Prior Probability Ratio on the Uncertainty of the Limit State Model

Previously, the model bias factor (c_1 in Equation 2.11) was back-calculated from the Bayesian mapping function assuming the prior probability ratio r = 1.53 that was based on the characteristics (or the make-up) of the entire database (75 intolerable cases and 49 tolerable cases). In the subsequent analyses, the prior probability ratio is assumed to vary in the range of 0.3 to 7.5 based on the make-up of each sample. For each sample,

a Bayesian mapping function is developed, which is then used as a reference to back-calculate the model bias factor of the limit state model (Equation 2.11).

Figure 2.5 and Figure 2.6 show plots of the calibrated mean model bias factor (μ_{c1}) versus the assumed prior probability ratio (r) and the COV of the model bias factor (COV_{c1}) versus r, respectively. Curve-fitting of the data shown in Figure 2.5 yields (R^2 = 0.96; residual standard error = 0.03):

$$\mu_{c1} = 2 - 1.27\left(\frac{r}{r+0.41}\right) \tag{2.12}$$

Curve-fitting of the data shown in Figure 2.6 yields (R^2 = 0.82; residual standard error = 0.02):

$$COV_{c1} = 0.70 - 0.45\left(\frac{r}{r+0.31}\right) \tag{2.13}$$

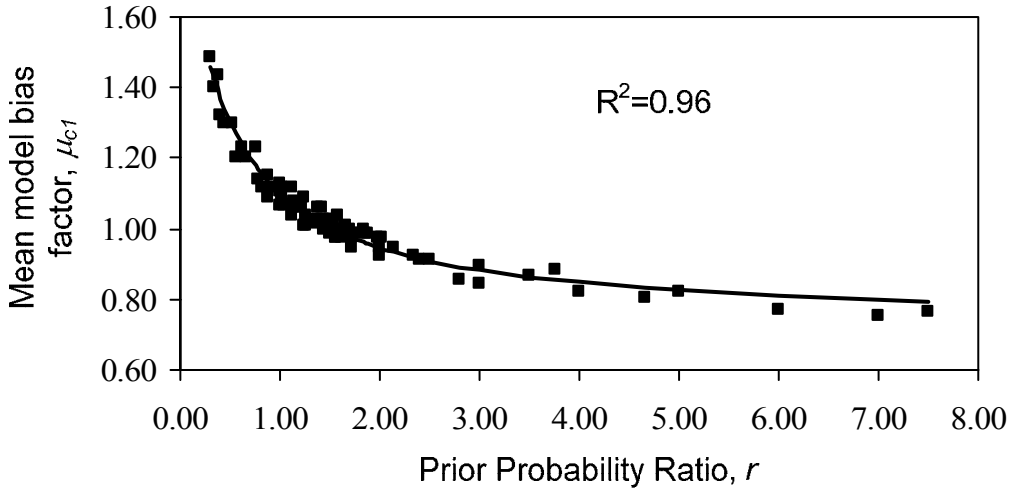

Figure 2.5 Mean model bias factor,μ_{c1} versus Prior Probability Ratio

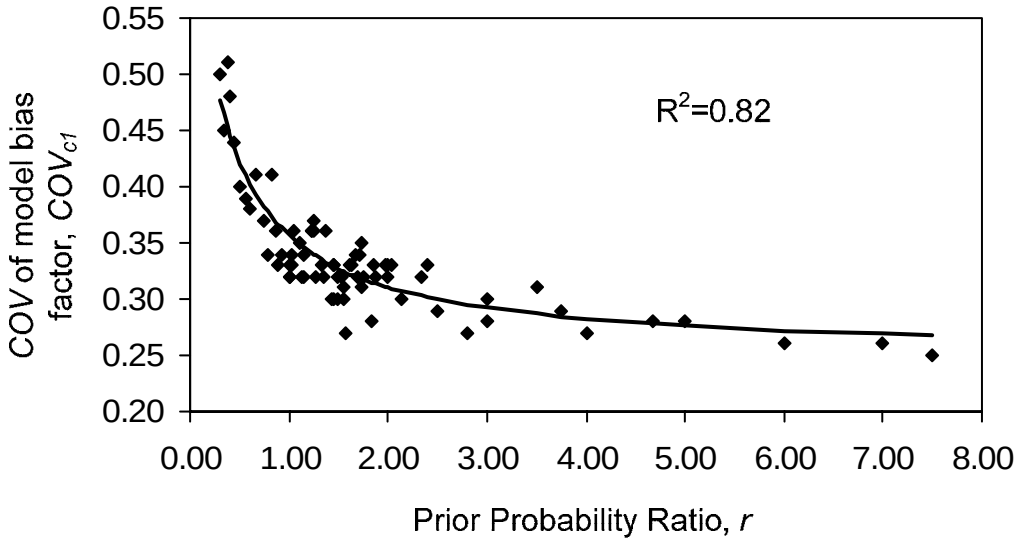

Figure 2.6 COV_{c1} versus Prior Probability Ratio

It is of interest to note that at r = 1.53, Equations 2.12 and 2.13 yield approximately μ_{c1} = 1.00 and COV_{c1} = 0.33, respectively. These statistics about the model bias factor are practically the same as those obtained previously using only samples with an assumed r = 1.53. Moreover, the residual standard errors in Equations 2.12 and 2.13, respectively, are approximately equal to the corresponding standard deviations of the μ_{c1} and COV_{c1} obtained previously using only samples with an assumed r = 1.53. As mentioned previously, it is desirable to combine the effect of $\sigma_{\mu c1}$ (the standard error in the use of Equation 2.12) and COV_{c1} so as to simplify the reliability analysis. As discussed previously, for samples with the assumed r = 1.53, a conservative estimate of the combined effect would result in an increase in COV_{c1} by approximately 0.04. An examination of both Equation 2.12 and Equation 2.13 and the associated standard errors reveals that this combined effect is quite consistent for all r values. Thus, Equation 2.13 may be modified to account for this combined effect:

$$COV_{c1} = 0.74 - 0.45\left(\frac{r}{r+0.31}\right) \tag{2.14}$$

In summary, for the limit state model defined in Equation 2.11 the model bias factor can be characterized by Equations 2.12 and 2.14 for a given *r* value. Based on this limit state, reliability index can be calculated using Equation 2.7 and the probability of building damage can be obtained from Equation 2.8.

Further Treatment of Prior Probability Ratio- An Iterative Procedure

The mean and coefficient of variation of the model bias factor are shown previously to be function of the prior probability ratio. This is not exactly a surprise, as the model bias factor was back-calculated based on the *reference* probability that was obtained from Equation 2.4 through calibration with the "observed" data. Although the reference probability obtained from Equation 2.4 is considered a "best estimate" of the "true" probability based on the given database, it depends on the knowledge of the prior probability. Thus, the back-calculated statistical parameters of the model bias factor, μ_{c1} and COV_{c1}, are both a function of the prior probability ratio.

Dependency of the model bias on the knowledge of prior probability, as expressed in Equations 2.12 and 2.14, presents a challenging situation as this knowledge may not be fully reflected in a given database (which is just a sample) and is thus generally unknown. To overcome this problem, an iterative procedure is established based on the relationships between the mean and COV of the model bias factor and the prior

probability ratio expressed in Equations 2.12 and 2.14. Intuitively, however, the model bias factor of a limit state model should not vary from case to case. To avoid violation of such intuition, the model bias factor is referred to hereinafter as the "*apparent*" model bias factor, meaning that it is not necessarily the "true" model bias factor but rather a factor that can be applied to a limit state model so that the probability of damage *for a specific case* obtained from Equations 2.7 and 2.8 matches the reference probability obtained from the calibrated Bayesian mapping function. This apparent model bias factor has the combined characteristics of both the "true" model bias factor and the "state" of

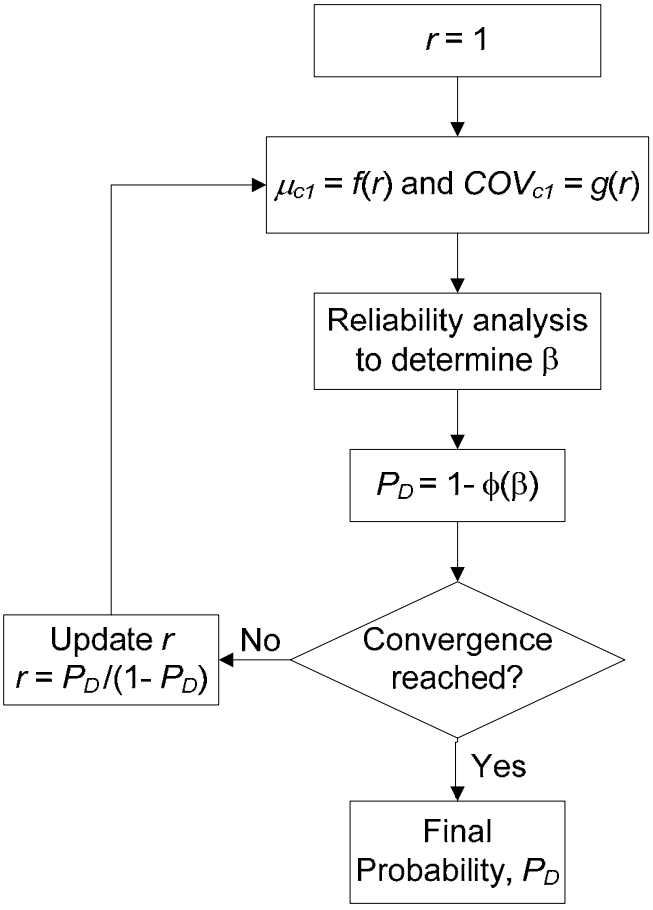

Figure 2.7 Steps of Iterative Procedure

information of the specific case.

The iterative procedure is illustrated in Figure 2.7. Initially, the prior probability of damage P_D is assumed to equal to 0.5 (since there is a lack of knowledge), and thus, the prior probability ratio r = 1. With this ratio, the apparent model bias factor can be estimated with Equations 2.12 and 2.14, and the reliability analysis can be performed. This will result in a new probability of damage P_D, which is considered an updated solution. With the updated P_D, a new ratio r is obtained, which in turn, yields an updated apparent model bias factor (through Equations 2.12 and 2.14, again). This process can be repeated until convergence where the final P_D is obtained along with the finalized apparent model bias factor (μ_{c1} and COV_{c1}). The significance and implication of the iterative procedure is further examined with two examples.

Example Case 1: M36-3

This example concerns an undamaged (*tolerable*) case in the database collected by Son (2003). The case, coded M36-3, was a numerical analysis of a 4-storey brick bearing structure on a stiff soil. The angular distortion and lateral strain of the case were 1.37×10^{-3} and 0.70×10^{-3} respectively leading to a principal strain of $\varepsilon_{p,L}=1.12\times10^{-3}$. Initially, the case is assessed herein based on the assumption that no information on the prior probability of building damage is available. Under this assumption, the prior probability ratio r = 1 based on the principle of the maximum entropy (Ang and Tang 2006), and the model uncertainty (μ_{c1} = 1.10 and COV_{c1} = 0.40) can be determined with Equations 2.12 and 2.14. Based on the limit state model defined

in Equation 2.11, reliability analysis is conducted using Equations 2.7 and 2.8, which yields $P_D = 0.41$.

For comparison, the same case, M36-3, is reanalyzed based on the assumption that r =1.53, the prior probability ratio estimated based on information revealed in the database, as presented previously. With this r value, the model bias factor can be characterized with $\mu_{c1} = 1.0$ and $COV_{c1} = 0.37$. Through reliability analysis, $P_D = 0.50$ is obtained. Both solutions seem to be quite high as this is an undamaged (*tolerable*) case where in theory P_D should be near 0.

Because the lack of prior knowledge of r value, the iterative procedure as shown in Figure 2.7 is applied to the same case, M36-3, to determine P_D. First, the prior probability ratio is assumed to be 1.0 (thus, $\mu_{c1} = 1.10$ and $COV_{c1} = 0.40$ based on Equations 2.12 and 2.14, respectively) and the P_D is found to be 0.41. In turn, the result of $P_D = 0.41$ suggests that $r = P_D/(1-P_D) = 0.71$ (thus, $\mu_{c1} = 1.20$ and $COV_{c1} = 0.43$) be used in the next round of the analysis. Using the updated apparent model bias factor, the P_D is recalculated to be 0.35 on the second iteration and the prior probability ratio and apparent model bias factor can be updated again. This process is repeated until the apparent model bias factor and P_D converge at $r = 0.37$. As shown in Figure 2.8, the apparent model bias factor and P_D converge simultaneously. At convergence, the P_D is equal to 0.27 with the apparent model bias factor characterized by $\mu_{c1} = 1.40$ and $COV_{c1} = 0.49$.

To test the effect of different initial guesses of the prior probability ratio (r) on the results of the iterative procedure, the same problem is solved with a number of different initial prior probability ratios (r =1, 2,…5). In all analyses, the same solution (r = 0.37 and P_D = 0.27) is obtained at convergence. The unique solution is also confirmed for all cases in the database using the iterative procedure.

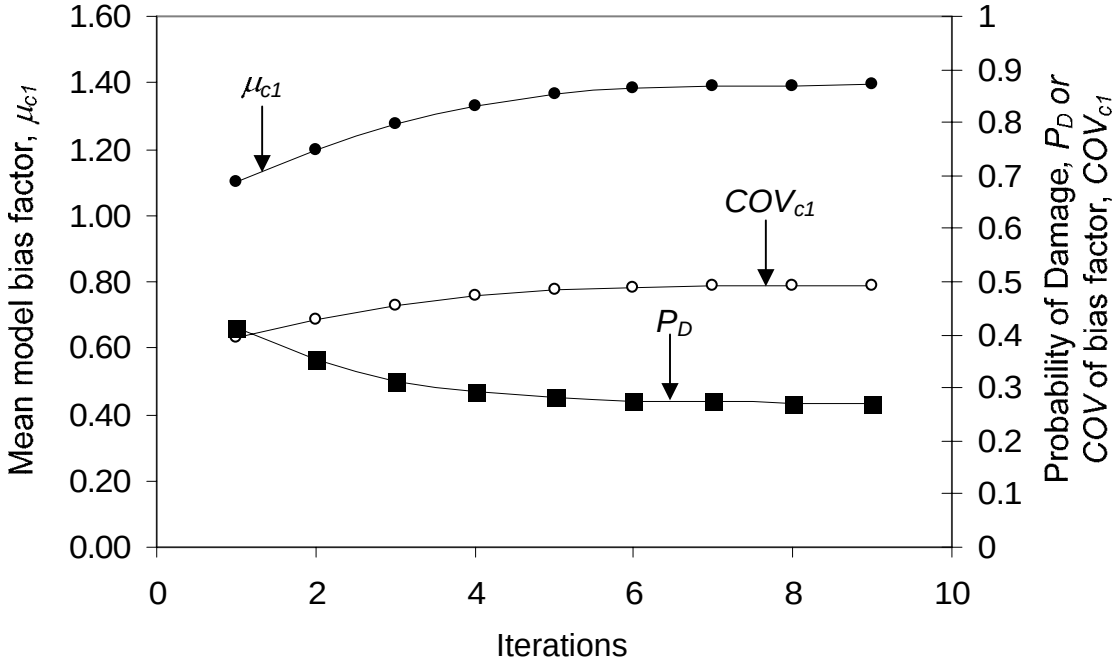

Figure 2.8 Convergence of Iterative Procedure

The finalized P_D of 0.27 obtained from the iterative procedure appears to be an improvement over the previous solutions of P_D = 0.41 (under the assumption of fixed r = 1) and P_D = 0.50 (under the assumption of fixed r = 1.53), as the "ideal" solution from the back-analysis of this undamaged (*tolerable*) case should be near 0.

The improvement in P_D due to the iterative procedure may be attributed to the knowledge about the specific case gained during the iterative process. In essence, the iterative procedure incorporates the case-specific information (for example, prior probability) into the calibration of the apparent model bias factor, which in turn, provides a basis for updating the information about this very case. At convergence, the apparent model bias factor is obtained and the probability for the case is determined.

Example Case 2: M20

This example concerns an intolerable case in the database collected by Son (2003). The case, coded M20, was a numerical analysis of a 2-storey brick bearing structure on a soft soil. The angular distortion and lateral strain of the case were 0.30×10^{-3} and 1.28×10^{-3}, respectively, which resulted in a loading principal strain, $\varepsilon_{P,L}=1.30\times10^{-3}$. Similar to the first example, if r =1 is assumed, the P_D can be calculated with Equations 2.7 and 2.8 to be 0.57. If r = 1.53 is assumed, the P_D is equal to 0.67.

Using the iterative procedure as detailed previously, the P_D is calculated to be 0.89 at convergence. Again, the P_D attained with the iterative procedure is the most consistent with the expected P_D (close to unity) from the back-analysis of this intolerable (damaged) case. Thus, this example demonstrates that the iterative procedure improves the estimation of P_D due to the knowledge gained on this case.

Summary

In this chapter, a P_D-ε_p mapping function was established based on the distributions of tolerable (undamaged) and intolerable (damaged) cases in an excavation-induced building damage database compiled by Son (2003) and Son and Cording (2005). In addition, a serviceability limit state model for evaluating damage potential to buildings adjacent to an excavation was initially established based on the data by Son and Cording (2005). Through calibration of the initial limit state model with the P_D-ε_p mapping functions, an unbiased limit state model was further developed. This unbiased limit state model, represented by Equation 2.11, was characterized with a model bias factor c_1 that has the following statistical parameters: $\mu_{c1} = 1.00$ and $COV_{c1} = 0.37$.

Since the P_D-ε_p mapping function was established based on Bayes' theorem, it requires the knowledge of prior probability. Thus, the model bias factor of the limit state model (Equation 2.11) determined through calibration with the P_D-ε_p mapping function depended on the assumed prior probability. The effect of the assumed prior probability on the model bias factor was studied, and Equations 2.12 and 2.14 were developed for estimating the mean and coefficient of variation of the model bias, μ_{c1} and COV_{c1}. With the model bias characterized, reliability analysis can then be performed with the limit state model expressed in Equation 2.11.

Since the prior probability is often unknown, an iterative procedure, illustrated in Figure 2.7, was developed to simultaneously calculate the model bias and the probability of damage P_D for a given case. From the cases examined and presented previously, the iterative procedure was shown to give improved results over those obtained by assuming

a fixed prior probability ratio. This improvement attained from the iterative procedure may be attributed to the knowledge about the specific case gained during the iterative process. In essence, the iterative procedure incorporates the case-specific information (for example, prior probability) into the calibration of the apparent model factor, which in turn, provides a basis for updating the information about this very case.

CHAPTER THREE

SIMPLIFIED MODEL FOR EVALUATING THE DAMAGE POTENTIAL OF BUILDINGS ADJACENT TO A BRACED EXCAVATION IN CLAYS[*]

Introduction

The design of an excavation in urban areas is a significant undertaking that requires both ensuring the stability of the excavation and maintaining the integrity of structures adjacent to an excavation. The latter, to prevent damage of buildings caused by an excavation, is the focus of this chapter. Specifically, an evaluation procedure with simplified models for assessing damage potential of buildings adjacent to an excavation is developed herein. Both the deterministic and the probabilistic assessments of the excavation-induced building damage potential can be performed within the framework of the proposed procedure.

A comprehensive procedure for the analysis of building damage caused by a nearby excavation involves three main components: 1) determination of the lateral and vertical ground movement profiles, 2) estimation of the angular distortion and lateral strain that develop in a building based on ground movement, building properties, and soil-structure interaction, and 3) assessment of the building damage based on the angular distortion and lateral strain induced in a building. Figure 3.1 illustrates the flow of various components of the proposed procedure for assessing excavation-induced building damage potential.

[*] A similar form of this chapter has been submitted for publication at the time of writing; co-authored by Schuster, M.J., Kung, G.T.C., Juang, C.H., and Hashash, Y.M.A.

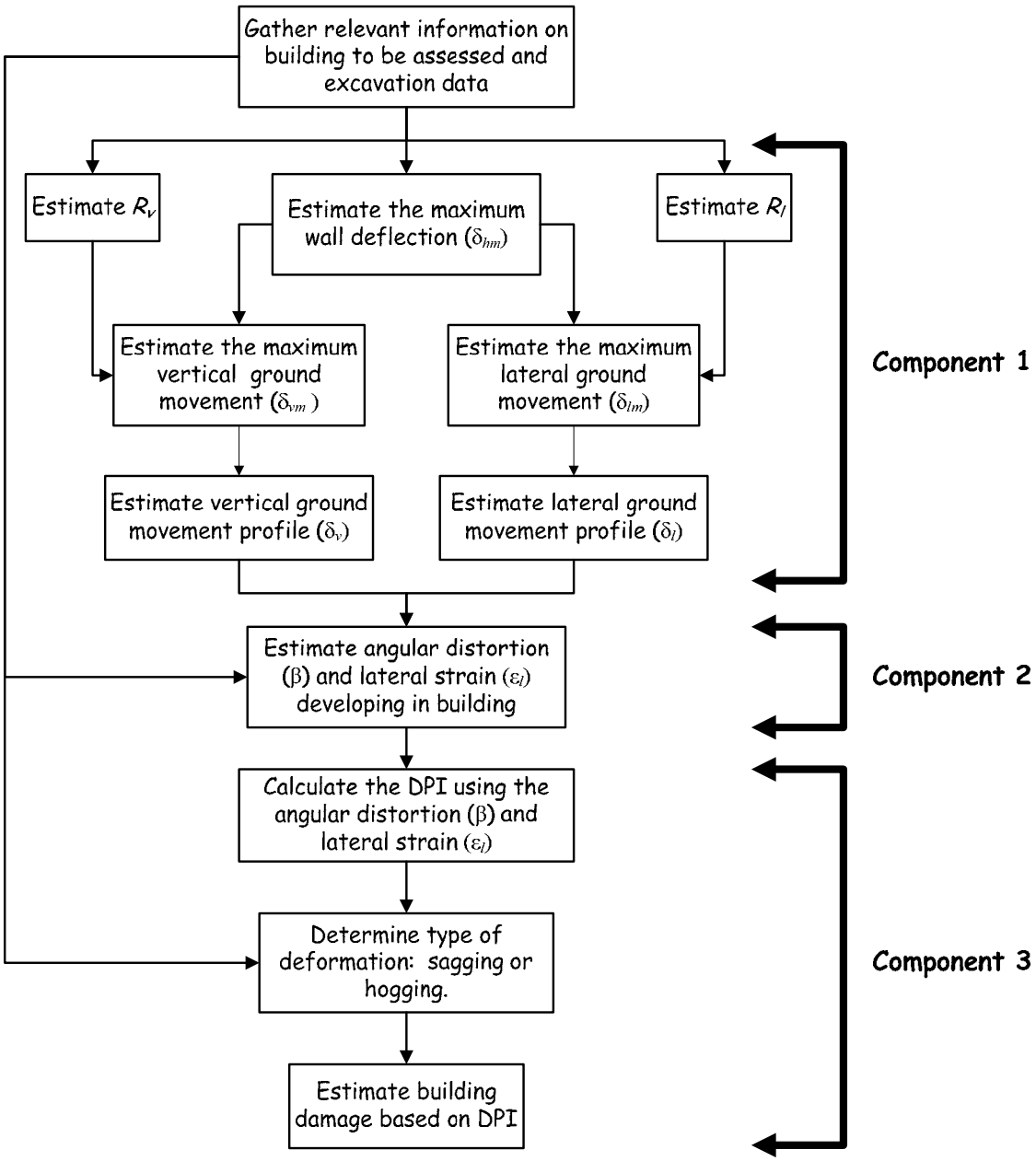

Figure 3.1 Procedure for evaluating excavation-induced building damage

The general framework of the proposed procedure as illustrated in Figure 3.1 is, of course, not new. In fact, a comprehensive procedure for evaluating excavation-induced building damage has recently been presented by Son and Cording (2005). Many other investigators (e.g., Skempton and MacDonald 1956; Polshin and Tokar 1957; Bjerrum 1963; Burland and Wroth 1974; O'Rourke et al. 1976; Boscardin and Cording 1989; Boone 1996; Finno et al. 2005) have also contributed to the development of evaluation criteria for assessing excavation-induced building damage. Nevertheless, the proposed procedure is augmented with various simplified semi-empirical models, which enables an easy implementation of the procedure in an engineering tool such as a spreadsheet for an efficient evaluation of building damage potential. Furthermore, the model uncertainty of the entire evaluation process is fully characterized, which enables a practical probabilistic assessment of building damage potential if so desired.

In this chapter, the various elements detailed in Figure 3.1 are developed to establish a framework for evaluating the building damage potential. To this end, simplified empirical models for estimating the excavation-induced ground movements are fully developed. For this task, the KJHH model developed by Kung et al. (2008) is adopted for estimating the vertical ground movement profile. Subsequently, the Kung-Schuster-Juang-Hashash (KSJH) model for estimating the lateral ground movement profile is developed herein using the KJHH model as a template. This is followed by the development of the empirical models for estimating the angular distortion and lateral strain that develop in a building, which are functions of building properties and the vertical and lateral ground movement profiles. A new evaluation criterion termed the

damage potential index (*DPI*), which is a function of angular distortion and lateral strain and represents a "normalized" value of principal strain, and its corresponding damage level criterion are then established. The step-by-step algorithm that further details the flowchart shown in Figure 3.1 is then presented along with examples that demonstrate the proposed procedure. Finally, the uncertainty of the entire evaluation process leading to the determination of *DPI* is fully characterized and an example for performing a probabilistic assessment of building damage potential is presented.

Models for Estimating Vertical and Lateral Ground Movement Profiles

Determination of angular distortion and lateral strain in a building caused by an excavation requires knowledge of the vertical ground movement profile as well as the lateral ground movement profile. A semi-empirical model for the vertical ground movement profile, called KJHH model, has been developed previously by Kung et al. (2007b). In this section, a similar model for the lateral ground movement profile is developed using the KJHH model as a template. This parallel model for estimation of lateral ground movement is termed the KSJH model for convenience of presentation hereinafter. Similar to the KJHH model, four tasks are required for the development of the KSJH model: 1) determination of the maximum lateral wall deflection δ_{hm}, 2) determination of R_l, a *lateral* deformation ratio defined as the ratio of the maximum lateral ground movement δ_{lm} over the maximum lateral wall deflection δ_{hm}, 3) determination of the maximum lateral ground movement (δ_{lm}), and 4) establishment of the lateral movement profile. To set the stage for development of the KSJH model, the

KJHH model is first summarized. Subsequently, the development of the KSJH model is presented.

Summary of KJHH model

In general, the vertical ground movement using the KJHH model can be estimated with the following approach:

(1) Determine the maximum wall deflection δ_{hm},

(2) Estimate the *vertical* deformation ratio R_v (=δ_{vm} /δ_{hm}), and

(3) Calculate the maximum vertical ground movement δ_{vm}.

(4) Determine the vertical ground movement profile.

In the KJHH model, five basic parameters are considered essential for predicting the maximum wall deflection (δ_{hm}) caused by excavation in soft to medium clays. These parameters include the excavation depth (H_e), the excavation width (B), the system stiffness [$EI/\gamma_w h_{avg}^4$ as defined in Clough and O'Rourke (1990), where E is the Young's modulus of wall material, I is the moment of inertia of the wall section, γ_w is the unit weight of water, and h_{avg} is the average support spacing], the ratio of shear strength over vertical effective stress (s_u/σ'_v), and the ratio of initial Young's tangent modulus over vertical effective stress (E_i/σ'_v). With these five input variables, the maximum lateral wall deflection δ_{hm} is calculated as (Kung et al. 2007a):

$$\delta_{hm} = a_0 + a_1X_1 + a_2X_2 + a_3X_3 + a_4X_4 + a_5X_5 + a_6X_1X_2 + a_7X_1X_3 + a_8X_1X_5 \qquad (3.1)$$

where $X_1 = t(H_e)$, $X_2 = t[\ln(EI/\gamma_w h_{avg}^4)]$, $X_3 = t(B/2)$, $X_4 = t(s_u/\sigma_v')$, and $X_5 = t(E_i/\sigma_v')$, and t is a transformation function defined in Eq. 3.2. The coefficients are as follows: a_0 = –13.41973, a_1 = –0.49351, a_2 = –0.09872, a_3 = 0.06025, a_4 = 0.23766, a_5 = –0.15406, a_6 = 0.00093, a_7 = 0.00285, and a_8 = 0.00198. It is noted that variables X_i (i = 1, 5) are the transformed variables of the five basic input variables defined as (Kung et al. 2007a):

$$X = t(x) = b_1 x^2 + b_2 x + b_3 \tag{3.2}$$

where x is each of the input variables (H_e, $\ln(EI/\gamma_w h_{avg}^4)$, $B/2$, s_u/σ_v', and E_i/σ_v'), X is the transformed variable, and the coefficients, b_1, b_2, and b_3 are listed in Table 3.1.

Table 3.1 Coefficients for linear transformation of five variables

Variables x	Applicable range	Coefficients of Equation 3.2		
		b_1	b_2	b_3
H_e (m)	0 – 30	-0.4	24	-50
$\ln(EI/\gamma_w h_{avg}^4)$	≥ 0	11.5	-295	2000
$B/2$ (m)	$0 \le B \le 100$	-0.04	4	90
s_u/σ_v'	0.2 – 0.4	3225	-2882	730
E_i/σ_v'	200 – 1200	0.00041	-1	500

The computed maximum wall deflection δ_{hm} should then be corrected for the presence of hard stratum near the bottom of the excavation. This may be carried out using the deflection reduction factor, K, which is defined as:

$$K = 1.5(T/B) + 0.4 \quad \text{for} \quad T/B \le 0.4 \tag{3.3}$$

where T is the distance from the bottom of the excavation to the hard stratum and B is and the width of the excavation. It should be noted that no modification is needed when $T/B > 0.4$.

Once the modified maximum wall deflection δ_{hm} is calculated with Equations 3.1-3.3, only the vertical deformation ratio is needed to estimate the maximum vertical ground movement. The vertical deformation ratio defined as the ratio of the maximum vertical ground movement over the modified maximum wall deflection, in clay-dominant sites is mainly influenced by three parameters, $\sum H_{clay}/H_{wall}$, s_u/σ'_v, and $E_i/1000\sigma'_v$. The parameter $\sum H_{clay}/H_{wall}$ is illustrated with Figure 3.2. The vertical deformation ratio R_v is expressed as:

$$R_v = c_0 + c_1 Y_1 + c_2 Y_2 + c_3 Y_3 + c_4 Y_1 Y_2 + c_5 Y_1 Y_3 + c_6 Y_2 Y_3 + c_7 Y_3^3 + c_8 Y_1 Y_2 Y_3 \tag{3.4}$$

where $Y_1 = \sum H_{clay}/H_{wall}$, $Y_2 = s_u/\sigma'_v$, $Y_3 = E_i/1000\sigma'_v$, and the coefficients for Equation 3.4 determined through the least-square regression are as follows: c_0 = 4.55622, c_1 = –3.40151, c_2 = –7.37697, c_3 = –4.99407, c_4 = 7.14106, c_5 = 4.60055, c_6 = 8.74863, c_7 = 0.38092, and c_8 = –10.58958.

The excavation-induced maximum ground movement δ_{vm} can be obtained by multiplying δ_{hm} with R_v and is expressed as:

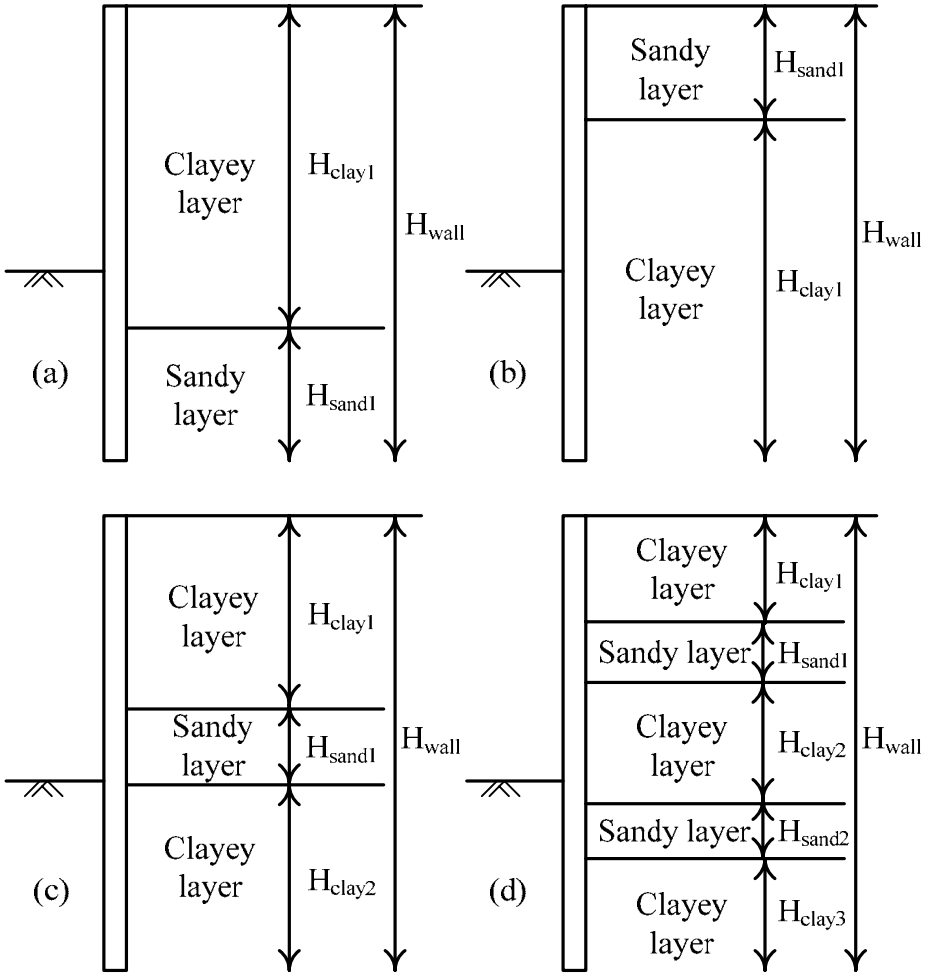

Note: 1. $\Sigma H_{clay} = H_{clay1}+H_{clay2}+...$

2. For a pure clay site, $\Sigma H_{clay} / H_{wall} = 1$

Figure 3.2 Determination of normalized clay layer thickness ($\sum H_{clay} / H_{wall}$)

$$\delta_{vm} = R_v \times \delta_{hm} \tag{3.5}$$

Finally, the vertical ground movement profile can be obtained using Figure 3.3. The ground movement profile illustrated in Figure 3.3 can be expressed as:

$$\delta_v / \delta_{vm} = \left(1.6 \times d / H_e + 0.2\right) \qquad \text{for } 0 \le d/H_e \le 0.5 \tag{3.6a}$$

$$\delta_v / \delta_{vm} = \left(-0.6 \times d / H_e + 1.3\right) \qquad \text{for } 0.5 \le d/H_e \le 2.0 \tag{3.6b}$$

$$\delta_v / \delta_{vm} = \left(-0.05 d / H_e + 0.2\right) \qquad \text{for } 2.0 \le d/H_e \le 4.0 \tag{3.6c}$$

where d is the distance from the wall, H_e is the excavation depth, δ_v is the vertical settlement at the distance d, and δ_{vm} is the maximum vertical settlement.

Simulated Data of Wall and Ground Responses through Numerical Experiments

The same numerical experiments as those employed in the development of the KJHH model are utilized in the development of the KSJH model. In fact, the same FEM

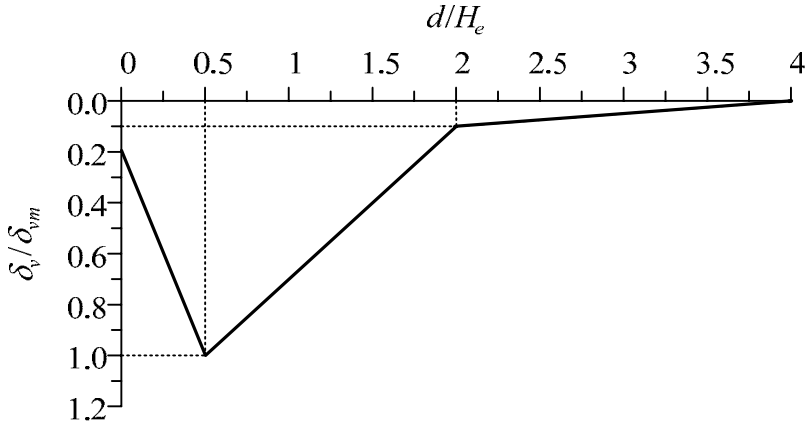

Figure 3.3 Excavation-induced settlement profile proposed by Kung et al. (2007b)

solutions of the hypothetical cases labeled previously as *numerical experiments* are employed. In the previous development of the KJHH model, the simulated data of the wall deflection and vertical ground movement obtained from these numerical experiments were used, and for the development of the KSJH model in this paper, the simulated data of the wall deflection and lateral ground movement are used.

Lateral Ground Movements Caused by Excavation

Figure 3.4 shows the lateral ground surface movements in selected representative hypothetical cases. Although significant scatter in the data presented, the trend of the normalized lateral ground surface movement profile is quite similar to one commonly observed for the vertical ground surface movement (ground surface settlement) profile reported in Hsieh and Ou (1998) and Kung et al. (2007b). Thus, a parallel development

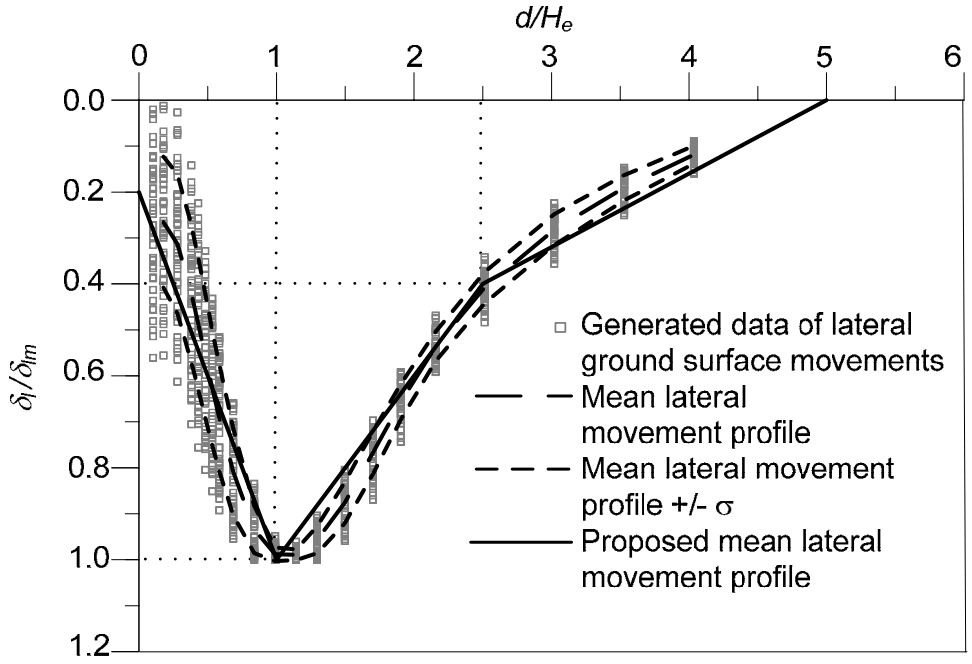

Figure 3.4 Ground surface lateral movement behavior in representative hypothetical cases

for an empirical model similar to the KJHH model that was used for estimating the ground surface settlement is feasible. Similar to the settlement profile suggested by Kung et al. (2007b), the proposed lateral ground surface movement profile is divided into three parts: $0 \le d/H_e \le 1$, $1 \le d/H_e \le 2.5$, and $2.5 \le d/H_e \le 5$ (Figure 3.4).

The proposed lateral ground surface movement profile is then verified with observed data from three excavation cases, the Taipei National Enterprise Center (TNEC case; Ou et al. 1998) and the Lurie Research Center case (Lurie case; Finno and Roboski 2005), and the Formosa case (Ou et al. 1993). Numerical simulations of the three excavation cases using finite element method (FEM) analysis with a small-strain soil model (Hsieh et al., 2003; Kung et al. 2007a) are also employed to complement field observations. Figure 3.5 shows the results of validation of the proposed lateral movement profile. The predictions in the range of $0 \le d/H_e \le 1$ are in good agreement with the observations and the FEM solutions. For the ranges of $1 \le d/H_e \le 2.5$ and $2.5 \le d/H_e \le 5$, no field observation data are available; nevertheless, the upper bound of the lateral ground surface movement profile presented in Figure 3.5 compared quite well with the FEM solutions.

Building foundations are generally constructed at certain depths rather than at the ground surface; thus the applicability of the proposed lateral ground surface movement profile (Figure 3.5) in estimating the lateral ground movement at depths needs further assessment. Figure 3.6 shows the FEM solutions of lateral ground movement profiles in

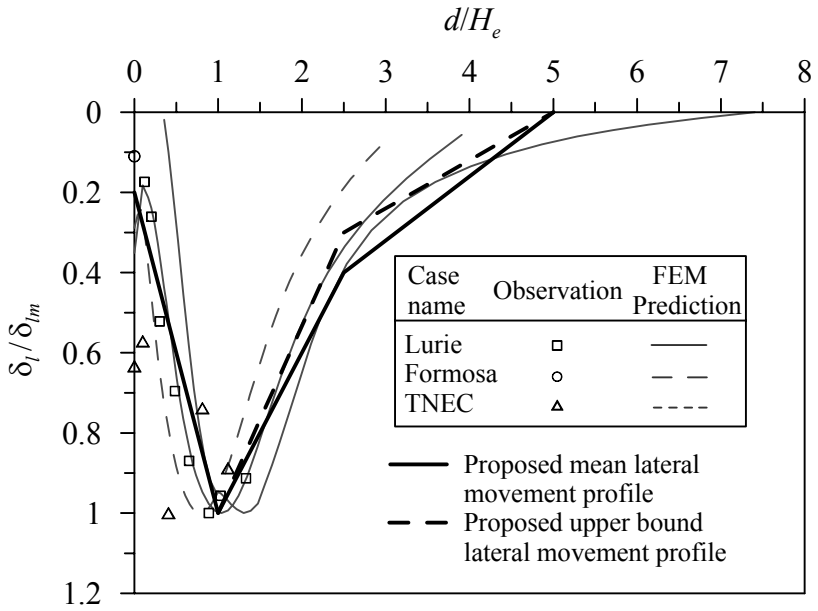

Figure 3.5 The proposed ground surface lateral profile with field observations and FEM simulations

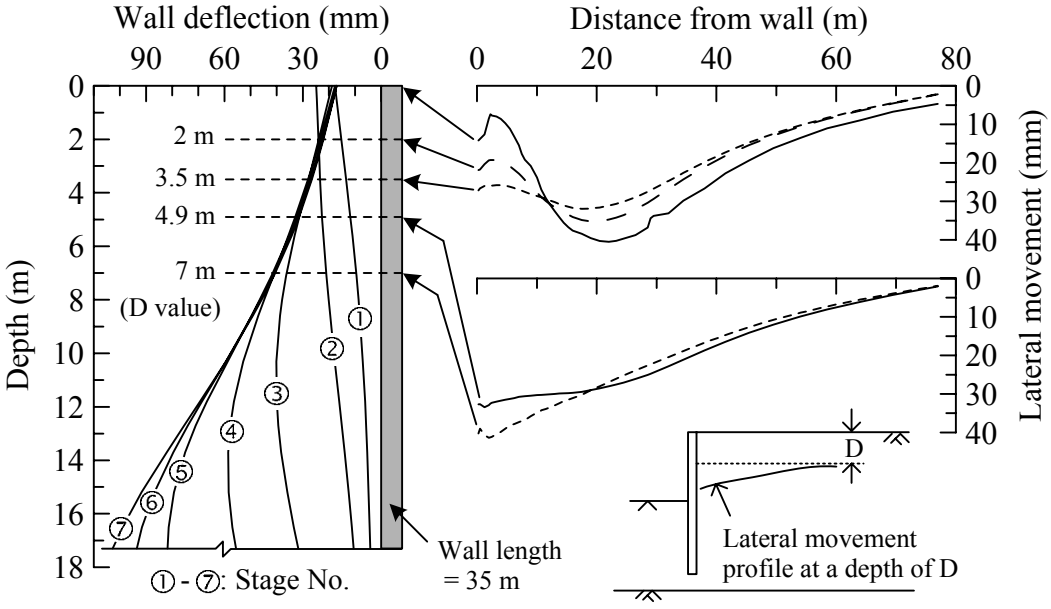

Figure 3.6 Excavation-induced lateral ground movement profiles at various depths based on FEM solutions of the TNEC case

the TNEC case at depths of 0 m (indicating ground surface), 2 m, 3.5 m, 4.9 m, and 7 m, respectively. Interestingly, the concave-type lateral movement profiles at depths of 0 m, 2 m, and 3.5 m significantly differ from the spandrel-type profiles at depths of 4.9 m and 7 m. At shallow depths, the concave-type profiles should be expected because the wall is supported by struts and thus difficult to deflect toward the excavation zone as the excavation proceeds. On the other hand, at larger depths (e.g., 7 m), the spandrel-type profiles are likely to occur because the wall can deflect unrestrainedly prior to the installation of struts at greater depths. Therefore, establishing lateral movement profiles at various depths for describing different scenarios of the response of the building foundations is desirable. Figure 3.7 shows a proposal of lateral movement profiles at various depths based on the results discussed previously. These lateral ground movement profiles include the concave-pattern profiles for depths from 0 m to 4 m and the spandrel-pattern profiles for depths from 5 m to 7 m. The observed data from the three case histories discussed previously including the TNEC case shown in Figure 3.7, tend to support the proposed lateral ground movement profiles. Further study on this issue to confirm the proposed lateral movement profiles is warranted.

The applicability of the ground surface settlement profile of the KJHH model to describe the settlement at various depths is also investigated herein. By examining the FEM solutions of the TNEC case and other hypothetical cases (Kung et al. 2007b), it is found that the settlements at various depths (in the range of 0 m to 7 m) is almost identical to that determined at the ground surface. This suggests that at these depths (e.g., depth $\leq$ 7 m), the settlement profile can also be estimated by the KJHH model.

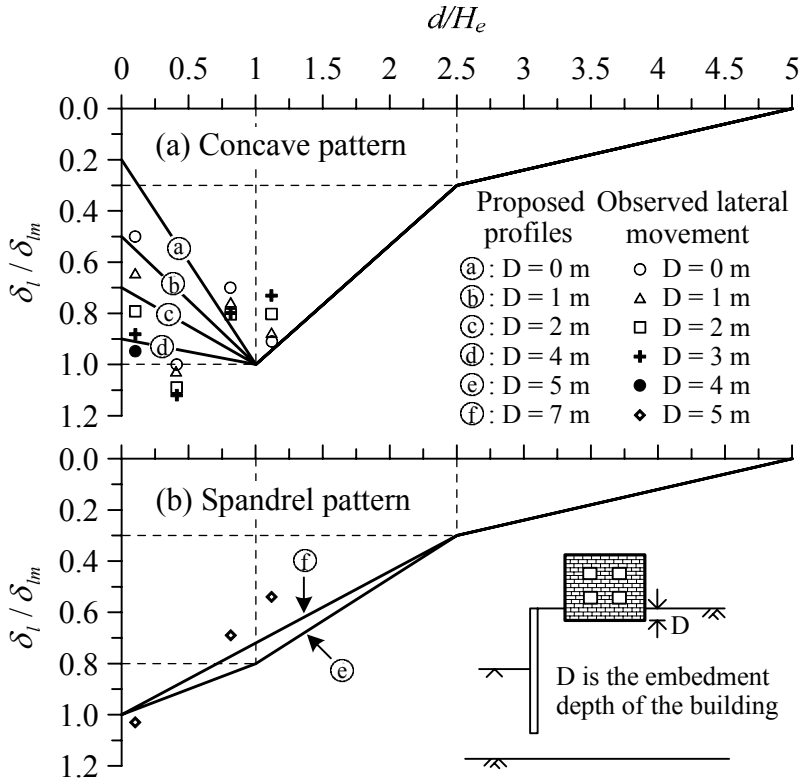

Figure 3.7 Proposed lateral movement profiles at various depths with field observations from the TNEC case

Semi-Empirical Model for Estimating Lateral Deformation Ratio R_l

The maximum lateral ground movement δ_{lm} may be determined through the lateral deformation ratio R_l:

$$\delta_{lm} = R_l \times \delta_{hm} \tag{3.7}$$

where the lateral deformation ratio R_l is established in a way similar to the development of the vertical deformation ratio R_v as described in Kung et al. (2007b). Based on curve-

fitting of the simulated data derived from FEM solutions, the following equation is obtained:

$$R_l = d_0 + d_1 Y_1 + d_2 Y_2 + d_3 Y_3 + d_4 Z_1 Y_2 + d_5 Z_1 Y_3 + d_6 Z_2 Y_3 \quad (3.8)$$

where Y_1, Y_2, *and* Y_3 are the same as defined in Equation 3.4, and the coefficients for Equation 3.8 determined through the least-square regression are as follows: $d_0 = 2.17807$, $d_1 = -1.19041$, $d_2 = -2.87994$, $d_3 = -0.96655$, $d_4 = 1.63969$, $d_5 = 0.16155$, and $d_6 = 1.46109$.

Figure 3.8 shows the scatter of Equation 3.8 in reproducing the results of FEM solutions that had previously been verified (Kung et al. 2007a). The accuracy and

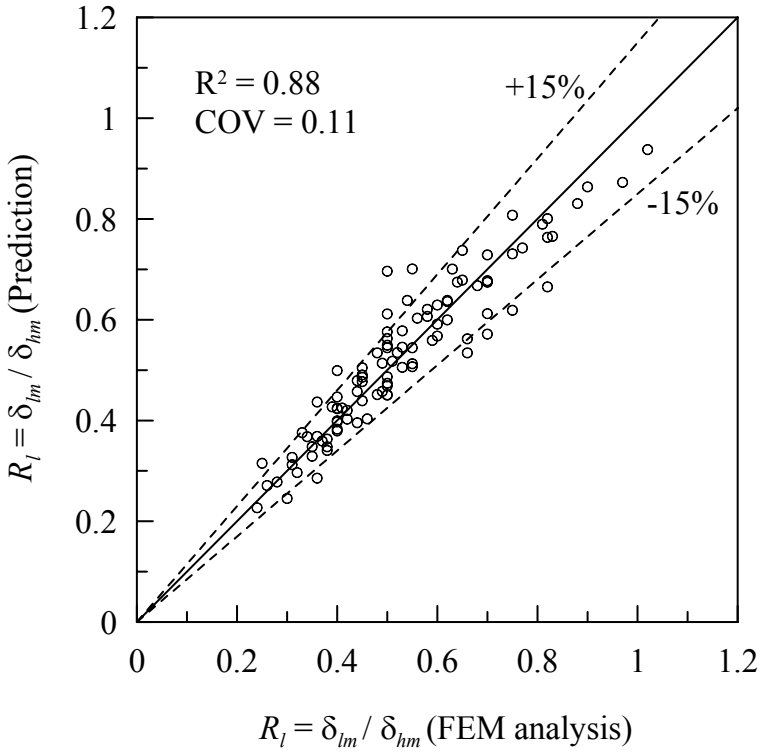

Figure 3.8 Performance of Equation 4 in various simulated ground conditions

precision of Equation 3.8 for predicting the lateral deformation ratio R_l is reflected by its R^2 (0.88) and *COV* (0.11) obtained in the regression analysis. In addition, almost all data points are within ±15% of the 1:1 line. Equation 3.8 is further verified with two available case histories (the TNEC case and the Lurie case). The observed and estimated values of R_l are 0.40 and 0.45, respectively, for the TNEC case, and are 0.93 and 0.91, respectively, for the Lurie case.

Summary of the KSJH Model for Lateral Ground Movement

The maximum wall deflection δ_{hm} is obtained from the KJHH model, and the lateral deformation ratio R_l is determined with Equation 3.8. It follows that the maximum lateral ground movement δ_{lm} can be determined with Equation 3.7. Once δ_{lm} is determined, the lateral ground movement profiles can be constructed following the proposed pattern shown in Figure 3.7. By combining the previously developed KJHH and newly developed KSJH model, both vertical and lateral ground movement profiles, which constitute Component 1 of the proposed procedure (Figure 3.1), can be determined.

Models for Angular Distortion and Lateral Strain in a Building

The strains that are induced in a building due to ground movement can essentially be characterized in terms of two parameters, angular distortion and lateral strain. In this section, regression-based simplified models are developed for determining these two parameters, which is Component 2 of the proposed procedure (Figure 3.1).

The formation of angular distortion and lateral strain in a building is heavily dependent on the soil-structure interaction. Recently, Son and Cording (2005 & 2007)

presented results of their comprehensive study that considered the effects of the soil-structure interaction for the estimation of angular distortion in the building. The angular distortion was approximated as a function of change in ground slope (ΔGS), structure cracking strain (ε_t), and soil-structure stiffness ratio ($E_s L^2/GHb$) where E_s is the soil stiffness in the region of footing influence, L is the length of building portion subjected to ground movement, G is the elastic shear modulus of the building, H is the height of the building, and b is the building wall thickness. Additionally, Boscardin and Cording (1989) provided a means to include the effect of building stiffness (in terms of grade beams) in the estimation of lateral strain. The lateral strain (ε_l) was characterized as a function of ε_{lg}, which is the lateral strain of the ground, and the grade beam-soil stiffness ratio ($E_g A/ E_s H S$) where E_s is soil stiffness, H is depth of excavation, S is the spacing of the grade beams perpendicular to the edge of the excavation, E_g is the modulus of elasticity of the grade beam, and A is the cross-sectional area of the grade beam.

The data presented by Son and Cording (2005) forms the basis for developing regression-based models for angular distortion and lateral strain in the present study. These models can facilitate both the deterministic and the probabilistic assessment of excavation-induced building damage using simple engineering tools such as spreadsheets.

Estimation of the Angular Distortion and Lateral Strain

To develop simplified empirical models for estimating the angular distortion and lateral strain in a building, a data set of 183 cases established by Son and Cording (2005) is employed. This data set is composed of cases with a wide range of surface settlements

and lateral ground movements applied to a wide range of buildings with different stiffness and cracking strains. For each case, detailed information on the ground movement and building properties along with the angular distortion and lateral strain that develop in a building are available.

As discussed previously, the estimation of angular distortion in a building requires information on the vertical ground movement profile (Kung et al. 2007b) and building properties. Therefore, the following parameters are included as inputs for the intended empirical model for angular distortion: the ground slope of the settlement trough GS ($\times 10^{-3}$), differential ground settlement of the settlement trough ΔS (mm), soil-structure stiffness ratio $E_s L^2/GHb$, and the structure cracking strain ε_t. These input parameters are similar to those used by Son and Cording (2005) in their chart-based solutions. Using these four parameters as the input variables and the angular distortion β ($\times 10^{-3}$) as the output variable, regression analysis of the 183 cases yields the following model (R^2 = 0.80):

$$\begin{aligned}\beta &= -0.105 + 0.413(GS) - 0.0466(\Delta S) - 0.304\left[\ln(E_s L^2 / GHb)\right] \\ &\quad + 0.108(GS/\varepsilon_t) + 0.267\left[\ln(E_s L^2 / GHb)\right](GS)\end{aligned} \tag{3.9}$$

Figure 3.9 shows the scatter of this regression model. The standard error of the prediction with this model is $\sigma = 0.42 \times 10^{-3}$. Note that the negative values of angular distortion indicate that the distortion of the building is compressive and that the building will distort inward.

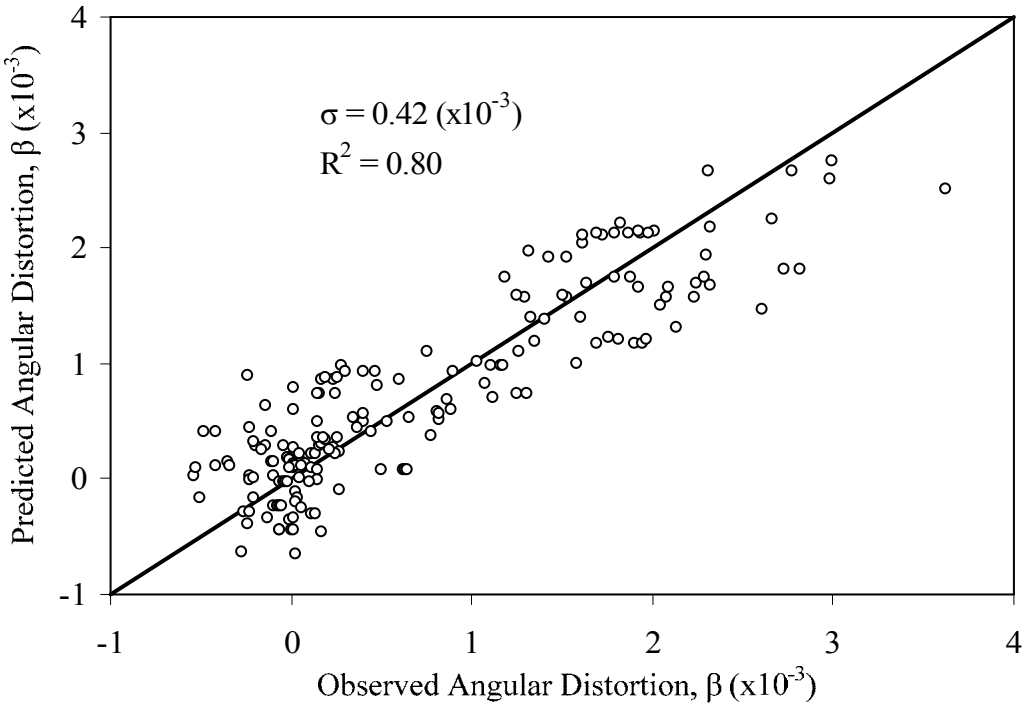

Figure 3.9 Results of regression analysis for angular distortion in a building

Similarly, the estimation of the lateral strain in a building requires information on the lateral ground movement profile and building properties. However, the estimation of lateral strain also requires information on the angular distortion since lateral strain can develop in the upper part of a building when angular distortion is high throughout a building (Son and Cording 2005). Therefore, the following parameters are included as inputs for estimating the lateral strain in a building: the soil-structure stiffness ratio E_sL^2/GHb, structure cracking strain ε_t, lateral strain of the ground ε_{lg} ($\times 10^{-3}$), and angular distortion β ($\times 10^{-3}$). Using these four parameters as the input variables and the lateral strain ε_l ($\times 10^{-3}$) as the output variable, regression analysis of the 183 cases yields the following model ($R^2 = 0.81$):

$$\varepsilon_l = -0.058 + 0.120(\beta) + 0.467(\varepsilon_{\mathrm{lg}}) - 0.200(\varepsilon_{\mathrm{t}}) + 0.062\left[\ln(E_s L^2 / GHb)\right] + 0.214(\beta / \varepsilon_{\mathrm{t}}) \quad (3.10)$$

Figure 3.10 shows the scatter of the predictions of lateral strains of the 183 cases estimated with Equation 3.10. The standard error of the prediction for this model is $\sigma = 0.45\times10^{-3}$. It should be noted that negative lateral strains are consistent with compressive strains in the building.

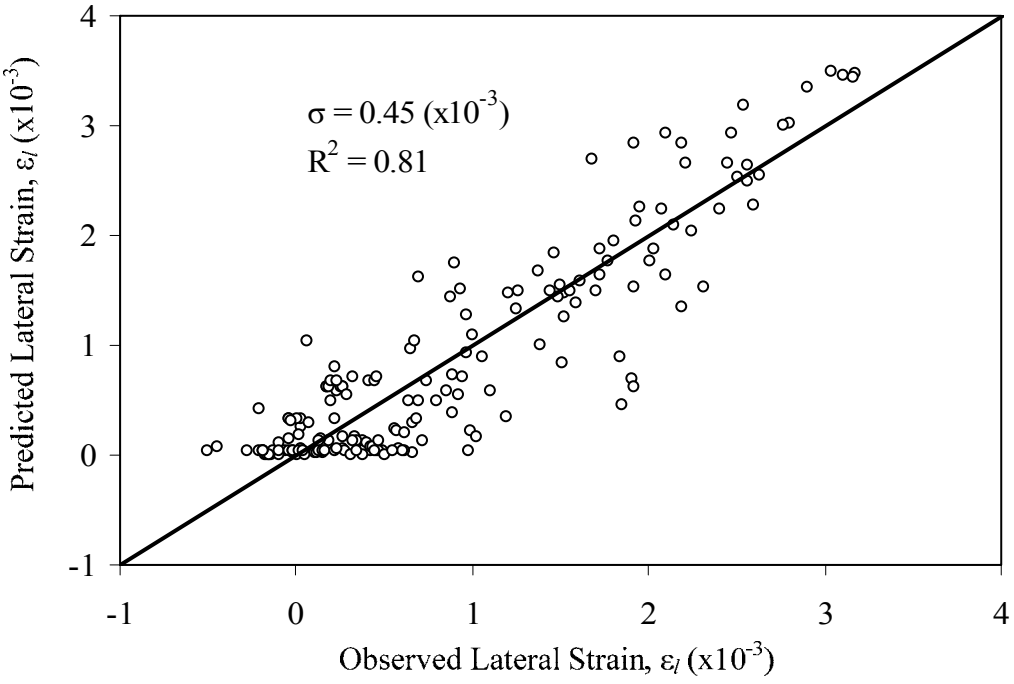

Figure 3.10 Results of regression analysis for lateral strain in a building

Criterion for Assessing Building Damage – "DPI" Model

The criterion used in the proposed procedure for evaluating building damage is a modification of the evaluation criterion of principal strain pioneered by Son and Cording

(2005) and presented previously in Chapter 2. In this section, the criterion of principal strain is normalized and expressed in terms of a new evaluation criterion called damage potential index (*DPI*).

Damage Potential Index (*DPI*)

As a means to implement the damage criteria in a way that would enable an efficient analysis of damage potential, either deterministically or probabilistically, a new term, called Damage Potential Index (*DPI*), is defined herein:

$$\begin{aligned} DPI &= \varepsilon_p /(1/200) \\ &= 20\times10^3 \ (\varepsilon_l \cos\theta_{\max}^2 + \beta \ \sin\theta_{\max} \cos\theta_{\max}) \end{aligned} \tag{3.11}$$

where β = angular distortion, ε_l = lateral strain (i.e. horizontal strain), and $\theta_{\max}$ = direction of crack formation measured from the vertical plane as defined in Chapter 2.

The rationale behind the concept of *DPI* is described in the following. Many previous studies (e.g., Bjerrum 1963; Burland and Wroth 1974; Grant et al. 1974; Boscardin and Cording 1989) showed that the *limiting* angular distortion, with which the structural damage of buildings is likely to occur, is approximately in the range of 1/100 to 1/200. Taking the upper bound of this angular distortion (thusly, β = 1/100) and assuming $\varepsilon_l = 0$ [thusly, $\theta_{\max} = 45^\circ$ according to Eq. (2.1b)], the "apparent" upper bound of ε_p is determined to be 1/200. By normalizing the maximum principal tensile strain ε_p calculated with Eq. (2.1a) with this "apparent" upper bound of ε_p, the index *DPI* is formulated, which falls in the range of 0 to 100. Of course, *DPI* can be greater than 100

if ε_p>1/200. However, in such cases the structural damage will definitely occur, and thusly, it will be unnecessary to conduct a detailed damage assessment. It should be noted that the *DPI* merely represents a normalization of the principal strain. Therefore, the study in Chapter 2 where principal strain is the evaluation criterion can be always be adopted to be applied to the *DPI*.

To develop criteria to interpret the calculated *DPI*, the effect of ground deformation pattern (sagging versus hogging, as illustrated in Figure 3.11) on building damage should be considered. In general, the building damage caused by the hogging pattern is more severe than the sagging pattern because with the former, tensile cracks develop earlier and faster in the upper part of the building. This phenomenon is well recognized by previous investigators (e.g., Burland and Wroth 1974; Son and Cording

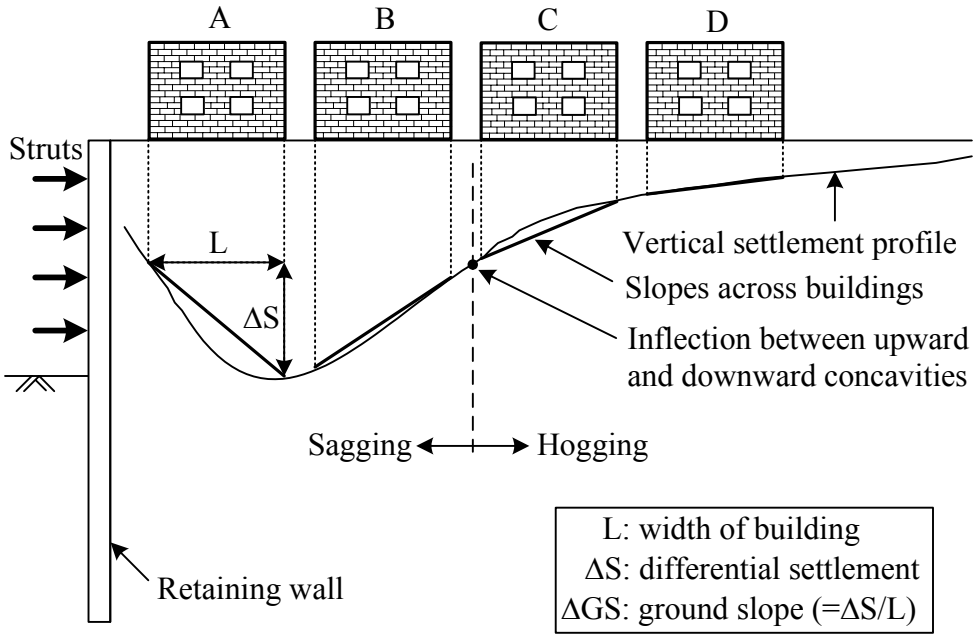

Figure 3.11 Sagging or hogging damage patterns of buildings

2005). However, no current evaluation scheme has *explicitly* incorporated this effect of ground deformation pattern into the analysis. In this chapter, a simplified scheme is proposed to account for this effect in the building damage evaluation. This simplified scheme is established based on an observation of the location of inflection point of the ground deformation pattern illustrated in Figure 3.12, which shows that buildings located within a distance of $d / H_e = 1.4$ from the excavation (where *d* is the distance the building

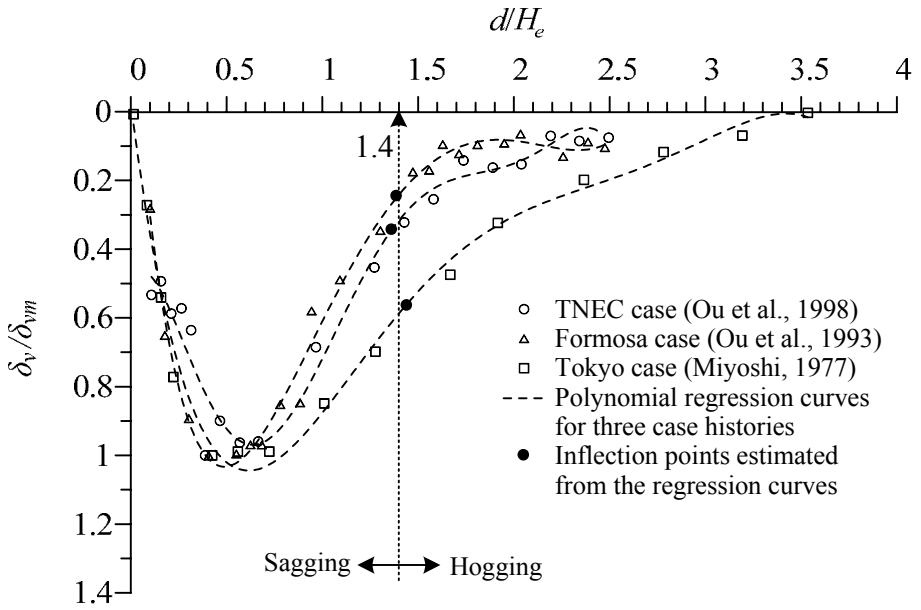

Figure 3.12 Inflection point that divides the damage patterns

is located from the excavation and H_e is excavation depth) tend to undergo *sagging* deformation, and buildings located at a distance farther than $d / H_e = 1.4$ from the excavation tend to undergo *hogging* deformation. This finding is based on a limited number of case histories and should be verified with additional studies. Nevertheless, the

trends are "strong" enough to support this preliminary rule for delineation of ground deformation pattern.

The effect of ground deformation pattern discussed previously is then incorporated into the *DPI*-based evaluation criteria listed in Table 3.2, in which six levels of building damage are delineated with *DPI* values. The ranges of *DPI* values for these damage levels are established primarily based on limiting conditions for building damages published in the literature (Bjerrum 1963; Burland and Wroth 1974; Burland et al. 1977; Boscardin and Cording 1989; Son and Cording 2005) and considering the effect

Table 3.2 Levels of building damage according to damage potential index

Level of building damage caused by excavation		Damage potential index (*DPI*)		Remedial measures
		Sagging $d/H_e \leq 1.4$	Hogging $d/H_e > 1.4$	
1	Negligible to very slight	0 – 15	0 – 10	Such damage levels are considered as *tolerable*, and no scheme to protect adjacent buildings is required.
2	Slight	15 – 25	10 – 20	
3	Slight to moderate	25 – 35	20 – 30	In this level, possible damage to adjacent buildings might be *intolerable*. A protection scheme might be required in the design stage. If not implemented, great caution must be exercised to monitor the building during the construction.
4	Moderate	35 – 60	30 – 50	These levels of damage are definitely *intolerable*. The excavation design should be re-examined and possibly changed. Or, a proper protection scheme must be implemented to protect adjacent buildings.
5	Severe	60 – 85	50 – 80	
6	Very severe	> 85	> 80	

of the ground deformation pattern (sagging versus hogging). The *DPI* model and the evaluation criteria constitute Component 3 of the proposed procedure (Figure 3.1).

Proposed Procedure for Building Damage Evaluation

A step-by-step procedure that further details the flowchart shown in Figure 3.1 for assessing the damage potential of buildings adjacent to an excavation is presented below:

1. Gather relevant information on the building to be assessed and excavation data (i.e. excavation height and width, soil stiffness, building geometry, building stiffness).
2. Estimate the maximum wall deflection δ_{hm} with Equations 3.1-3.3. Six variables, H_e, $\ln(EI/\gamma_w h_{avg}^4)$, $B/2$, s_u/σ'_v, E_i/σ'_v, and T are required for estimating δ_{hm}.
3. Estimate vertical and lateral deformation ratios, R_v and R_l with Equations 3.4 and 3.8. Three parameters, $\sum H_{clay}/H_{wall}$, s_u/σ'_v and $E_i/1000\sigma'_v$, are required for estimating R_v and R_l.
4. Calculate the maximum surface settlement δ_{vm} and the maximum lateral ground movement δ_{lm} with Equations 3.5 and 3.7 respectively.
5. Estimate the depth of the building foundation (or the embedment depth of the building).
6. Determine the vertical settlement and lateral movement profiles at the depth of the building foundation based on the estimated δ_{vm} (Equation 3.6 or Figure 3.3) and δ_{lm} (Figure 3.7).

7. Estimate the angular distortion (β) and lateral strain (ε_l) in the building considering the soil-structure interaction using Equations 3.9 and 3.10.
8. Determine the pattern of the possible building damage based on its location relative to the wall. For $0 \le d / H_e \le 1.4$, the pattern is judged to be sagging; for $1.4 \le d / H_e \le 4$, the pattern is judged to be hogging.
9. Calculate the *DPI* of the building using Equation 3.11 and then interpret the damage level based on Table 3.2.

Uncertainty of the Proposed "DPI" Model

A significant advantage of the evaluation procedure presented in this paper is its easy adaptability for probabilistic analysis. To conduct a simplified probabilistic analysis, the uncertainty of the entire process for computing *DPI*, referred to herein as the *DPI* model, must be examined first. With the knowledge on the uncertainty of the *DPI* model, an engineer can easily evaluate the probability of the excavation-induced building damage.

The uncertainty of the *DPI* model results mainly from the propagation of model uncertainty of the component models (KSJH and KJJH models). The uncertainty of the KJHH model was characterized previously (Kung et al. 2007b), whereas the uncertainty of the KSJH model is assessed in this paper.

Model Uncertainty of the KSJH Model

The procedure employed by Kung et al (2007b) for characterizing the uncertainty of the KJHH model is followed here for assessing the model uncertainty (or model bias)

of the KSJH model. The model bias for each component of the KSJH model can be estimated in terms of bias factor (*BF*):

$$BF = \frac{observed\ value\ (or\ "true"\ value)}{estimated\ value} \tag{3.12}$$

The model bias factor is a normal random variable with a mean and a standard deviation. If the model is unbiased, the bias factor will have a mean of 1.0 (denoted as $\mu = 1.0$). The model bias of the maximum wall deflection δ_{hm} has previously been characterized with a mean of $\mu_{\delta_{lm}} = 1.0$ and a standard deviation of $\sigma_{\delta_{hm}} = 0.25$ (Kung et al. 2007b). The model bias of the lateral deformation ratio R_l, which is determined with Equation 3.12, is characterized with $\mu_{R_l} = 1.0$ and $\sigma_{R_l} = 0.11$ based on analysis of the finite element simulations results that were used for the development of the R_l model. Since the maximum lateral ground movement δ_{lm} is determined with Equation 3.7 by multiplying δ_{hm} with R_l, the mean of the bias factor for the maximum lateral ground movement can be calculated as shown below:

$$\mu_{\delta_{lm}} = \mu_{R_l}(\mu_{\delta_{hm}}) = 1.0(1.0) = 1.0.$$

The standard deviation of the bias factor can then be determined using the first order Taylor series approximation (Ang and Tang 2006) as shown below:

$$\sigma_{\delta_{lm}} = \sqrt{\mu_{R_l}^2 \sigma_{R_l}^2 + \mu_{\delta_{hm}}^2 \sigma_{\delta_{hm}}^2 + 2\rho\mu_{R_l}\sigma_{R_l}\mu_{\delta_{hm}}\sigma_{\delta_{hm}}} = 0.31.$$

It should be noted that in estimating the standard deviation here, the correlation between the maximum wall deflection and lateral deformation ratio was estimated to be 0.3 based on the analysis of the maximum wall deflection and lateral deformation ratios obtained from the FEM generated cases. This estimate is considered reasonable; besides, a small to moderate change in this estimate will result in a negligible change in the resulting standard deviation.

Finally, the model uncertainty of a lateral ground movement δ_l at any distance from the excavation must be estimated. Since the maximum lateral ground movement and lateral ground movement generated with the FEM analysis are strongly correlated, the uncertainty of both the maximum lateral ground movement and lateral ground movement may be assumed to be equal. Thus, the model bias of the lateral ground movement can be characterized with a mean of 1.0 and a standard deviation of 0.31. This result is quite consistent with the mean of 1.0 and the standard deviation of 0.35 obtained for the model bias factor of the vertical ground movement model reported by Kung et al. (2007b).

Uncertainty of the DPI Model

The uncertainty of the *DPI* model may be characterized by the standard deviation (σ_{DPI}) of the computed *DPI*. To this end, the procedure described by Duncan (2000), which is a simplified version of the first order second moment (FOSM) method, is employed to determine σ_{DPI}.

The mean *DPI*, denoted herein as μ_{DPI}, can simply be taken as the value calculated using the mean values or the most probable values of the input parameters of

the *DPI* model. The standard deviation σ_{DPI} is, however, dependent on the propagation of the component model uncertainty and can be different in different ranges of input parameters. To estimate this standard deviation, all the cases in the database of Son and Cording (2005) were analyzed using Duncan's (2000) simplified FOSM procedure. The results are shown in Figure 3.13. Additionally, as shown in Figure 3.14, use of the point

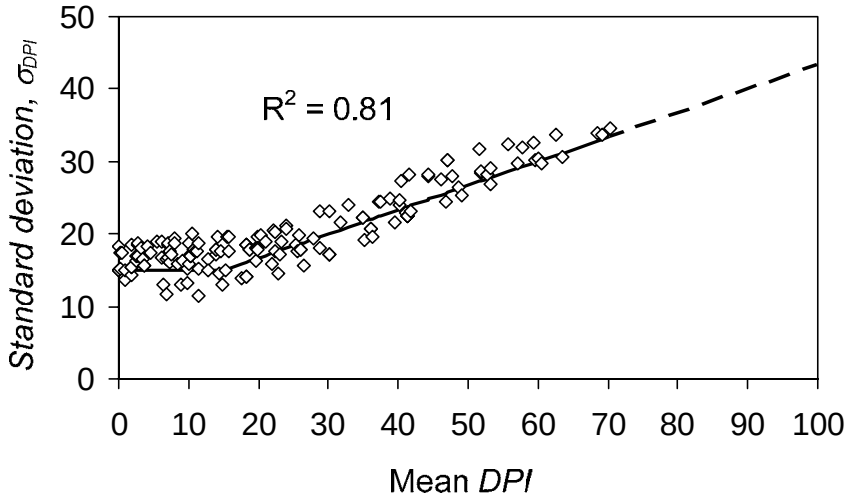

Figure 3.13 Model uncertainty of DPI

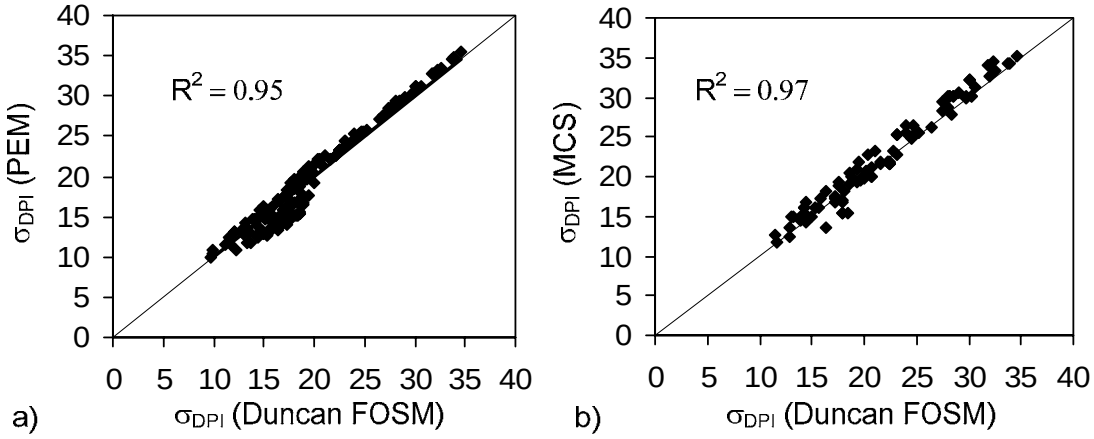

Figure 3.14 Estimation of σ_{DPI} for Different Evaluation Procedures

estimate method (PEM) and Monte Carlo simulation (MCS) methods to compute the propagation of component model uncertainties yielded practically the same results as those attained with Duncan's simplified FOSM approach. Based on the data shown in Figure 3.13, the following simplified equation is proposed for estimating the standard deviation σ_{DPI}:

$$\begin{aligned} \sigma_{DPI} &= 15, \ \text{if } DPI \le 15 \\ \sigma_{DPI} &= 15 + (DPI - 15)/3, \ \text{if } DPI > 15 \end{aligned} \tag{3.13}$$

With the knowledge of the mean and standard deviation of *DPI* for a given future case, the probability of exceeding a specified *DPI* value can be readily determined and the probabilistic assessment of building damage can be made. For example, if the mean *DPI* is computed to be 18, then the standard deviation will be σ_{DPI} = 16 according to Equation 3.13. Assuming that *DPI* follows lognormal distribution (Phoon 2005), the probability of exceeding a threshold *DPI* value that corresponds to a specified damage level, say, "Slight" damage, can be easily obtained as follows:

$$P_D = \Pr[DPI > 20] = 30\% \tag{3.14}$$

where 20 is a threshold value of *DPI*, taken in this example as the upper bound of "Slight" damage (hogging deformation pattern listed in Table 3.1). This probability of 30% is the probability of sustaining a damage level exceeding "Slight" damage.

To facilitate probabilistic assessments, a simplified chart is developed for assessing building damage probability caused by excavation, as shown in Figure 3.15.

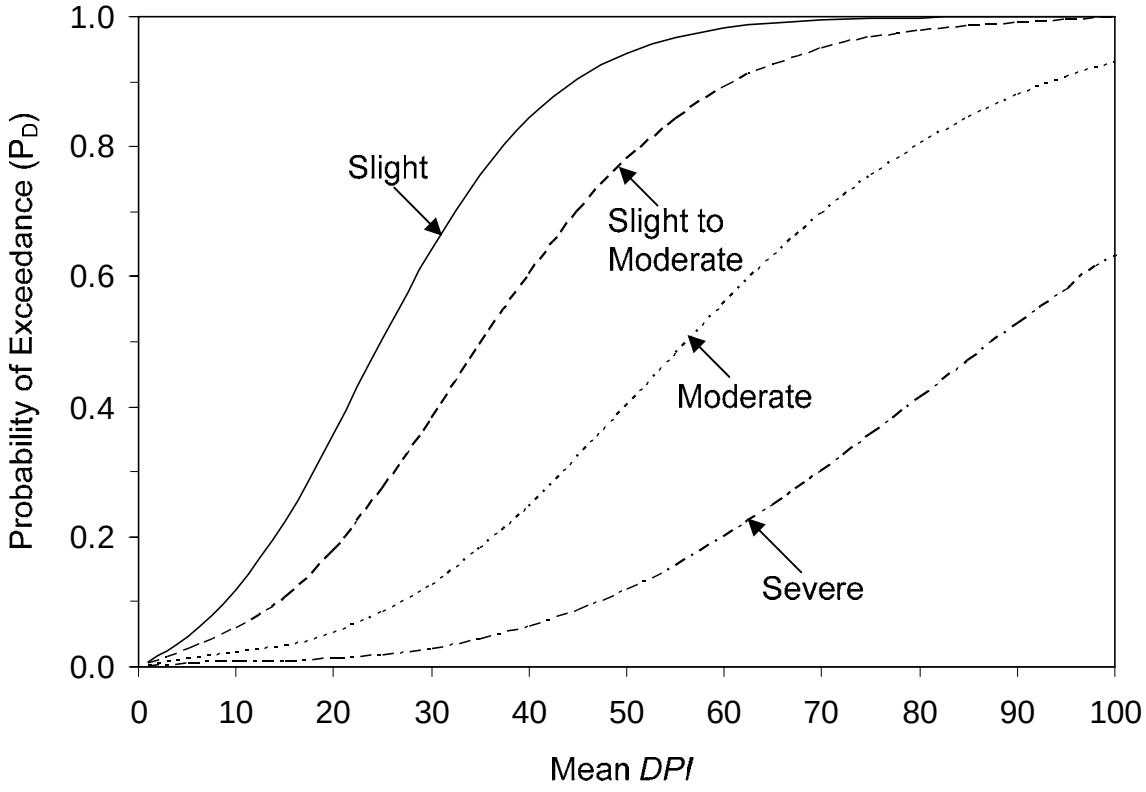

Figure 3.15 Simplified chart for building damage probability caused by excavation

The curves shown in this chart are obtained through repeated analyses of the above probability calculation for various mean *DPI* values at different specified damage levels. From a user's perspective, the probability of sustaining a building damage exceeding a specified level, such as Slight, Slight to moderate, Moderate, or Severe, can be read off the chart with a calculated *DPI* value. For example, entering a mean *DPI* of 18 yields a probability of exceeding "Slight" damage of 30%; the same calculated *DPI* value will suggest a probability of 15% that the damage will exceed "Slight to moderate" damage.

It should be noted that probabilistic analysis facilitated with Figure 3.15 represents only a simplified assessment. In actuality, a fully-probabilistic assessment considers uncertainty in both the loading and the resistance as well as uncertainty in the

input variables required in the *DPI* model. However, the present analysis only considers the model uncertainty in the loading.

Example Application of the Proposed Procedure

In this section, the proposed procedure is demonstrated with a number of numerical case histories from Son and Cording's database (2005) as well as a real-world excavation case history (Ou et al. 1998).

Analysis of Son and Cording (2005) Numerical Cases

To illustrate the application of the proposed procedure, ten randomly selected numerical cases by Son and Cording (2005) are evaluated and the results are shown in Table 3.3. The purpose of this exercise is to show the applicability of the proposed procedure in a deterministic analysis especially for damaged cases.

For these numerical cases analyzed, there is insufficient information to apply the KJHH and KSJH models for estimating the lateral and vertical ground movements. Thus, the analysis is started with the knowledge of the ground slope, differential settlement of the ground, and horizontal strain of the ground. With this information, empirical models (Equations 3.9 and 3.10) are used to determine the angular distortion and lateral strain in the building. Subsequently, the *DPI* is calculated with Equation 3.11 and the damage levels of these cases are assessed based on criteria listed in Table 3.2. As shown in Table 3.3, the damage levels determined with the proposed procedure are generally consistent with the damage levels assessed by Son and Cording (2005). Because steps involving the KJHH and KSJH models are skipped (assuming that in these cases, the ground slope,

Table 3.3 Analysis of Numerical Cases of Son and Cording (2005) with the proposed procedure

Case	EsL^2/GHb	GS (10^{-3})	ΔS (mm)	ε_t	ε_{lg} ($x10^{-3}$)	β ($x10^{-3}$)	ε_l ($x10^{-3}$)	Type of Deformation	*DPI*	Damage based on *DPI*	Damage assessed by Son and Cording
F1-2	3.10	3.03	36.97	0.25	1.13	1.30	1.76	Hogging	40	Moderate	Moderate
F4-2	6.20	3.06	37.33	0.25	1.13	1.68	2.17	Hogging	49	Moderate	Severe
F17-2	6.20	3.08	37.58	0.25	0.00	1.69	1.66	Hogging	40	Moderate	Moderate
F3-2	12.40	3.16	38.55	0.25	1.13	2.13	2.65	Hogging	61	Severe	Severe
F8-3	27.90	3.18	58.19	0.25	0.00	1.68	1.74	Hogging	42	Moderate	Moderate
M10	5.93	4.36	79.79	0.67	1.95	0.21	0.92	Hogging	19	Slight	Slight
F11-3	206.7	3.21	58.74	2.50	1.15	1.57	0.63	Hogging	23	Slight to Moderate	Slight
M4	11.02	5.00	91.50	0.33	1.95	1.81	2.32	Hogging	53	Severe	Severe
M20	5.91	4.36	79.79	0.33	1.60	0.93	1.45	Hogging	32	Moderate	Moderate
F12	12.70	3.23	39.41	0.25	0.00	2.21	2.20	Hogging	53	Severe	Moderate

differential settlement of the ground, and horizontal strain of the ground are accurate as per Son and Cording 2005), the issue of model uncertainty is not considered in this example application.

Taipei, TNEC Case – Building D Adjacent to the Excavation

The Taipei, TNEC case (Ou et al. 1998), involves a 19.7 m excavation for the construction of the Taipei National Enterprise Center (TNEC) building. The damage potential of a nearby four-story building (Building D; see Figure 3.16), which is a frame structure with infill walls, is selected for this demonstration analysis. This building is located in the central part of the long-side diaphragm wall, where the excavation-induced ground responses can be fairly accurately modeled as the plane-strain condition, and its performance observation during the excavation is available (Ou et al. 2000). In this demonstration analysis, the damage potential of this building with four bays in the section

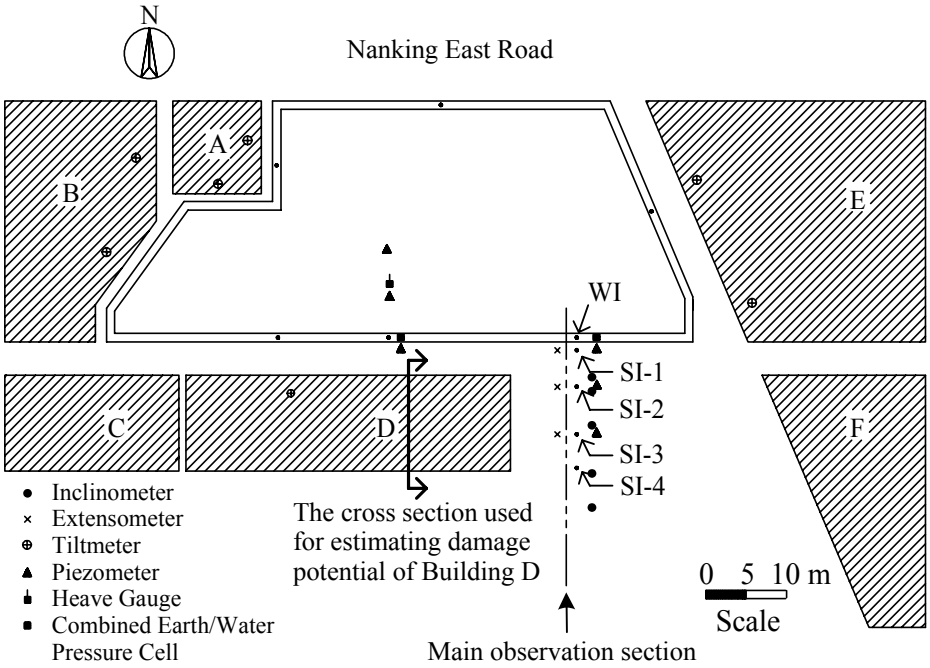

Figure 3.16 Plan view of the TNEC case and the instrumentation plan (Adapted from Ou et al. 1998)

perpendicular to the wall is assessed. The location of the Building D, supported by footing foundations, is 9 m to 31 m away from the diaphragm wall. The damage potential of Building D is analyzed as follows:

Steps 1: Relevant information on the building conditions and excavation data are collected.

***Step 2*:** Determine the required parameters as follows: (1) H_e = 19.7 *m* is determined for the final stage of excavation; (2) *EI* = 1507 $MN/m^2/m$ and h_{avg} = 3.3 m yield $\ln(EI/\gamma_w h_{avg}^4) = 7.166$; (3) *B/2* = 20.6 *m*; (4) $s_u/\sigma'_v = 0.32$ is obtained for this case; (5) $E_i/\sigma'_v = 650$ is obtained based on the results of triaxial tests at strains equal to 10^{-5} (Kung 2003) Thus, δ_{hm} = 96 mm can be obtained using a semi-empirical models presented in Equations 3.1-3.3.

Step 3: Determining additional parameters as follows: $\sum H_{clay} / H_{wall} = 0.87$ can be obtained based on the stratigraphy in this case. With $s_u/\sigma'_v = 0.32$, $E_i/1000\sigma'_v = 0.65$, and $\sum H_{clay} / H_{wall} = 0.87$, R_v = 0.6 (Eq. 3.4) and R_l = 0.45 (Equation 3.8).

Step 4: Based on δ_{hm} = 96 mm, R_v = 0.6, and R_l = 0.45, the maximum ground surface settlement and the maximum lateral movement, δ_{vm} = 58 mm (Equation 3.5) and δ_{lm} = 43 mm (Equation 3.7), can be determined.

Step 5: According to Ou et al. (2000), Building D is supported by spread footings. The depth of the footings is estimated to be in the range of 3 m to 4 m. In this analysis, the depth of 4 m is used.

Step 6: The vertical settlement (Figure 3.3) and lateral movement profiles (Figure 3.7) at the depth of 4 m are constructed and the results are shown in Figure 3.16.

Step 7: Equations 3.9 and 3.10 are used to estimate the angular distortion (β) and lateral strain (ε_l) in Building D for bay Nos. 1, 2, 3 and 4 using GS, ΔS, ε_{lg}, (E_sL^2/GHb), and ε_t obtained from the lateral and vertical ground movement curves and characteristics of the building. Consequently, β is estimated to be 0.00×10^{-3}, 0.82×10^{-3}, 0.82×10^{-3}, and 0.82×10^{-3}, and ε_l is estimated to be 0.00×10^{-3}, 0.22×10^{-3}, 0.71×10^{-3}, and 0.71×10^{-3} for bays Nos. 1, 2, 3 and 4, respectively.

Step 8: With the computed β and ε_l values, the *DPI* for bay Nos. 1, 2, 3 and 4 are determined to be equal to 0, 11, 18, and 18 respectively.

***Step 9*:** As shown in Figure 3.17, bay Nos. 1 to 3 of this building are located in the sagging zone, and bay No. 4 is located in both the sagging and hogging zones. The damage levels of bay Nos. 1 and 2 of the Building D are both negligible to very slight, and the damage levels for bay Nos. 3 and 4 are classified as level 2 (slight) according to

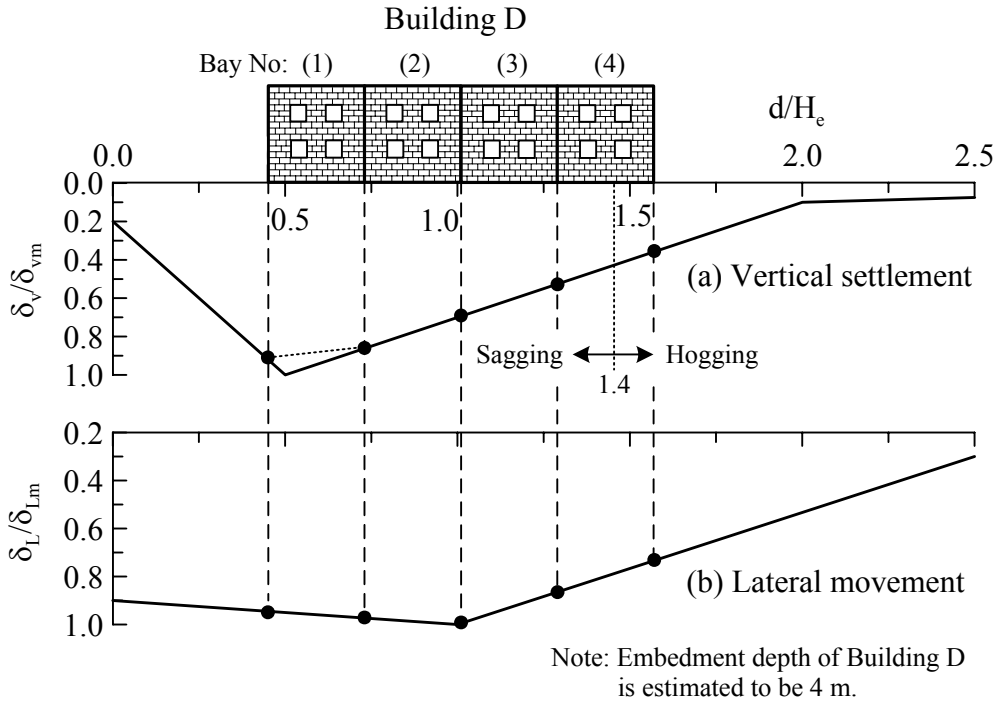

Figure 3.17 Estimated profiles of vertical settlement and lateral movement of the ground for assessing damage potential of Building D in the excavation of TNEC

criteria listed in Table 3.2. The result indicates that the original excavation design is sufficient and no protection measure for Building D would be required.

The above analysis represents a deterministic assessment of damage potential of a building adjacent to an excavation. To demonstrate how the proposed procedure can be used in a probabilistic assessment, the damage potential in Bay No. 4 of the TNEC case history is reassessed. For Bay No. 4 of the TNEC case history, the calculated *DPI* has a mean of $\mu_{DPI} = 18$. Using the chart shown in Figure 3.15, the probability of exceeding "Slight" damage is found to be 30%; the probability of exceeding "Slight to moderate" damage is found to be 15%; and the probabilities of exceeding "Moderate" and "Severe" damages are practically negligible (less than 5% and 1%, respectively).

J.T Liao (2007, personal communication) recalled that there was no change in excavation design in this project, and that no protection scheme was implemented for Building D (presumably no assessment was performed or if an assessment was done, no chance of building damage was judged). Field observations (Liao 1996; Ou et al. 2000) during and after the construction showed that some cracks were found on the internal walls of bay Nos. 3 and 4 in this building; this level of building damage would be characterized as "slight damage" according to the Boscardin and Cording's (1989) evaluation system. The results of the demonstration analysis of Building D during the construction of the TNEC agree well with these field observations.

Summary

In this chapter, a step-by-step procedure for assessing the damage potential of a building adjacent to an excavation, which is illustrated in Figure 3.1, is established. In this procedure, a newly developed evaluation criterion termed *DPI* is established for

evaluating the potential for building damage. The component models that are required in this procedure to calculate the *DPI* are clearly formulated and their model uncertainties are characterized. Furthermore, with the model uncertainties of the component models fully characterized, Equation 3.13 is developed for estimating the model uncertainty of the *DPI* enabling a simplified probabilistic analysis. Subsequently, both deterministic and simplified probabilistic assessments of excavation-induced building damage potential are presented with example applications to demonstrate the applicability of the newly developed procedure.

CHAPTER FOUR

FULLY-PROBABILISTIC APPROACH FOR EVALUATING THE POTENTIAL FOR EXCAVATION-INDUCED BUILDING DAMAGE*

Introduction

With the development of a simplified evaluation procedure in Chapter 3 of this dissertation, the damage potential index (*DPI*) can be adopted as an evaluation criteria for assessing the potential for building damage adjacent to an excavation. Consequently, the building serviceability requirements can be established in terms of *DPI*. In the context of this dissertation, the capacity or *resistance* of the building to damage is referred to herein as the "limiting" *DPI*, while the demand or *load* applied to the building is referred to herein as the "applied" *DPI*. It is noted that the limiting *DPI* may be specified empirically based on the observed building performance data while the applied *DPI* is the *DPI* calculated for a specific case.

In a deterministic analysis, a building is assumed to be undamaged if the applied *DPI* (load) is less than the limiting *DPI* (resistance). On the other hand, if the calculated *DPI* for a specific case exceeds the limiting *DPI*, the violation of serviceability requirements occurs and building damage is said to occur. In reality, both the load and the resistance can be uncertain quantities because of a number of possible sources of uncertainties as demonstrated in Chapters 2 and 3; thus, a more rational approach would be to treat both quantities as random variables and then to assess the potential for excavation-induced building damage with a reliability analysis. Therefore, the purpose of

* A version of this chapter is being prepared for publication; co-authored by Juang, C.H, Schuster, M.J., Ou, C.Y., and Phoon, K.K.

this chapter is to develop a fully-probabilistic framework and procedure for evaluating the excavation-induced building damage considering all of the uncertainty in the analysis.

Previous studies (Zhang and Ng 2005, Hsiao et al 2008) including those presented in Chapters 2 and 3 of this dissertation have contributed to the development of probabilistic analysis for assessing serviceability damage potential of buildings. These studies have adopted previously developed evaluation criteria (Skempton and MacDonald 1956; Polshin and Tokar 1957; Bjerrum 1963; Burland and Wroth 1974; O'Rourke et al. 1976; Boscardin and Cording 1989; Boone 1996; Finno et al. 2005), and generally have focused on either the resistance or loading side of the serviceability limit state equation. However, none of the evaluation criteria have been implemented within the framework of a fully-probabilistic analysis, which considers uncertainty in both the resistance and loading side.

In this chapter, the deterministic procedure developed in Chapter 3 is adopted as a basis for a fully probabilistic analysis using the *DPI* criterion. Furthermore, contrary to the reliability analyses presented in Chapters 2 and 3 of this dissertation, the fully-probabilistic procedure within this chapter considers the uncertainty of both the applied *DPI* (load) and the limiting *DPI* (resistance). Specifically, both the parameter and model uncertainty of the *DPI*-based limit state, in both the resistance side and loading side, are fully characterized and incorporated into the reliability analysis. A step-by-step procedure for performing a fully-probabilistic analysis of building damage potential is established and implemented in an engineering tool such as Excel. The versatility of the developed framework is illustrated with a well-documented case history. A sensitivity analysis is further conducted to examine the influence of individual input parameters, and

the effect of the various assumptions, on the calculated probability of building damage caused by an excavation.

DPI-based Serviceability Limit State

To assess the potential for the excavation-induced building damage using the *DPI* as a basis, a serviceability limit state is formulated as:

$$g(x) = DPI_R - DPI_L \tag{4.1}$$

where DPI_R is the limiting *DPI* (resistance); DPI_L is the applied *DPI* (load); and x is the vector of variables that determine DPI_R and DPI_L. As noted previously, the DPI_R may be specified empirically based on the observed building performance data while the DPI_L is the *DPI* calculated for a specific case. In a deterministic analysis, building damage occurs when $g(x) < 0$.

In this section, the parameter and model uncertainty of DPI_R and DPI_L are characterized. It should be noted that the *DPI* calculated with the procedure presented in Chapter 3 represents the applied *DPI* (DPI_L) in the limit state (Equation 4.1). Possible uncertainty in the required input parameters and the uncertainty associated with the entire procedure are the reason the applied *DPI* (DPI_L) should be treated as a random variable.

Parameter and Model Uncertainties in the Applied *DPI*

To determine the parameter uncertainty for the applied *DPI*, the input parameters (i.e. H_e, $B/2, EI/\gamma_w h_{avg}^4$, $\sum H_{clay}/H_{wall}$ s_u/σ'_v, E_i/σ'_v, etc.), that are required for computing the *DPI* must be assessed for a given case. In particular, the mean and standard deviation for each input parameter must be determined along with the

distribution type. In a previous study, Hsiao et al. (2008) found that it is reasonable to assume normal distribution for each parameter in the analysis of excavation-induced building damage potential. The standard deviation of each input parameter may be estimated based on data collected for a specific case or published coefficients of variation, and guidance is available for such estimate (Duncan 2000). When there is doubt, sensitivity analysis to determine the effect of any assumptions made about the parameter uncertainty should be investigated. This approach is taken in the present study.

To simplify the fully-probabilistic analysis based on the limit state defined in Equation 4.1, the uncertainties associated with all intermediate calculation steps leading to the evaluation of the applied *DPI* are combined. In other words, the entire calculation process presented in Chapter 3 is treated as a model and the uncertainty of this model is assessed in a single quantity. Symbolically, the applied *DPI*, which is denoted as DPI_L in Equation 4.1, is expressed as:

$$DPI_L = c_2 \, DPI \tag{4.2}$$

where *DPI* is the computed damage potential index based on the procedure presented in Chapter 3, and c_2 is a model bias factor (in terms of μ_{c_2} and COV_{c_2}) to account for the uncertainty in the entire process of computing *DPI*.

Based on their uncertainty propagation analysis using Duncan's first order second moment (FOSM) analysis presented in Chapter 3, the standard deviation of the computed *DPI*, denoted as σ_{DPI}, can be estimated with the Equation 3.13. Additionally, the computed *DPI* for a given case using the best estimate (or mean) value for each and every

input parameter can be treated as the mean value of DPI_L. Thus, the mean value of the model bias factor, denoted as μ_{c_2}, can reasonably assumed to be μ_{c_2} = 1.0 [note: the results of sensitivity analysis with ranging from 0.9 to 1.1 further supports this claim]. The coefficient of variation of c_2, denoted as COV_{c_2}, can be determined for a given case, since both the mean value of DPI_L and σ_{DPI} can be calculated. Based on curve-fitting of the *COVs* computed for each of the 124 cases in the database originally presented in Chapter 3, the following empirical equation is established (Figure 4.1 shows the scatter of curve-fitting):

$$COV_{c_2} = 0.32 + 11/DPI \tag{4.3}$$

Thus, the model bias factor c_2 is statistically characterized. For the present analysis, the model bias factor is assumed to follow a lognormal distribution (Phoon and Kulhawy 2005), although the normal distribution can also be used.

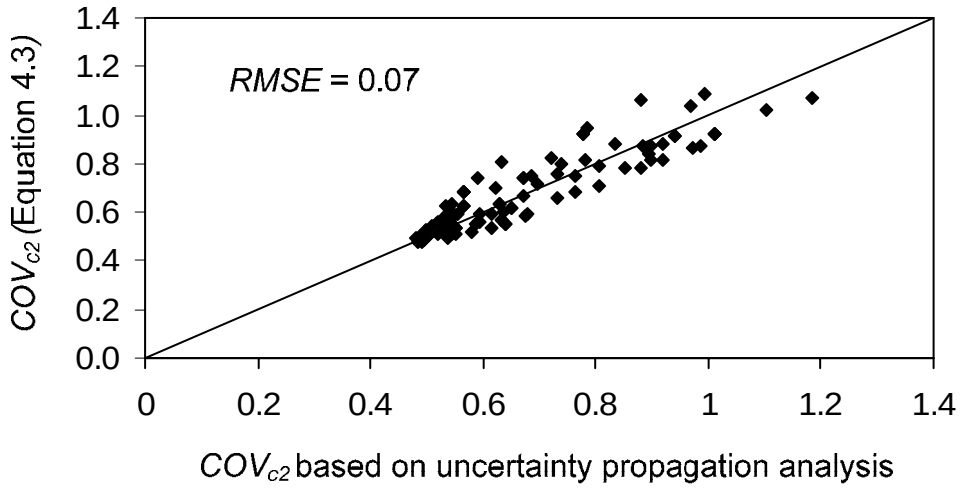

Figure 4.1 Scatter of the curve-fitting for COV_{c_2} (Equation 4.3)

Uncertainty of the Limiting *DPI*

The resistance DPI_R in Equation 4.1 is the limiting *DPI*. As noted previously, the DPI_R may be specified empirically based on the observed building performance data. In fact, in Chapter 2 of the dissertation, a limiting principal strain of 1.19×10^{-3} was established for building damage evaluation based on the database developed by Son and Cording (2005). The significance of this limiting principal strain ε_p of 1.19×10^{-3} is that a building is likely to experience damage that exceeds the "slight damage" level, if the computed principal strain exceeds that level. As defined previously in Chapter 2, a building that undergoes "moderate", "severe", and "very severe" damage is considered intolerable and one that undergoes "negligible", "very slight", and "slight" damage is classified as "tolerable". Thus, a building that sustains a damage that exceeds the "slight damage" level is classified as "intolerable." It should be noted that the bracket $(\varepsilon_l \times (\cos\theta_{\max})^2 + \beta \sin\theta_{\max}\cos\theta_{\max})$ in Equation 2.1a is the principal tensile strain (ε_p) originally defined by Son and Cording (2005). Thus, the variable $DPI = [20\times10^3(\varepsilon_p)]$, can be thought of being a "normalized" principal strain and will assume the probability distribution properties of ε_p. Taking $\varepsilon_p = 1.19\times10^{-3}$, the limiting *DPI* will be: $DPI_R = 20\times10^3(1.19\times10^{-3}) = 23.8$. Because $\varepsilon_p = 1.19\times10^{-3}$ was determined empirically from observed performance data and with the assumption that building damage exceeding the "slight damage" level is intolerable, the uncertainty exists in this limiting principal strain and the resulting DPI_R should be more appropriately treated as a random variable. Similar to the expression of DPI_L in Equation 4.2, the limiting *DPI* may be expressed as:

$$DPI_R = 23.8\ (c_1) \tag{4.4}$$

Unlike the DPI_L, which is case specific, the DPI_R model expressed in Equation 4.4 does not involve the input parameters, as it is the general evaluation criterion that is applicable to all cases. Hence, only the model uncertainty, represented by the model bias factor c_1, needs to be characterized.

Since the DPI_R follows the probability distribution of ε_p, the model bias factor c_1 characterized in Chapter 2 of this dissertation using the database developed by Son and Cording (2005) is readily applicable for computing DPI_R. Thus, the mean and the *COV* of this model bias factor, denoted as μ_{c_1} and COV_{c_1} respectively, can be estimated with Equations 2.12 and 2.14.

It should be noted that Equations 2.12 and 2.14 are dependent on *r*, the prior probability ratio [*P(D)*/*P(ND)*] where *P*(*D*) is prior probability of building damage and *P*(*ND*) is prior probability of no building damage of a given case. Since there is a lack of knowledge as to what *r* should be for a future case, the iterative procedure presented in Chapter 2 and illustrated in Figure 2.7 can be utilized. In the present study, this iterative approach is incorporated into the proposed fully probabilistic procedure (see Figure 4.2).

Revised Serviceability Limit State

Based on the previous discussions, the serviceability limit state expressed in Equation 4.1 can be re-written as:

$$g(x) = (23.8)(c_1) - (DPI)(c_2) \tag{4.5}$$

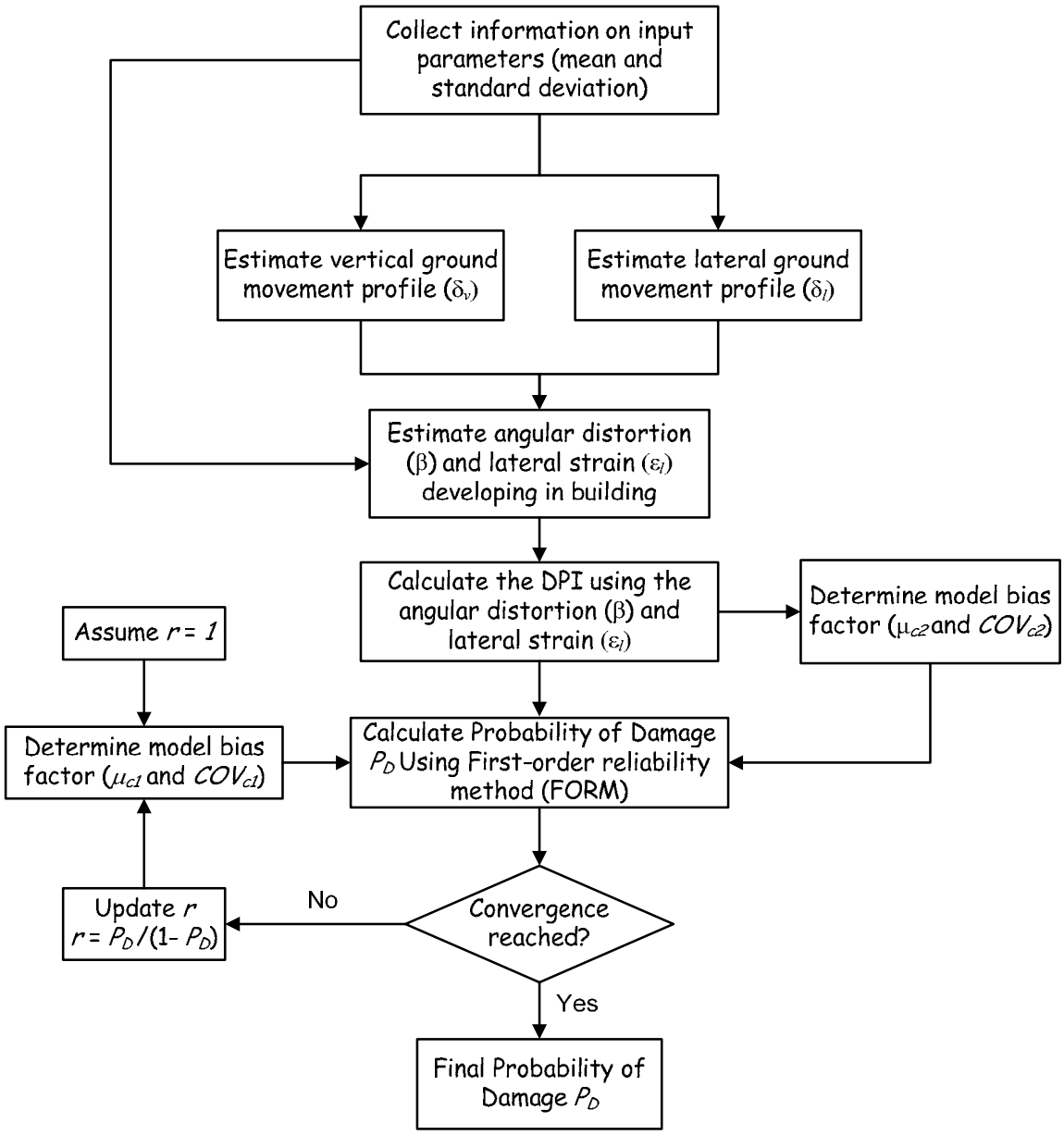

Figure 4.2 Fully-probabilistic procedure for evaluating the potential for excavation-induced building damage

In Equation 4.5, the variables c_1 and c_2 represent the respective model bias factors that have been characterized; the variable *DPI* is the quantity computed based on the input parameters for a specific case following the procedure described previously in Chapter 3. The computed *DPI* is treated as a random variable to account for the uncertainty in the input parameters.

In summary, a serviceability limit state has been established and expressed in Equation 4.5 and all uncertainties, associated with either input parameters or models, have been fully characterized. Reliability analysis using routine techniques such as the first order reliability method (FORM) can readily be performed to determine the probability of building damage caused by an excavation. This is the probability that the building will suffer an intolerable damage, as defined previously.

Fully-probabilistic Analysis of Excavation-induced Building Damage

Procedure for Fully-probabilistic Analysis

In reference to Figure 4.2, the proposed framework for fully-probabilistic analysis of excavation-induced building damage potential is summarized in a step-by-step procedure as follows:

(a) Obtain the mean values and *COVs* (or standard deviations) for all input variables necessary for the calculation of the applied *DPI* presented in Chapter 3. For estimating the mean and *COVs* of the soil parameters, the published literature (for example, Duncan 2000) can be used as a guide when no or inadequate data are available. For the example application presented later in this paper, the small-strain (10^{-5}) triaxial tests conducted by Kung (2003) are used to determine the

mean and *COV* of the soil parameters. The mean values for the non-soil parameters can be determined from the design specifications for an excavation. For the example application presented later, the *COVs* of the non-soil parameters are assumed to be 0.05 as suggested by Hsiao et al. (2008), but this assumption is further investigated with sensitivity analysis.

(b) Calculate the maximum vertical and lateral ground movements with Equations 3.1-3.8 and develop the vertical and lateral ground movement profiles based on Figures 3.3 and 3.7.

(c) Determine the angular distortion and lateral strain in the building using Equations 3.9 and 3.10. Subsequently, calculate the "applied" *DPI* based on Equation 3.11.

(d) Characterize the model bias factor c_2 by taking $\mu_{c_2} = 1$ and computing COV_{c_2} with Equation 4.3.

(e) Initially assume prior probability ratio $r = 1$, and characterize the model bias factor c_1 by computing μ_{c_1} and COV_{c_1} with Equations 2.12 and 2.14.

(f) Perform a reliability analysis with the limit state defined in Equation 4.5 using the first order reliability method (FORM) to obtain the reliability index (Hasofer and Lind 1974, Ang and Tang 1984, Baecher and Christian, 2003) and the probability of damage (P_D).

(g) Update the prior probability ratio *r* based on the calculated probability of damage (i.e. $r = P_D/(1-P_D)$). Then repeat Steps 5, 6, and 7 until the probability of damage converges.

Example Application - Taipei National Enterprise Center (TNEC) case

To illustrate the developed fully-probabilistic analysis framework and procedure, the TNEC case documented by Ou et al. (1998, 2000) and utilized in Chapter 3 is reanalyzed. The soil conditions at the TNEC site are typical of the Taipei basin with a thick alluvium deposit (Sungshan Formation) overlain by a gravel deposit (Chingmei Formation) where the hard stratum is at a depth of 46 m (Kung et al. 2007). The Sungshan Formation is predominantly a slightly overconsolidated soft to medium clay with low plasticity. An analysis of the soil properties at the TNEC site reveals that s_u/σ'_v and E_i/s_u are slightly correlated ($\rho = 0.3$) and can be characterized with mean values of 0.31 and 650, respectively and the coefficients of variation (*COV*) for both parameters are 0.16, as shown in Table 4.1.

Table 4.1 Mean values of input parameters TNEC case history

Factor	Excavation sequence (Stage No.)				
	3	4	5	6	7
Depth, H_e (m)	8.6	11.8	15.2	17.3	19.7
System stiffness, $EI/\gamma_w h_{avg}^4$	1023	966	1109	1115	1294

- Mean of other input parameters for predicting ground movement profiles: $B/2$ = 20.6 m, s_u/σ'_v = 0.25 and E_i/σ'_v = 500, $\sum H_{clay}H_{wall}$ = 0.87, T = (46 - H_e) m, and embedment depth (D) = 4 m.
- Characteristics of Critical Building Section: d_1 = 25.5 m and d_2 = 31.0 m from edge of excavation, embedment depth (D) = 4 m, (E_sL^2/GHb) =15, and ε_t = 0.9.
- *COV*s of s_u/σ'_v and E_i/σ'_v = 0.16
- *COV*s of B, $\sum H_{clay}H_{wall}$, T, D, E_sL^2/GHb, and ε_t = 0.05
- Coefficient of correlation between s_u/σ'_v and E_i/σ'_v = 0.3

Figure 4.3 illustrates the design of the braced excavation at the TNEC site and Figure 4.4 shows the location of the building adjacent to this excavation that is to be assessed for its damage potential. As shown in Figure 4.3, the excavation width is equal to 41.2 m and supported by a diaphragm wall that is 0.9 m thick and 35 m deep. The excavation was performed in seven stages, and the excavation depths and system stiffnesses for Stages 3 through 7 are summarized in Table 4.1. It should be noted that the vertical and lateral ground movements for Stages 1 and 2 are negligible, which leads to negligible probabilities of damage at Building D (Figure 4.4). The mean and *COV* values of all other input parameters related to the design of the excavation, including $B/2$, $\sum H_{clay} H_{wall}$, T, and embedment depth (D), are listed in Table 4.1.

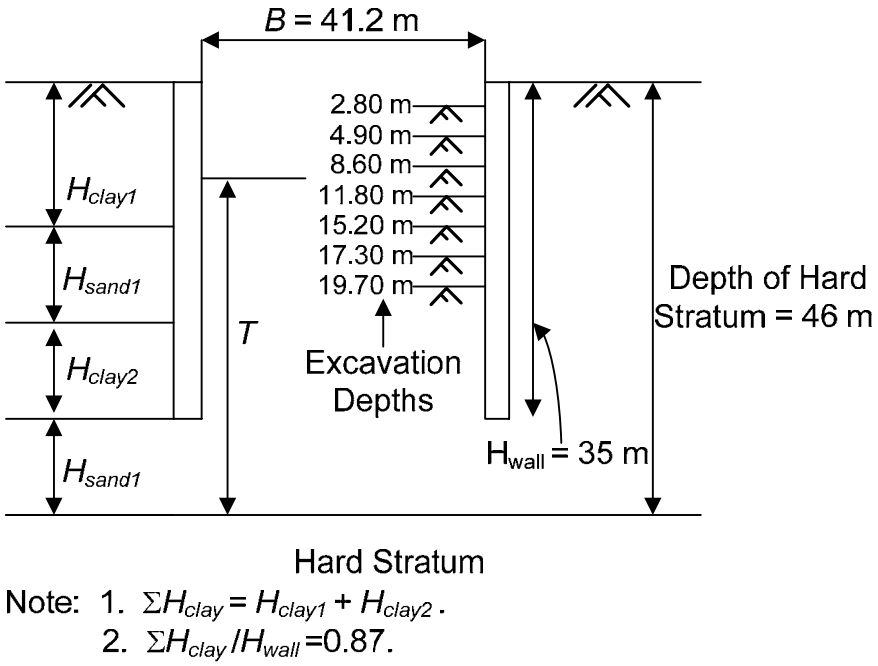

Figure 4.3 Design of Braced Excavation for TNEC case

As shown in Figure 4.4, Building D is located perpendicular to the excavation with the front and back of the building spanning a distance of 9 m to 31 m from the excavation. Building D is a four-story frame structure with infill walls that can be divided into 4 bays each supported by footing foundations with embedment depths of 4 m. The bay spanning from d_1 = 25.5 to d_2 = 31 m has been identified as the critical bay; slight damage was observed after the excavation (Liao 1996; Ou et al. 2000). Based on the description of Building D, the critical cracking strain ε_t and the soil structure stiffness ratio E_sL^2/GHb are estimated to be 0.9 and 15 respectively, as shown in Table 4.1. The *COV*s of the non-soil parameters are assumed to be 0.05 (Hsiao et al. 2008).

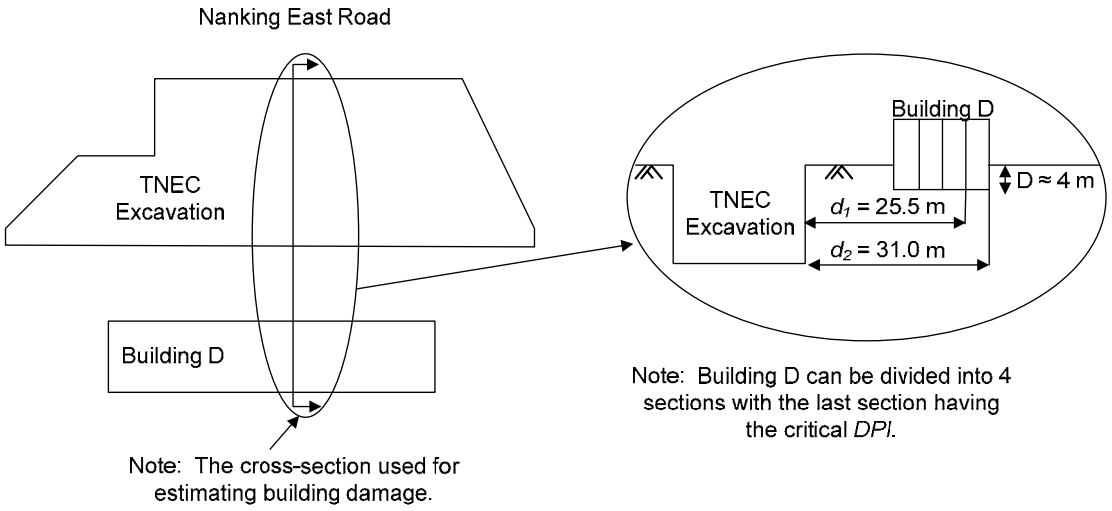

Figure 4.4 Location of Excavation and Building D in TNEC case

The procedure for fully probabilistic analysis presented previously is followed. Specifically, reliability analysis using FORM is conducted. Figure 4.5 shows a spreadsheet implementation (after Low 1997, Phoon 2004) of the FORM analysis for this

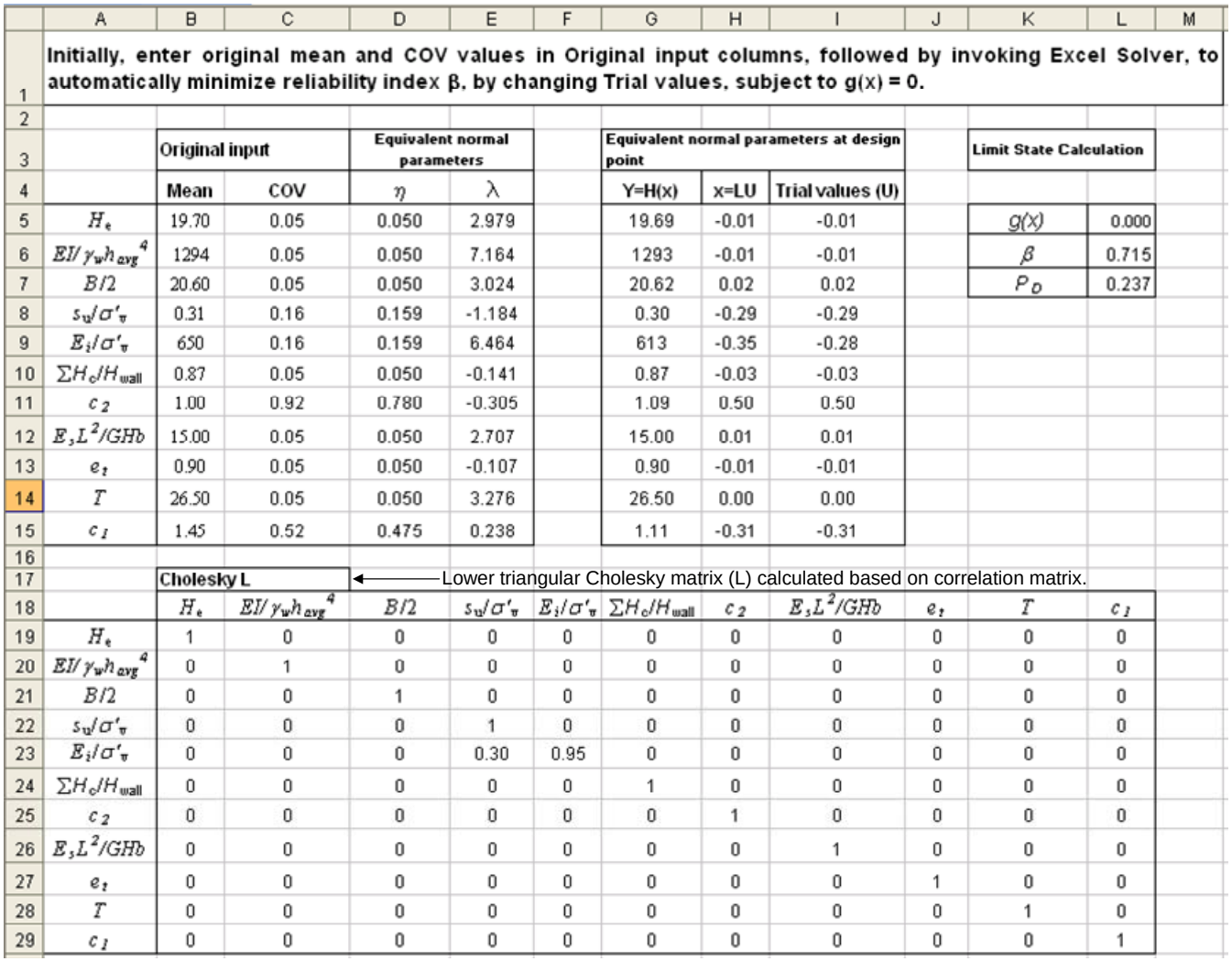

Initially, enter original mean and COV values in Original input columns, followed by invoking Excel Solver, to automatically minimize reliability index β, by changing Trial values, subject to g(x) = 0.

	Original input		Equivalent normal parameters		Equivalent normal parameters at design point			Limit State Calculation	
	Mean	COV	η	λ	Y=H(x)	x=LU	Trial values (U)		
H_e	19.70	0.05	0.050	2.979	19.69	-0.01	-0.01	$g(x)$	0.000
$EI/\gamma_w h_{avg}^4$	1294	0.05	0.050	7.164	1293	-0.01	-0.01	β	0.715
$B/2$	20.60	0.05	0.050	3.024	20.62	0.02	0.02	P_D	0.237
s_u/σ'_v	0.31	0.16	0.159	-1.184	0.30	-0.29	-0.29		
E_i/σ'_v	650	0.16	0.159	6.464	613	-0.35	-0.28		
$\Sigma H_c/H_{wall}$	0.87	0.05	0.050	-0.141	0.87	-0.03	-0.03		
c_2	1.00	0.92	0.780	-0.305	1.09	0.50	0.50		
$E_s L^2/GHb$	15.00	0.05	0.050	2.707	15.00	0.01	0.01		
e_t	0.90	0.05	0.050	-0.107	0.90	-0.01	-0.01		
T	26.50	0.05	0.050	3.276	26.50	0.00	0.00		
c_1	1.45	0.52	0.475	0.238	1.11	-0.31	-0.31		

Cholesky L ← Lower triangular Cholesky matrix (L) calculated based on correlation matrix.

	H_e	$EI/\gamma_w h_{avg}^4$	$B/2$	s_u/σ'_v	E_i/σ'_v	$\Sigma H_c/H_{wall}$	c_2	$E_s L^2/GHb$	e_t	T	c_1
H_e	1	0	0	0	0	0	0	0	0	0	0
$EI/\gamma_w h_{avg}^4$	0	1	0	0	0	0	0	0	0	0	0
$B/2$	0	0	1	0	0	0	0	0	0	0	0
s_u/σ'_v	0	0	0	1	0	0	0	0	0	0	0
E_i/σ'_v	0	0	0	0.30	0.95	0	0	0	0	0	0
$\Sigma H_c/H_{wall}$	0	0	0	0	0	1	0	0	0	0	0
c_2	0	0	0	0	0	0	1	0	0	0	0
$E_s L^2/GHb$	0	0	0	0	0	0	0	1	0	0	0
e_t	0	0	0	0	0	0	0	0	1	0	0
T	0	0	0	0	0	0	0	0	0	1	0
c_1	0	0	0	0	0	0	0	0	0	0	1

Figure 4.5 The proposed reliability-based procedure in a spreadsheet

case, and Figure 4.6 shows the results of the computed probability of damage of Building D at various excavation stages and the corresponding depths.

To illustrate how the iterative procedure works, the convergence of the computed probability of damage at Stage 7 is used as an example and the results are shown in Figure 4.7. In this case, as well as in most other cases, it took only a few iterations to converge. Furthermore, to provide a comparison, the results obtained using the non-iterative approach, in which the parameter r is assumed to be 1.0 in Equations 2.12 and 2.14, are also shown in Figure 4.6. As shown in Figure 4.6, at each excavation stage, the probability of damage P_D obtained with the iterative procedure is slightly lower than that obtained with the non-iterative approach. Considering that the damage level of Building

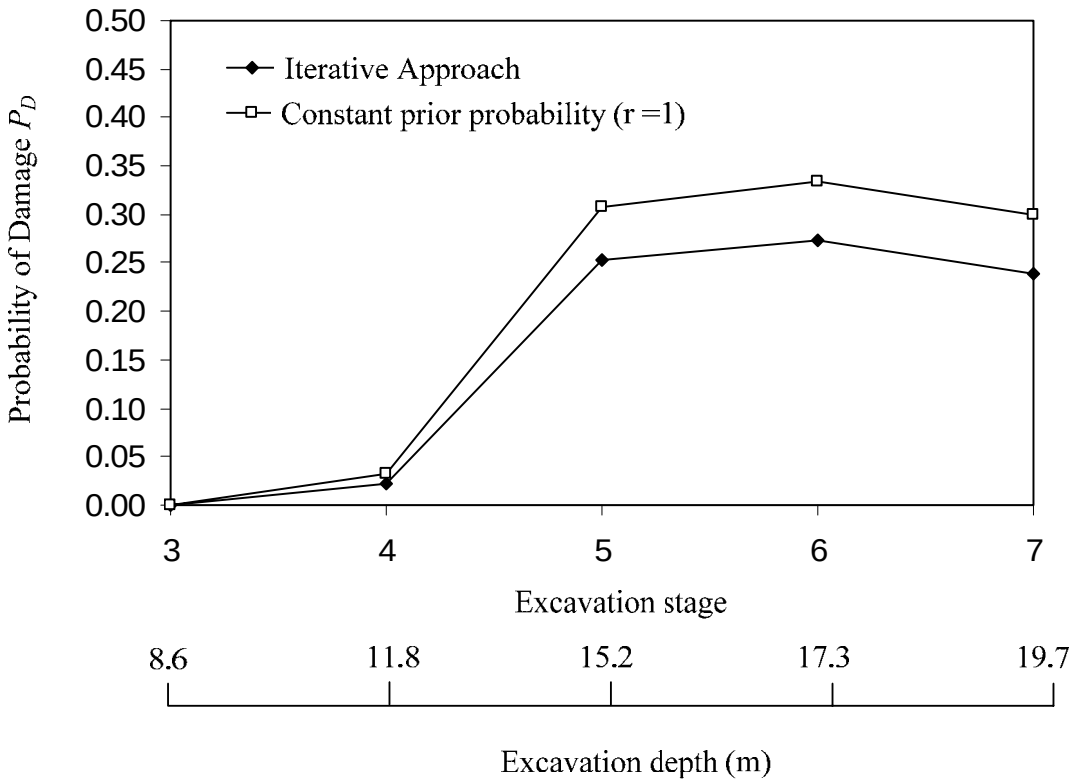

Figure 4.6 Estimated Probability of Damage to Building D

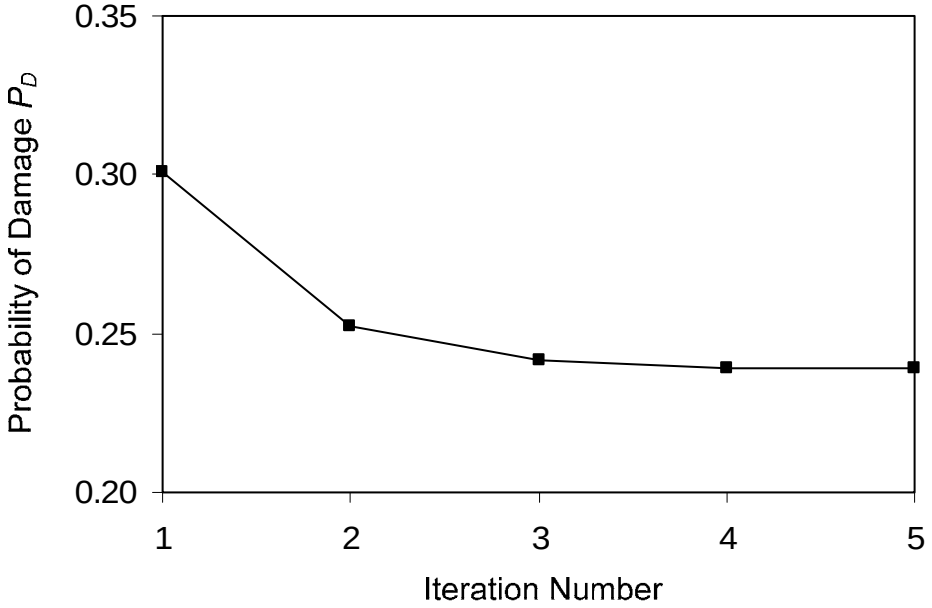

Figure 4.7 Probability of damage to Building D at Stage 7

D is characterized through field observations as "slight damage" and "tolerable," lower probabilities obtained with the iterative procedure are considered more accurate. However, the difference between the two approaches is quite small and the results are quite comparable in terms of the magnitude and the overall trend; thusly, it is not unreasonable to assume $r = 1$ for a simplified solution. Nevertheless, the reader is cautioned that the iterative procedure can have a more significant effect, depending on the case analyzed, as evidenced by the results presented in Chapter 2.

Figure 4.6 also shows that the probability of damage to Building D is negligible at Stages 3 and 4; and as excavation proceeds and the excavation depth increases, this probability is increased, and at the depths corresponding to Stages 5, 6, and 7 (the final stage), the probability is approximately equal to 0.25. Recalling that the probability of damage is the probability that damage will be intolerable (exceeding slight damage), a

probability of damage of 0.25 implies that Building D is unlikely to exceed slight damage and will more likely incur slight damage or less as a result of the excavation. This result is quite consistent with field observation of slight damage in only one portion of Building D.

Finally, although not shown herein, it should be noted that the effect of assuming μ_{c_2} = 1.0 on the probability of damage was examined by varying μ_{c_2} between 0.9 and 1.1 in a sensitivity analysis. Practically the same probabilities of damage were obtained in this case for all values of μ_{c_2} analyzed.

Significance of Fully-Probabilistic Approach

To illustrate the significance of the fully-probabilistic approach, Building D of the TNEC case is reevaluated at Stage 7 of excavation with the inclusion of only specific sources of uncertainty. As shown in Table 4.2, Stage 7 of excavation was reevaluated with five different scenarios of parameter and model uncertainty. As a reference, a deterministic analysis was conducted and no uncertainty was included. For all other analyses, only specific sources of uncertainty are included in the probabilistic analyses. Based on the result of the deterministic analysis, the *DPI* = 18, and according to the deterministic evaluation criteria established in Chapter 3, the probability of damage (in the context of this paper, the probability of exceeding the slight damage) will be zero, as *DPI* > 20 is required for this condition. With model and/or parameter uncertainty included in the analysis, different probabilities are obtained in this case for different uncertainty scenarios even with the same *DPI* value. Thusly, it is to the advantage of the

engineer to perform a fully probabilistic assessment whenever possible. Even if the parameter uncertainty cannot be ascertained, it would be better off to perform some sensitivity analysis with different assumed *COVs* to gain additional insight for making better engineering decisions.

Table 4.2 Analysis of the TNEC case history (Building D) with different scenarios of parameter and model uncertainties

Scenario	Constraint for the Analysis	DPI	Probability of Damage
1	Deterministic – no uncertainty	18	N/A*
2	Only model uncertainty c_1	18	0.13
3	Only model uncertainty c_1 and c_2	18	0.18
4	Fully-probabilistic (all uncertainties included; *COV*s of s_u/σ'_v and $E_i/\sigma'_v = 0.16$)	18	0.25
5	Fully-probabilistic (all uncertainties included; *COV*s of s_u/σ'_v and $E_i/\sigma'_v = 0.40$)	18	0.37

*In a deterministic analysis, the probability is either 1 or 0. Based on the deterministic evaluation criteria presented in Chapter 3, exceeding the "slight damage" requires that DPI > 20. Thus, this probability may be assessed to be 0.

The fully probabilistic analysis can easily be implemented in a spreadsheet, and in fact, a spreadsheet that implements the proposed methodology (Figure 4.5) is available from the dissertation author upon request. Nevertheless, to further facilitate the use of the

proposed methodology, additional simplified evaluation charts are prepared and presented below.

Simplified Charts for Assessing the Probability of Damage

To develop the simplified charts, only the model uncertainty is included in the probabilistic analysis since the parameter uncertainty is case specific. In other words, the charts are based on the results of the analysis referred to as Scenario 3 shown in Table 4.2. Thus, the results obtained from the simplified charts will be most accurate if the *COVs* of the input parameters are low. A concerted effort on the part of the user will be required to accurately assess the input parameters. Alternatively but less desirably, the user could perform a "what if" analysis to gauge the variation in the estimated probability of damage by varying the results of the deterministic solution.

Previously, Boscardin and Cording (1989) and Son and Cording (2005) have developed deterministic evaluation charts. To show the transition, a new chart similar to these previous charts is first developed, as shown in Figure 4.8. This chart shows a family of probability curves (or contours), in which the probability is obtained with the proposed framework by considering the model uncertainty but not parameter uncertainty. The data points shown in this chart are those compiled by Son and Cording (2005) but only two damage classes (tolerable and intolerable) are identified. Again, the probability of damage here is referred to the probability of exceeding the slight damage level. The obtained probability of damage relates quite well with the damage data points, as cases with intolerable damage generally have high probabilities of damage while those with tolerable damage generally have low probabilities of damage.

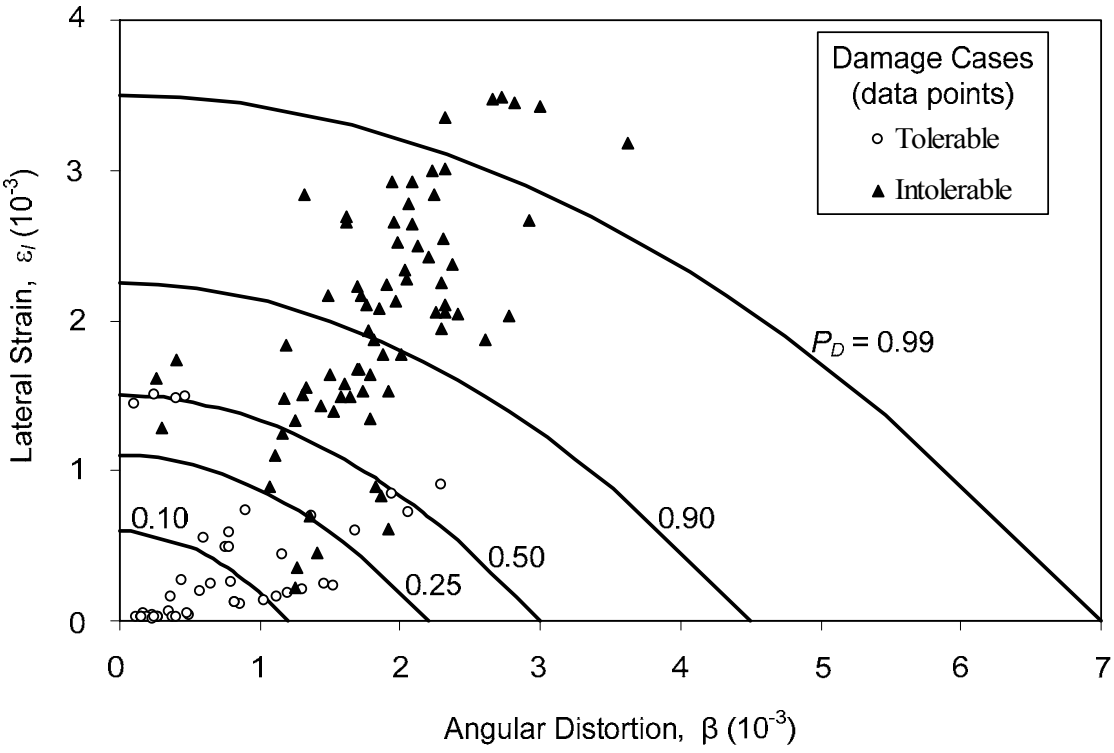

Figure 4.8 Probability-based Simplified Evaluation Chart

Although the probability contour presented in Figure 4.8 is useful, an improved simplified chart can be created. Figure 4.9 shows a simplified chart where the probability of damage can be read out directly for a given *DPI*. For the TNEC case, the building D is assessed with *DPI* = 18 (with considering the parameter uncertainty). Using Figure 4.9, the probability of damage is found to be 0.18, which is the same as the solution listed in Table 4.2 for the analysis scenario that considers only model uncertainty. Obviously, this chart, like the one shown in Figure 4.8, is developed considering only the model uncertainty. Therefore, a concerted effort on the part of the user must be made to accurately assess the input parameters in order to derive an accurate estimate of the probability of building damage.

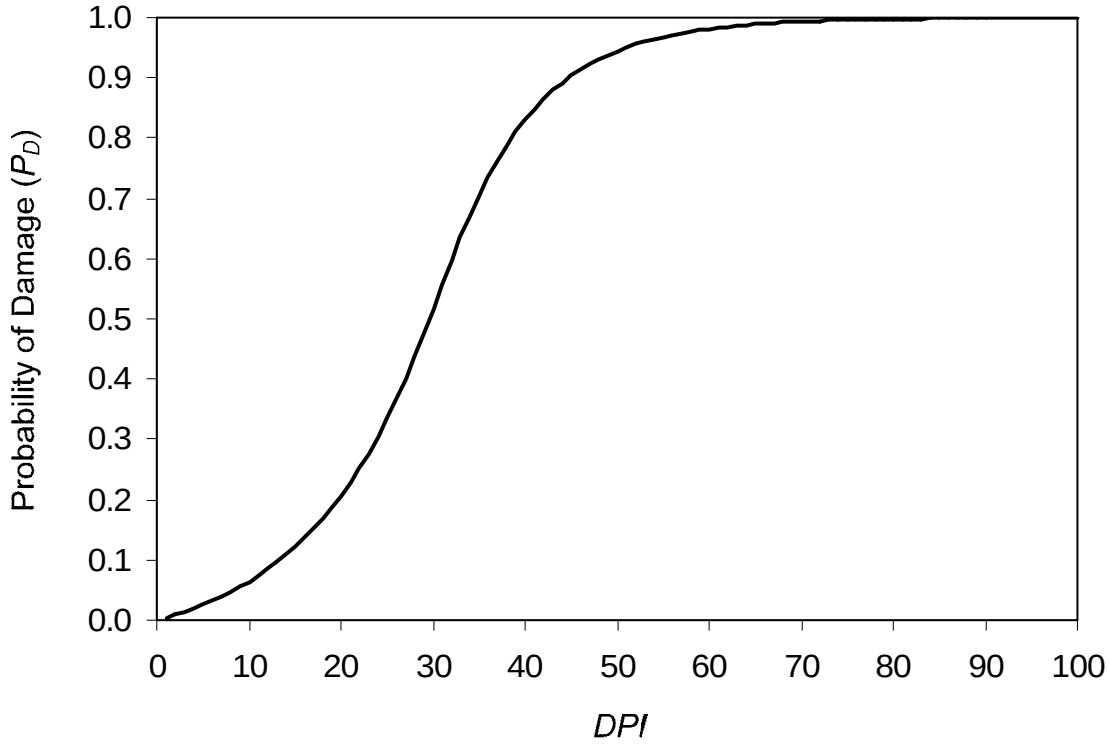

Figure 4.9 DPI-based Simplified Probabilistic Assessment Chart

Sensitivity Analysis

Using the TNEC case history previously analyzed, a "gamma" sensitivity analysis (Der Kiureghian and Ke 1985) is first performed to determine the sensitivity of the computed probability of damage to each of the various input variables, from which the relative importance of each of the input parameters is assessed. Additionally, the effects of the various assumptions about the input parameters on the resultant probability of damage are analyzed.

Gamma Sensitivity Index

The gamma sensitivity index is expressed as (Der Kiureghian and Ke 1985):

$$\gamma_i = \frac{\left|\alpha J_{y,x} D\right|}{\| \alpha J_{y,x} D \|} \tag{4.6}$$

where γ_i is the gamma sensitivity index for each of the parameters considered in the reliability analysis, including model bias factors; α is directional cosine at the design point in the original random variable space; $J_{y,x}$ is the Jacobian matrix of elements $\frac{\partial y}{\partial x}$ with $y = T(x)$ and $T(.)$ being an orthogonal transformation function; y_i are uncorrelated standard normal random variables; and D is the diagonal matrix of the standard deviation of each parameter x_i. These parameters include $x_1 = H_e$, $x_2 = EI/\gamma_w h_{avg}^4$ (or S for short), $x_3 = B/2$, $x_4 = s_u/\sigma'_v$, $x_5 = E_i/\sigma'_v$, $x_6 = \sum H_{clay}/H_{wall}$, $x_7 = c_2$, $x_8 = E_s L^2/GHb$, $x_9 = \varepsilon_t$, $x_{10} = T$, and $x_{11} = c_1$.

Once the probability of damage is calculated with the FORM analysis, Equation 4.6 can be used to calculate the gamma sensitivity index of each parameter. Since the gamma sensitivity index measures the relative contribution of each parameter to the probability of damage, the probability of damage is most sensitive to the parameters with the highest gamma sensitivity indices.

The gamma sensitivity index for each parameter is shown in Figure 4.10. The model bias factor c_2 is found to be the most important among all parameters, followed by the model bias factor c_1, and the two normalized soil parameters s_u/σ'_v and E_i/σ'_v. The

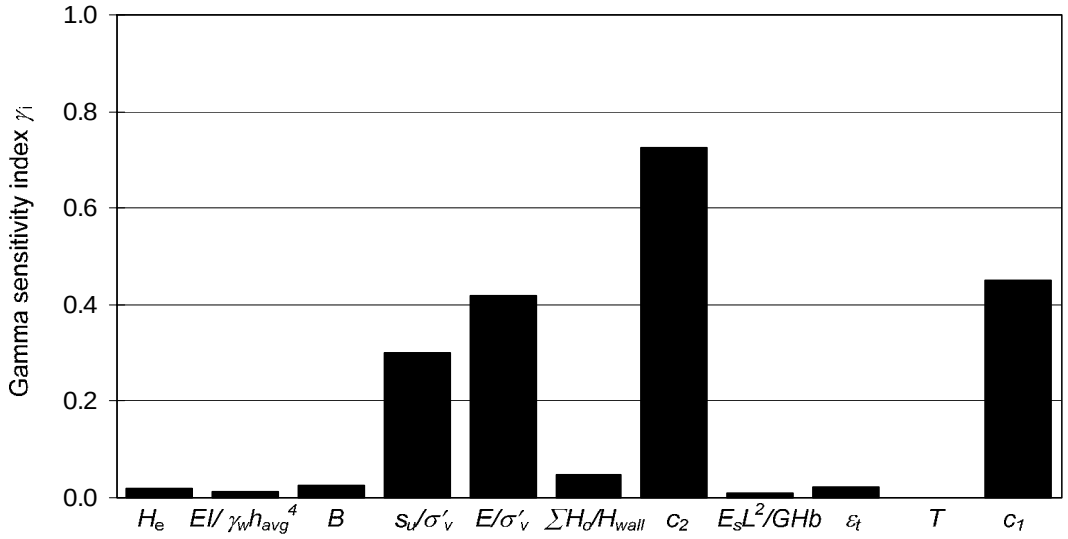

Figure 4.10 Sensitivity Index of Input Parameters

probability of damage is found to be much less sensitive to all other parameters. The highest influence of the two bias factors is obvious, as they are applied directly to the limiting *DPI* and the applied *DPI*. The higher influence of the two normalized soil parameters and the lower influence of the non-soil parameters confirm the findings of the previous reliability study by Hsiao et al. (2008).

To see if the importance of the non-soil parameters would increase if the *COV* was assumed to be a higher value, the probability of damage and gamma sensitivity indices for the TNEC case were recalculated under the assumption that the *COV* of the non-soil parameters was equal to 0.10 and 0.20. However, practically the same results were obtained with these two *COV* assumptions.

The results and discussions presented previously underline the importance of properly characterizing the soil parameters. Thus, it would be of interest to further examine the effect of assuming different levels of the soil parameters uncertainty on the

computed probability of damage. These additional sensitivity analyses are presented in the sub-section that follows.

Additional Sensitivity Analyses Focusing on Soil Parameters

By repeating the sensitivity analysis reported in Figure 4.10 with different uncertainty levels for the parameter s_u/σ'_v [ranging from COV = 0.1 to 0.6], the effect of the uncertainty in this soil parameter on its relative contribution to the probability of damage can be evaluated, and thusly, the importance of this parameter can be assessed. The results are summarized in Figure 4.11, which shows that as the COV of s_u/σ'_v increases, the sensitivity of the probability of damage to this parameter also increases. In

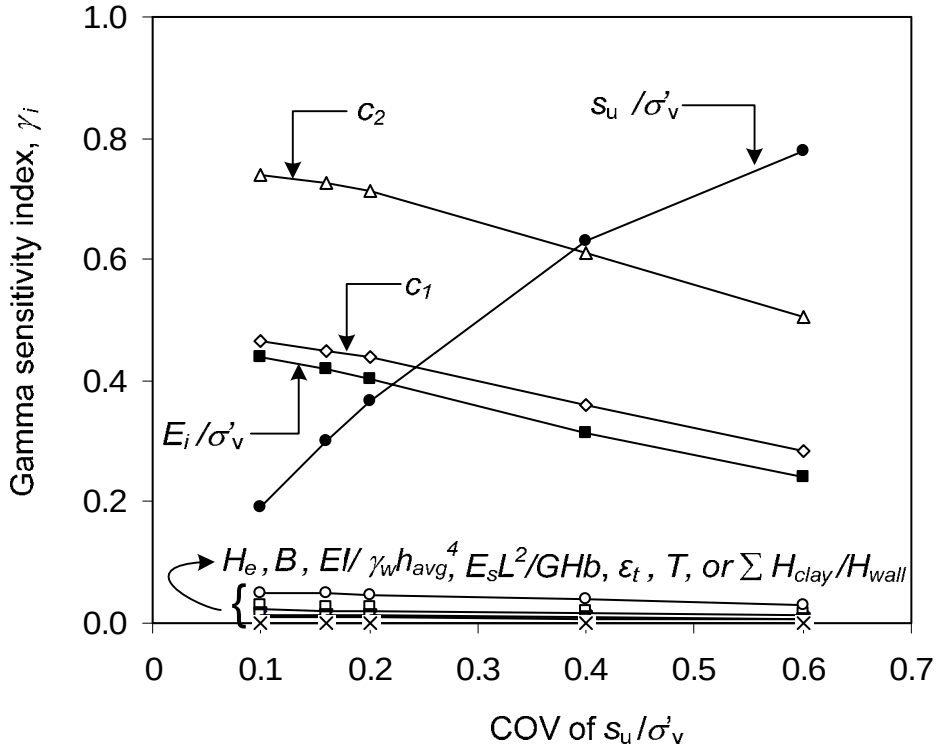

Figure 4.11 Gamma sensitivity index for various $COVs$ of s_u/σ'_v

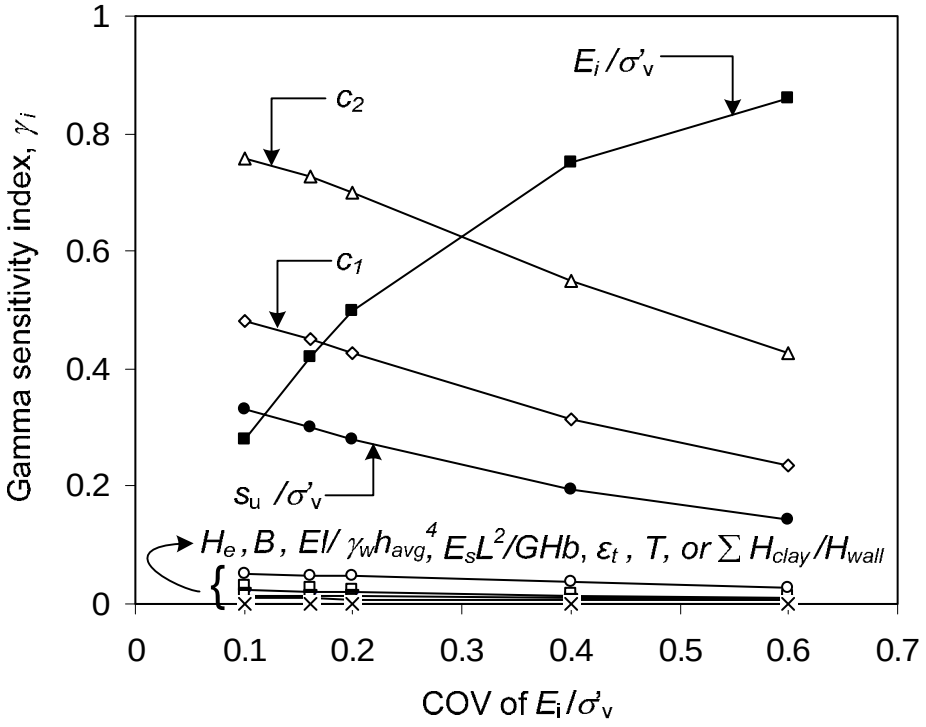

Figure 4.12 Gamma sensitivity index for various *COVs* of E_i/σ'_v

fact, when the *COV* of s_u/σ'_v reaches a certain value, the probability of damage becomes most sensitive to s_u/σ'_v, exceeding the importance of c_1 or c_2.

Similarly, Figure 4.12 shows the effect of assuming different levels of uncertainty in the parameter E_i/σ'_v. Similar trends as those observed in Figure 4.11 regarding the effect of s_u/σ'_v are displayed in Figure 4.12 for the effect of E_i/σ'_v. The cross over point in sensitivity between c_1 and E_i/σ'_v is approximately equal to a *COV* of 17%, and between c_2 and E_i/σ'_v is approximately equal to a *COV* of 30%. The results shown in Figures 4.11 and 4.12 highlight the importance of properly characterizing the soil parameters stated previously. In this regard, it is interesting to note that a *COV* of 0.30 to

0.50 for E_i/σ'_v is quite possible in typical geotechnical practice (Phoon and Kulhawy 1999). Thus, the E_i/σ'_v can be a controlling input parameter in many excavation applications.

To assess how the probability of damage changes as the *COVs* of s_u/σ'_v and E_i/σ'_v change, the *COVs* of both parameters were varied between 0.05-0.60 and the probabilities of damage were calculated. The results are presented in Figure 4.13, which shows that for the example case analyzed, the probability of damage can increase from about 0.2 at the uncertainty level of *COV* = 0.2 to about 0.4 at the uncertainty level of 0.6. This further illustrates the necessity to accurately characterize the soil parameters, especially the *COV*.

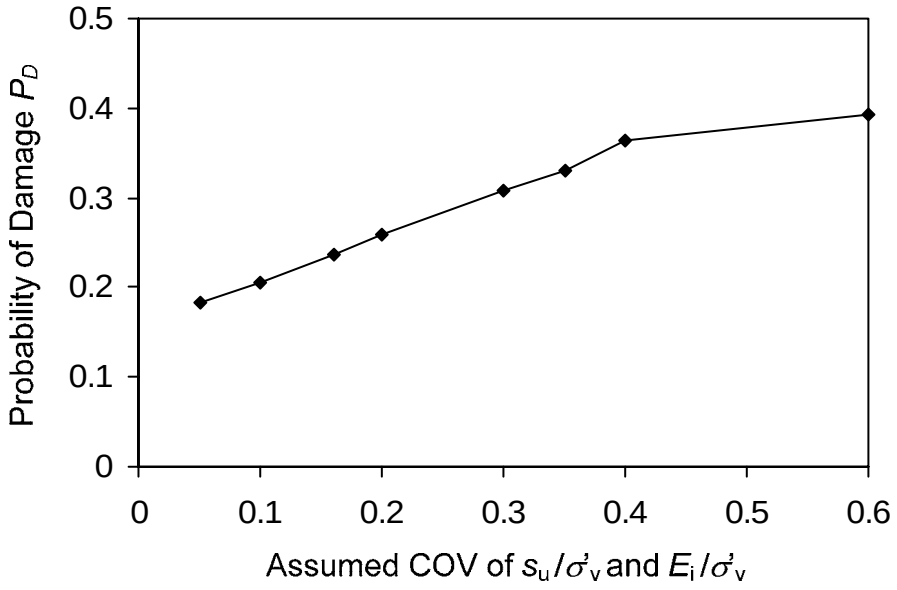

Figure 4.13 Probability of Damage for Different Levels of Uncertainty in the Soil Parameters

Summary

In this paper, a fully-probabilistic framework and procedure for assessing the potential for excavation-induced building damage is developed. To this end, a serviceability limit state based on the Damage Potential Index (*DPI*) is established. Subsequently, the resistance and the loading of the serviceability limit state, including parameter uncertainty and model uncertainty, are characterized. This procedure is then implemented in a spreadsheet-based framework and demonstrated with a well-documented case history. Subsequently, simplified probabilistic evaluation charts are presented to facilitate a simplified analysis of the potential for excavation-induced building damage. Additionally, sensitivity analyses are conducted and further validate the proposed analyses.

CHAPTER FIVE

UPDATING SOIL PARAMETERS FOR EXCAVATION-INDUCED BUILDING DAMAGE POTENTIAL ASSESSMENT [*]

Introduction

The observational method has long been used to aid in the deep excavation work. Traditionally, the finite element method (FEM) is utilized in the analysis and design of the support system for a deep excavation (Whittle et al 1993, Hsieh and Ou 1997, Calvello and Finno 2004, Finno and Calvello 2005, and Kung et al. 2007a). The process generally involves a few steps described in the following. First, the wall deflection and vertical ground movement, referred to as ground settlement herein, caused by the excavation are calculated, and the potential for damage to adjacent buildings are assessed based on available evaluation criteria (i.e., Boscardin and Cording 1989, Boone 1996, Son and Cording 2005, and Finno et al. 2005). The results are factored into the final design. Then, as the excavation work begins and proceeds, the wall deflection and ground settlement are measured at a given excavation stage. These "observations" are used as a basis to fine-tune or update the previous estimate of soil parameters that went into the wall deflection and ground settlement "predictions." Finally, the updated soil parameters, which represent the "best" knowledge of the soil parameters at that stage, are used to repeat the analysis to update the predictions of wall deflection and ground settlement at the planned subsequent stages of excavation (Ou and Tang 1994, Calvello

[*] A similar version of this chapter is being prepared for publication; co-authored by Schuster, M.J., Juang, C.H, and Ou, C.Y.

and Finno 2004, and Finno and Calvello 2005). This process continues until the completion of the excavation.

Hashash et al. (2004) presented a new methodology in the updating, in which soil's stress-strain behavior is updated at the "element" level based on field observations. In their methodology, artificial neural networks are used to simulate the stress-strain behavior of soil elements in the FEM analysis, and the updating in the stress-strain behavior is carried out through neural networks updated with field observations. The updated stress-strain behavior is then used in the FEM analysis of subsequent stages of excavation. This methodology is attractive fundamentally, but requires more intensive computational efforts than the traditional FEM-based inverse analysis.

Although, traditionally, the observational method is often applied in conjunction with a finite element analysis, it is also possible to utilize the observational method with the simplified comprehensive procedure, where damage potential is measured in terms of Damage Potential Index (*DPI*), as presented in Chapter 3. For guidance, the reliability-based updating procedure presented by Hsiao et al. (2008) is studied. In their study, the maximum ground settlement observed during the excavation is used as a basis for updating. However, rather than using the FEM, they used a semi-empirical model for computing (or predicting) the maximum ground settlement. Furthermore, rather than updating the soil parameters to "match" the prediction to the measured maximum settlement, they chose to update the model bias factor of the predictive model of ground settlement. By taking these steps, Hsiao et al. (2008) were able to establish a simple

reliability-based updating scheme that can easily be implemented in a spreadsheet for practical applications.

Although the approach developed by Hsiao et al. (2008) is effective and efficient for improving the prediction of the maximum ground settlement at the subsequent stages of excavation based on the observations at the prior stage, use of the maximum settlement *alone* as a proxy to the building damage potential may not be ideal. This is understandable because the *DPI* depends on *both* the ground settlement and the lateral ground movement, whereas the updating procedure by Hsiao et al. (2008) focuses *only* on the ground settlement as it relies on the updating of the bias factor of the settlement prediction model. Since the updating of the soil parameters tends to improve the predictions of both settlement and lateral ground movement, the two parameters required for determining the *DPI*, it would be desirable to develop a framework for updating the soil parameters so as to update the *DPI* for improving excavation-induced building damage assessment.

Previous study by Hsiao et al. (2008) has shown that among the input variables that are required in the predictive model for settlement, the normalized shear strength (s_u / σ'_v) and the normalized initial modulus of elasticity (E_i / σ'_v) have the most influence on the computed settlement. Thus, it may be possible to update these soil parameters based on the maximum settlement measured during the excavation. Ideally, the wall deflection, ground settlement, and lateral ground movement should all be measured and used together as a basis for updating the soil parameters. In reality, the lateral ground movement is difficult to measure in the field. Nevertheless, both the maximum wall

deflection and the maximum lateral ground movement are related quite well with the maximum ground settlement; thus, it is quite feasible to update the soil parameters based only on the measured maximum settlement. However, it might also be advantageous to adopt an updating scheme in which field observations of both the maximum wall deflection and the maximum settlement are used in the updating process.

Therefore, in this chapter, simplified updating schemes are developed using observations of the maximum settlement and/or the maximum wall deflection as a basis. The updating scheme requiring only the observations of the maximum settlement is first presented. In order to update the soil parameters, an algorithm is first developed to back-calculate the soil parameters based on the observed settlement. Subsequently, an updating scheme is established based on the concept of *relaxation*. This updating procedure is then demonstrated with an analysis of case histories. Next, a similar procedure for updating the soil parameters based on the measurements of both maximum wall deflection and maximum settlement is presented.

Updating Soil Parameters with Observed Maximum Settlement

In this section, the procedure for updating soil parameters based on the observed maximum settlement alone is developed. To document this procedure, an algorithm for back-calculating these soil parameters is first presented, followed by the discussion of a soil parameter updating scheme. Finally, an example application is presented to demonstrate the effectiveness of the developed approach for improving the prediction of the maximum settlement.

Algorithm for Back-Calculation of Soil Parameters

To back-calculate the soil parameters based on an observed maximum settlement at a given stage of excavation, the predictive equation for the maximum settlement, which is presented in full in Chapter 3, needs to be re-defined as a function of the two soil parameters. As shown in Chapter 3, the semi-empirical model for predicting the ground settlement developed by Kung et al. (2007b) can be expressed symbolically as:

$$\delta_{vm} = R_v \delta_{hm} \tag{5.1}$$

where R_v is the deformation ratio and δ_{hm} is the maximum wall deflection.

In the Kung et al. (2007b) model, R_v and δ_{hm} are both multi-variable equations that are dependent on the normalized soil parameters s_u/σ'_v and E_i/σ'_v. In particular, the empirical model for R_v is dependent on s_u/σ'_v, E_i/σ'_v, and the normalized clay layer thickness $\sum H_{clay}/H_{wall}$ [where $\sum H_{clay}$ is the total height of all clay layers and H_{wall} is the height of the wall]. The empirical model for δ_{hm} is a function of s_u/σ'_v, E_i/σ'_v, and the excavation depth (H_e), the excavation width (*B/2)*, the depth from bottom of excavation to hard stratum (T), and the system stiffness [$S = EI/\gamma_w h_{avg}^4$ as defined in Clough and O'Rourke (1990), where E is the modulus of elasticity of wall material, I is the moment of inertia of the wall section, γ_w is the unit weight of water, and h_{avg} is the average support spacing].

Since the non-soil parameters ($\sum H_{clay} / H_{wall}$, H_e, $B/2$, $EI/\gamma_w h_{avg}^4$, and T) in the Kung et al. (2007b) model are *known* quantities for a given excavation case, the predictive equation for the maximum settlement can be treated as follows:

$$\delta_{vm,predicted} = f(s_u / \sigma'_v, E_i / \sigma'_v) \tag{5.2}$$

In the back-calculation, the normalized soil parameters s_u / σ'_v and E_i / σ'_v are adjusted until the difference between the observed settlement and predicted settlement is minimized:

$$\left| \delta_{vm,observed} - \delta_{vm,predicted} \right| = \min \tag{5.3}$$

Because the two soil parameters are correlated and they are to be updated simultaneously when minimizing Equation 5.3, the correlation between these two parameters must be maintained in the back-calculation to ensure the updated parameters do not change drastically from one stage to the next. To maintain the correlation between the two soil parameters, the adjustment or updating is performed on the "transformed" space where the uncorrelated standard normal variables are defined, not in the original space where the actual soil parameters are defined. Once the two parameters are updated, the uncorrelated standard normal values of the soil parameters are transformed back to the actual values of the soil parameters in the original space. Assuming a normal distribution for simplicity, this transformation process is shown below (Phoon 2004):

$$Y = LU + m \tag{5.4}$$

where Y is a vector of the soil parameters, L is the lower triangular Cholesky matrix derived from the covariance matrix, U represents a matrix of the uncorrelated standard normal values of the soil parameters, and m is a vector of the initial soil parameter values. For the problem at hand, the vector Y represents the two soil parameters that are required for the ground settlement prediction (Equation 5.2). The transformation from the updated uncorrelated standard normal values back to the original space allows for the inclusion of the unaltered correlation in the back-calculated soil parameters.

Figure 5.1 illustrates the procedure described previously for updating the soil parameters. For a given stage, the non-soil parameters (i.e. H_e, S, etc.), which are constant, and the initial estimates of mean values of the soil parameters, which are to be adjusted, are inputted. Additionally, to maintain the correlation between the two soil parameters, the coefficient of variation (COV), which indicates the uncertainty of the soil parameters, and the covariance matrix (ρ), which provides a measure of the correlation between the two soil parameters and is used to calculate the Cholesky matrix (L), must be inputted. In the automated procedure implemented in the spreadsheet shown in Figure 5.1, the matrix of the uncorrelated standard normal values of soil parameters, U, is initiated or adjusted, followed by the computation of the vector of soil parameters Y and the maximum settlement. The error (or difference) between the observed and predicted maximum settlement is then calculated with Eq. (5.3). Using Excel "Solver" (a function in Excel that can perform optimization), U is automatically and continuously adjusted until the error is minimized.

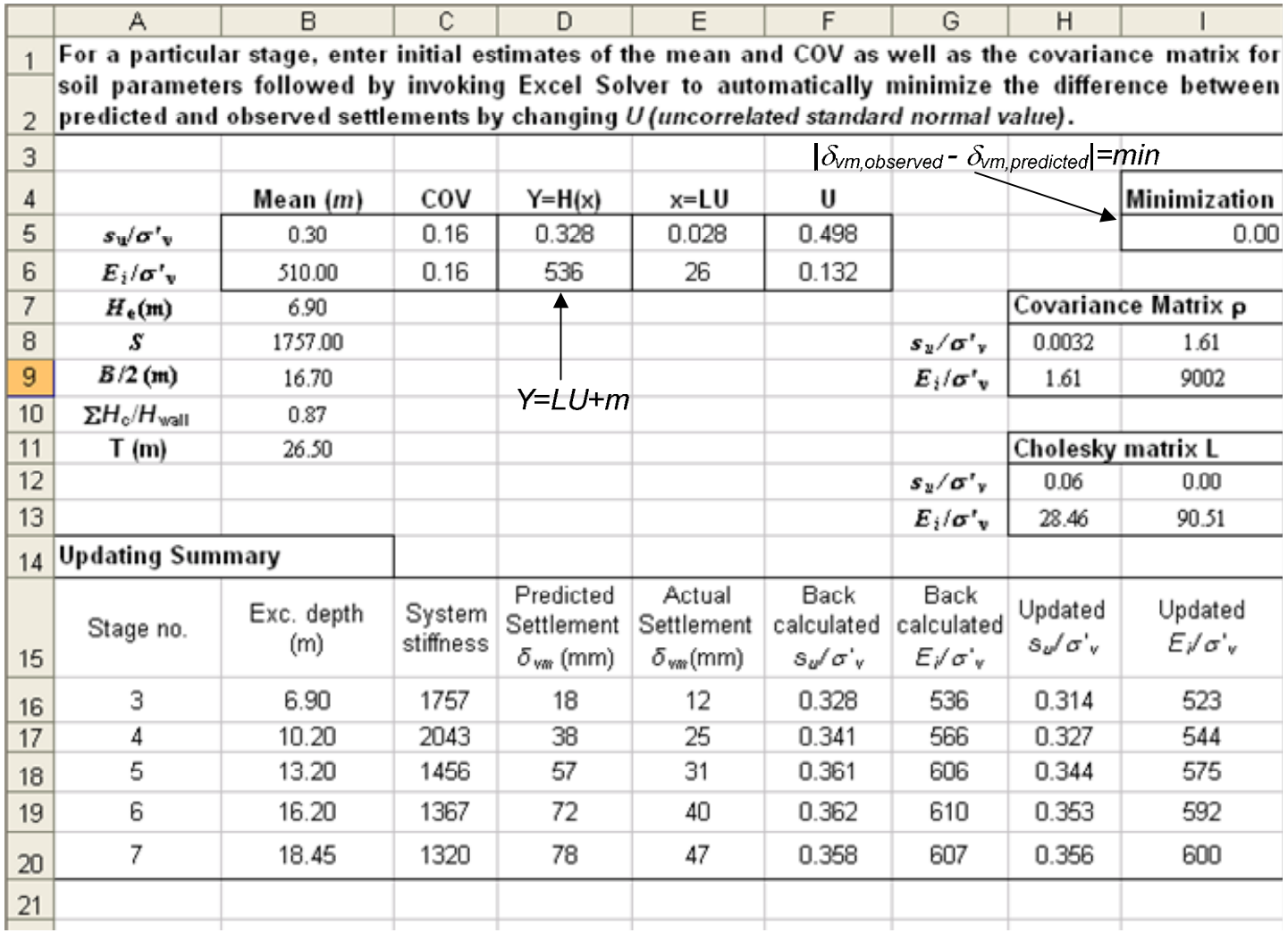

For a particular stage, enter initial estimates of the mean and COV as well as the covariance matrix for soil parameters followed by invoking Excel Solver to automatically minimize the difference between predicted and observed settlements by changing *U (uncorrelated standard normal value)*.

$|\delta_{vm,observed} - \delta_{vm,predicted}| = min$

	Mean (*m*)	COV	Y=H(x)	x=LU	U
s_u/σ'_v	0.30	0.16	0.328	0.028	0.498
E_i/σ'_v	510.00	0.16	536	26	0.132

Y=LU+m

H_e(m)	6.90
S	1757.00
$B/2$ (m)	16.70
$\Sigma H_c/H_{wall}$	0.87
T (m)	26.50

Minimization: 0.00

Covariance Matrix ρ

s_u/σ'_v	0.0032	1.61
E_i/σ'_v	1.61	9002

Cholesky matrix L

s_u/σ'_v	0.06	0.00
E_i/σ'_v	28.46	90.51

Updating Summary

Stage no.	Exc. depth (m)	System stiffness	Predicted Settlement δ_{vm} (mm)	Actual Settlement δ_{vm}(mm)	Back calculated s_u/σ'_v	Back calculated E_i/σ'_v	Updated s_u/σ'_v	Updated E_i/σ'_v
3	6.90	1757	18	12	0.328	536	0.314	523
4	10.20	2043	38	25	0.341	566	0.327	544
5	13.20	1456	57	31	0.361	606	0.344	575
6	16.20	1367	72	40	0.362	610	0.353	592
7	18.45	1320	78	47	0.358	607	0.356	600

Figure 5.1 Spreadsheet Setup for Updating Soil Parameters

To demonstrate the back-calculation algorithm, the Formosa case history presented by Hsiao et al. (2008) is analyzed here. The Formosa case history involves a 7-stage excavation, the details of which have been previously shown in Figure 5.2 and essential data listed in Table 5.1. The soil conditions at the Formosa site are typical of the Taipei basin (Ou et al. 1993) and can generally be described as a soft to medium clay.

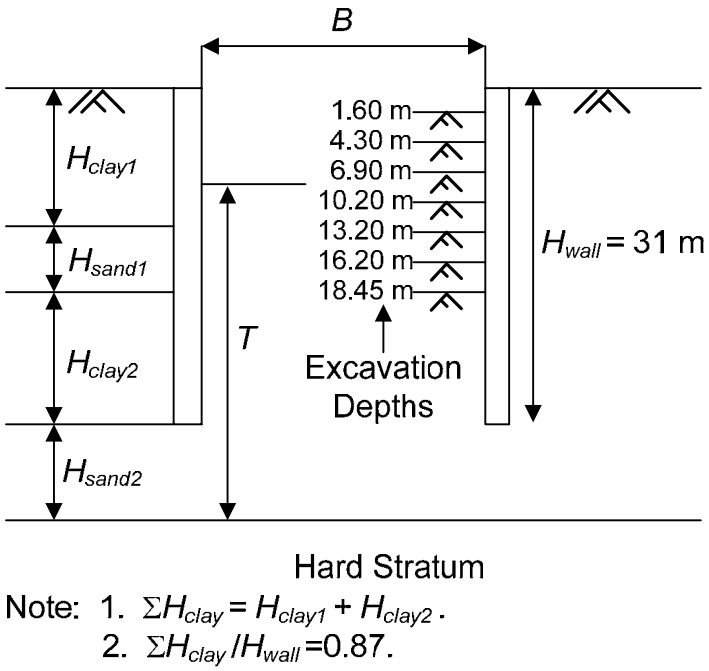

Figure 5.2 Setup of Formosa excavation

As shown in Table 5.1, the soil parameters s_u/σ'_v and E_i/σ'_v can initially be characterized with mean values of 0.30 and 510, respectively, and a *COV* of 0.16 for both parameters (Kung 2003). Additionally, the covariance matrix in Figure 5.1 can be calculated based on a coefficient of correlation between the soil parameters of 0.3. As suggested by Hsiao et al. (2008), the first two stages of excavation are not included in the

updating because of negligible observed settlements. Therefore, back-calculation of the soil parameters will start with Stage 3 of the excavation.

Table 5.1 Mean values of excavation depths and system stiffness of Formosa case history

Factor	Excavation sequence (Stage No.)				
	3	4	5	6	7
Depth, H_e (m)	6.9	10.2	13.2	16.2	18.45
System stiffness, $EI/\gamma_w h_{avg}^4$	1757	2043	1456	1367	1320
Observed Maximum Settlement (mm)	12	25	31	40	47
Observed Maximum Wall Deflection (mm)	25	42	49	59	62

- Mean of other input parameters: $B/2$ = 16.7 m, s_u/σ'_v = 0.30 and E_i/σ'_v = 510, T = (31 - H_e)m, and $\sum H_{clay} H_{wall}$ = 0.87.
- *COV*s of s_u/σ'_v and E_i/σ'_v = 0.16
- Coefficient of correlation of s_u/σ'_v and E_i/σ'_v = 0.3
- Mean and COV for Maximum Vertical Settlement: $BF_{\delta vm}$ = 1.00 and $COV_{\delta vm}$ = 0.35.
- Mean and COV for Maximum Lateral Settlement: $BF_{\delta lm}$ = 1.00 and $COV_{\delta lm}$ = 0.31.

As shown in Figure 5.1, the target excavation depth for Stage 3 is 6.9 m, and the normalized system stiffness is 1757. Prior to Stage 3 excavation, the predicted maximum settlement is 18 mm based on the initial estimates of the soil parameters of s_u/σ'_v = 0.30 and E_i/σ'_v = 510. Since the observed settlement is 12 mm at this stage, the soil parameters are back-calculated to minimize the difference between the actual settlement and the predicted settlement as shown below:

$$\left| \delta_{vm,observed} - \delta_{vm,predicted} \right| = \left| [12 - f(s_u / \sigma'_v,\ E / \sigma'_v)] \right| = \min \tag{5.5}$$

Using Excel solver as shown in Figure 5.1, the difference between the observed and predicted maximum settlement is minimized (i.e., *min* is set to 0). The soil parameters are back-calculated to be $s_u / \sigma'_v = 0.328$ and $E_i / \sigma'_v = 536$, respectively, with $min \approx 0$. With these soil parameters, the maximum settlement is predicted to be 12 mm at this stage.

Relaxation and Soil Parameters Updating for Improving Settlement Predictions

While the soil parameters can be back-calculated so that the predicted maximum settlement matches the observed value well for a given excavation stage, as presented previously, an updating strategy is needed to achieve the best predictive results in the subsequent stages of excavation. In this study, a relaxation technique is adopted, and the soil parameters are updated at the end of each stage of excavation as follows:

$$x_{i+1} = \lambda (x_{\text{back}}) + (1 - \lambda) x_i \tag{5.6}$$

where x_{i+1} represents the updated soil parameter value, λ represents the weighting factor, x_{back} represents the back-calculated soil parameter value at a given stage, and x_i represents the prior value of the soil parameters. The rationale behind this strategy is that the soil parameters can be "over-corrected" if the back-calculated values of soil parameters from a given stage are used *directly* in the subsequent analysis of the maximum settlement. Relaxation in the soil parameters updating often produces better results. In Equation 5.6, when λ = 1 is adopted, the back-calculated value is taken as the updated value, implying

no relaxation. When $\lambda = 0.5$ is adopted, the updated value is taken as the average of the prior value and the back-calculated value. In general, the choice of the best λ value to use is problem-specific and can only be determined through a trial-and-error process.

To continue the discussion of soil parameters updating in the Formosa case, recall that no updating is performed prior to Stage 3. Thus, the settlement predictions prior to Stage 3 are essentially those made initially ("as-design" values). Prior to Stage 3 of excavation, the maximum settlement prediction at the target depth of 6.9 m is 18 mm. At the completion of Stage 3 excavation, where the excavation depth is at 6.9 m, the observed maximum settlement is 12 mm. Based on this observed settlement at the completion of Stage 3 excavation, and using a relaxation with $\lambda = 0.75$ (note: use of other values will be presented and compared later), the soil parameters are updated. Then, based on the updated soil parameters, the settlement predictions at various target depths are updated prior to Stage 4 of excavation.

Figure 5.3 shows the updated maximum settlement predictions at various target depths in the Formosa excavation case. For example, prior to stage 4 of excavation, the maximum settlements are predicted for the target excavation depths of 10.15 m, 13.2 m, 16.2 m, and 18.45 m [these are the target depths at the end of stages 4, 5, 6, and 7 of excavation, respectively]. As shown in Figure 5.3, prior to stage 4 of excavation, the predicted maximum settlement is 32 mm at the target depth of 10.15 m, is 48 mm at the target depth of 13.2 m, is 62 mm at the target depth of 16.2 m, and is 70 mm at the target depth of 18.45 m. These settlement predictions made prior to stage 4 of excavation are shown with a "triangle" (Δ) symbol in Figure 5.3.

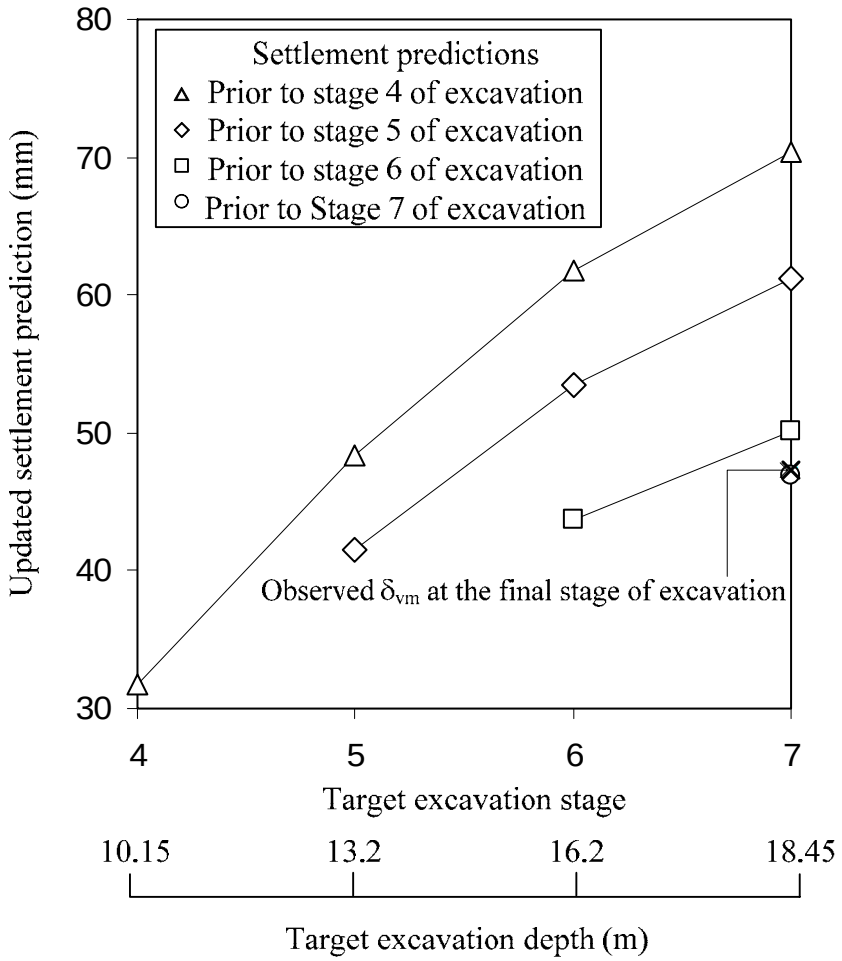

Figure 5.3 Updating of Settlement Predictions

Similarly, at the end of stage 4 excavation, the observed maximum settlement is available and can be used to update the soil parameters. The updated soil parameters can be used to predict the maximum settlements at the target depths of 13.2 m, 16.2 m, and 18.45 m [corresponding to stage 5, 6, and 7]. Of course, at the end of stage 4 excavation, there is no longer a need to "predict" the settlement at the depth of 10.15 m. Thus, prior to stage 5 of excavation, the maximum settlements are predicted at only three depths, shown with a "diamond" (◊) symbol in Figure 5.3.

In a similar manner, two settlements predictions are made at the target depths of 16.2 m and 18.45 m prior to stage 6 of excavation, and one settlement prediction is made at the target depth of 18.45 m prior to stage 7 of excavation. Also shown in Figure 5.3 is the observed settlement at the end of final stage (Stage 7) of excavation, which is at the depth of 18.45 m. The results shown in Figure 5.3 indicate that as the excavation proceeds, and with more chances of soil parameters updating based on the observed settlement, the settlement prediction made for the final target depth of 18.45 m becomes more *accurate*.

Figure 5.4 shows the updated settlement predictions *only* at the target depth of 18.45 m prior to Stages 3, 4, 5, 6, and 7, respectively, along with the observed maximum settlement at the depth of 18.45 m. It should be noted that prior to Stage 3, no updating

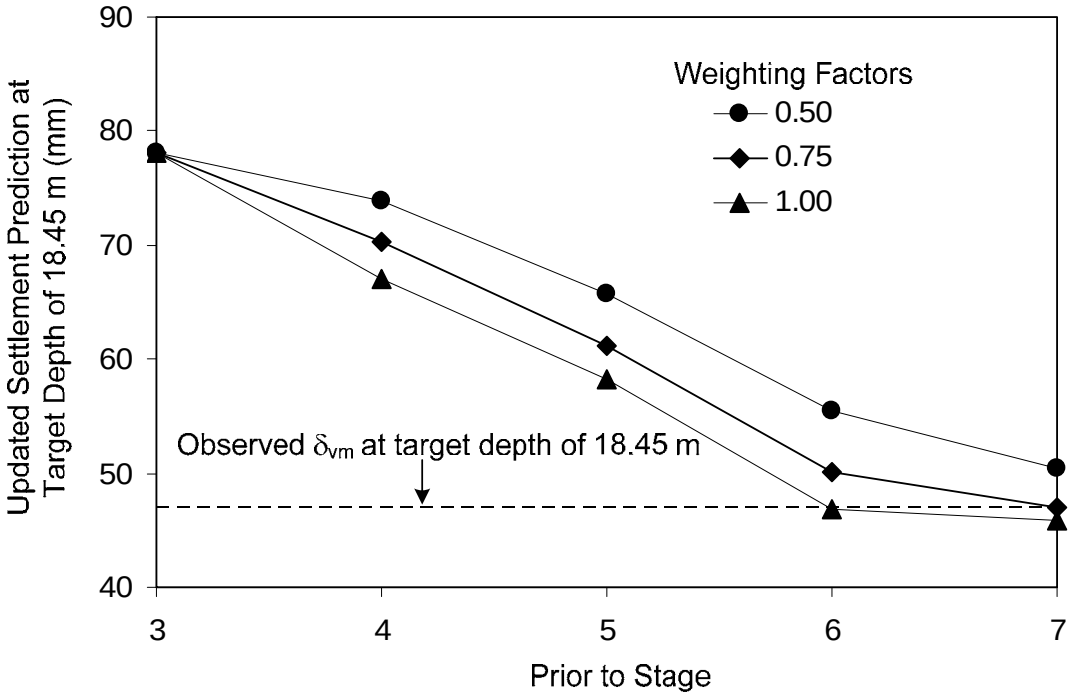

Figure 5.4 Updated Settlement Predictions at Target Depth of 18.45 m for Different Weighting Factors

has occurred yet, and the predicted settlement is 78 mm (shown in Figure 5.3) based on the initial (as-design) soil parameters. Prior to Stages 4, 5, 6, and 7, however, the soil parameters have been updated based on the observed settlement from all previous stages and the settlements are re-calculated with the updated soil parameters. The accuracy of the predicted settlement is shown to drastically improve with each successive updating of soil parameters. It is noted that for soil parameter updating, three λ values are used in the relaxation, and the results of all three scenarios are quite similar in this case. Thus, choice of the weighting factor here is a matter of preference. In the subsequent analysis, the weighting factor $\lambda = 0.75$ is adopted as it converges upon the observed maximum settlement efficiently and is generally less susceptible to overcorrection. As in numerical solutions of many engineering problems, however, the issue of the weighting factor for relaxation could be problem-specific, and should be carefully examined.

To further examine the proposed updating scheme, the effect that the initial estimate of the soil parameters has on the updated settlement predictions is analyzed. To analyze this effect, the Formosa case is reanalyzed assuming different initial values of soil parameters (with four different scenarios, $s_u / \sigma'_v = 0.30$ and $E_i / \sigma'_v = 510$, $s_u / \sigma'_v = 0.28$ and $E_i / \sigma'_v = 550$, $s_u / \sigma'_v = 0.36$ and $E_i / \sigma'_v = 750$, and $s_u / \sigma'_v = 0.31$ and $E_i / \sigma'_v = 650$) with a weighting factor of 0.75. The updated settlement predictions *only* at the target depth of 18.45 m prior to Stages 3, 4, 5, 6, and 7, respectively, is shown along with the observed settlement at the target depth of 18.45 m in Figure 5.5. As can be seen from Figure 5.5, the updating in soil parameters based on the settlement observed in the prior stage can improve the settlement predictions at the final stage regardless of what initial

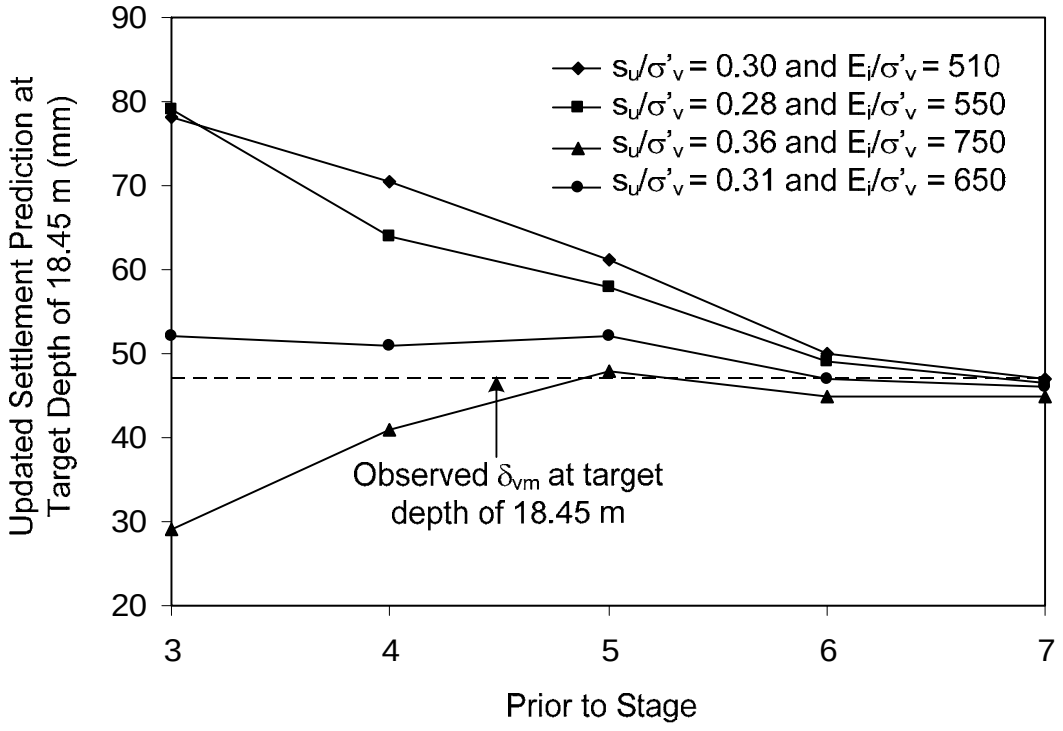

Figure 5.5 Effect of Initial Value of Soil Parameters

estimates of soil parameters were used. Thus, the proposed updating scheme is considered effective.

Finally, it should be of interest to compare the settlement predictions made with the updated soil parameters to those made with the updated model bias factor as reported by Hsiao et al. (2008). Figure 5.6 shows such a comparison, where updated settlement predictions at the target depth of 18.45 m prior to Stage 4, 5, 6, and 7 are shown. The predicted settlement prior to Stage 3, which is essentially the "as-design" prediction, is also shown. Both methods are found to be effective in improving the accuracy of prediction of the maximum settlement at the final excavation depth of 18.45 m, although the results based on the updated soil parameters are shown to be more accurate compared to the observed maximum settlement. The updating of soil parameters also has an added

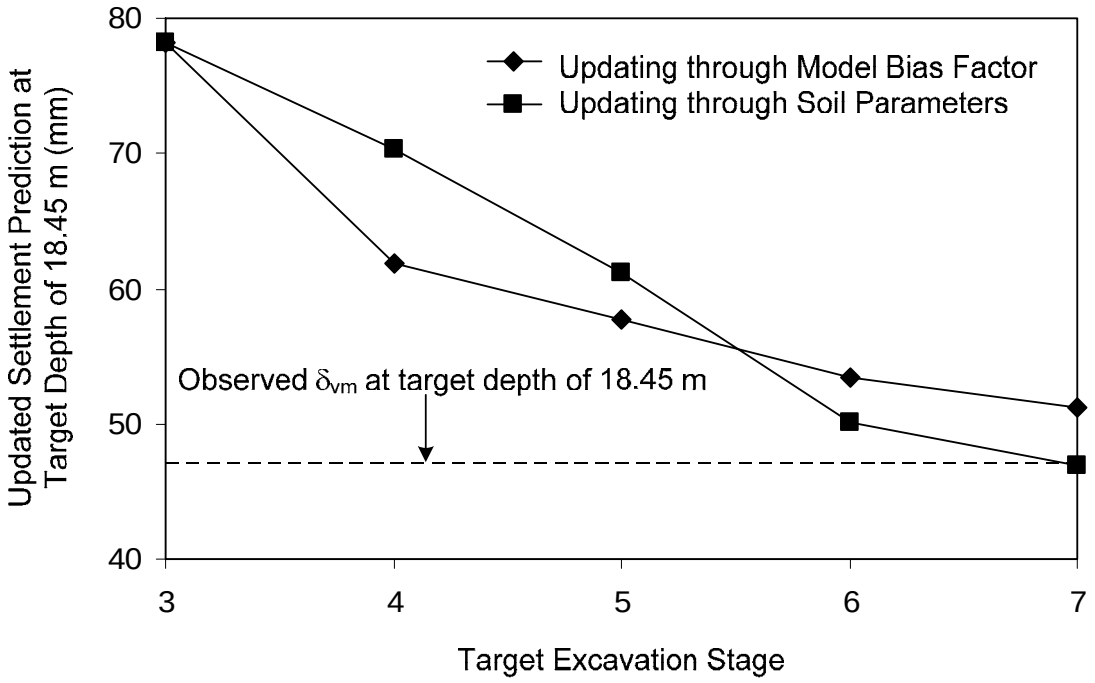

Figure 5.6 Comparison between settlements updated through model bias factor and those updated through soil parameters

effect in improving the prediction of lateral ground movements, and thusly, improving the accuracy of building damage assessment, which will be demonstrated in a latter section of this paper.

Updating Soil Parameters Using Both Maximum Settlement and Maximum Wall Deflection Observations

As shown previously, the observed maximum settlement from the prior stage can be used as a basis for updating soil parameters, and the accuracy of the settlement predictions for subsequent stages can be improved with the updated soil parameters. Although not shown here, the observed maximum wall deflection can also be used as a basis for updating soil parameters, and comparable results of settlement predictions are obtained. While the updating of soil parameters using the observed maximum settlement or wall deflection *alone* is shown to be effective, it would seem advantageous to update

the soil parameters based on both observations when both are available. To this end, the soil updating procedure presented previously is modified so that both the maximum wall deflection and maximum settlement are utilized in the updating.

Back-calculation and Updating of Soil Parameters

To update the soil parameters based on the observations of both maximum settlement and maximum wall deflection, the same framework as presented previously is followed. Initially, the soil parameters are back-calculated based on the observed maximum settlement and wall deflection. Subsequently, the soil parameters are updated based on the prior estimate of soil parameters and the present or back-calculated soil parameters.

The algorithm to back-calculate soil parameters based on the observed maximum settlement has previously been presented (in reference to Figure 5.1). This algorithm is modified to consider as an updating basis both the observed maximum wall deflection δ_{hm} and the maximum settlement δ_{vm}. In the revised algorithm, the root mean square error (RMSE) between the observed and predicted responses is minimized:

$$RMSE = \sqrt{\left(\frac{\delta_{hm,pred} - \delta_{hm,obs}}{\delta_{hm,obs}}\right)^2 + \left(\frac{\delta_{vm,pred} - \delta_{vm,obs}}{\delta_{vm,obs}}\right)^2} = \min \tag{5.7}$$

where $\delta_{hm,pred}$ is the predicted maximum wall deflection, $\delta_{hm,obs}$ is the observed maximum wall deflection, $\delta_{vm,pred}$ is the predicted maximum settlement, and $\delta_{vm,obs}$ is the observed maximum settlement.

As presented previously, the soil parameters are adjusted in the uncorrelated standard normal space and then transformed back to the actual values in the original space through Equation 5.4. The actual values of the soil parameters computed with Equation 5.4 are then inputted into Equation 5.7 to determine the RMSE. Using Excel Solver, the uncorrelated standard normal soil parameters are readjusted and the process is repeated until the RSME is minimized. It should be noted that an additional constraint is implemented in this updating algorithm. Here, to avoid extrapolation of the empirical models used to predict the maximum wall deflection and settlement, the ratio E_i / σ'_v divided by s_u / σ'_v, which can be expressed as E_i / s_u, is limited to a range of 1500-3000. This range is selected based on the range of data that was used in the development of the empirical models for the maximum wall deflection and settlement (Kung et al 2007b).

Once the soil parameters are back-calculated, the relaxation technique can again be used to update the soil parameters as presented previously. In the analysis presented herein, a weighting factor of 0.75 is applied.

Updating of Predicted Wall Deflection and Settlement

To demonstrate the newly developed updating scheme, the Formosa case history is reanalyzed. Here, the soil parameters are updated with both the observed maximum settlement and the observed maximum wall deflection. The results of this analysis are then compared with the results of updating merely with either the observed maximum settlement or the observed maximum wall deflection. Figures 5.7 and 5.8 show such a comparison. In Figure 5.7, the predictions of the maximum wall deflection at an excavation depth of 18.45 m made with the updated soil parameters using the three updating schemes (updating with the observed maximum settlement alone, with the

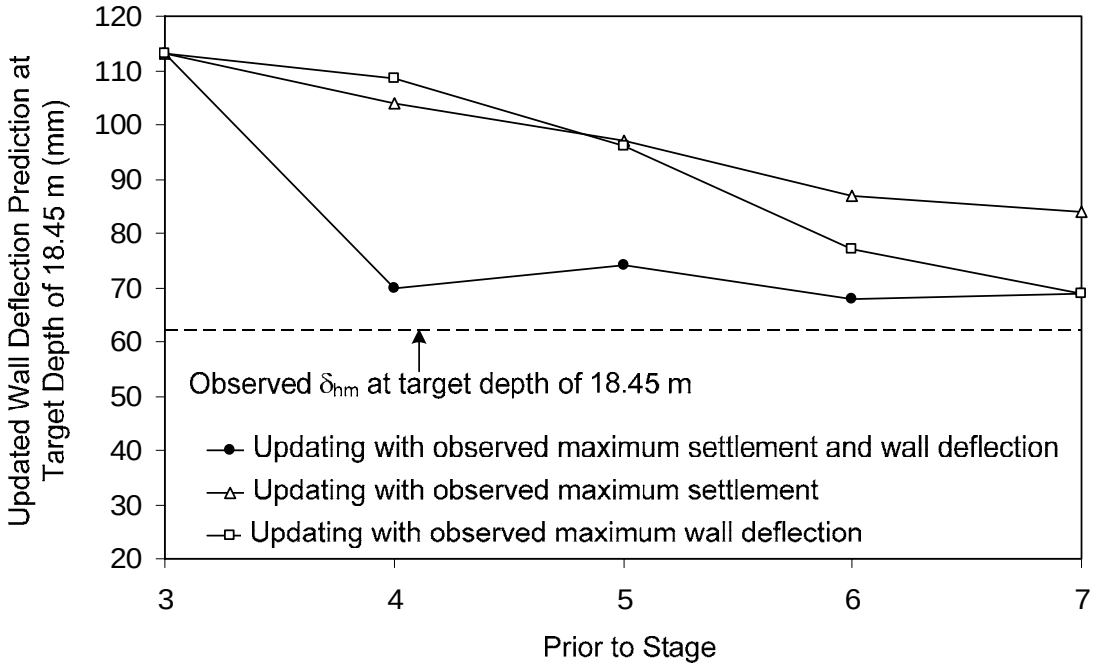

Figure 5.7 Comparison of the maximum wall deflection predictions with three different updating schemes

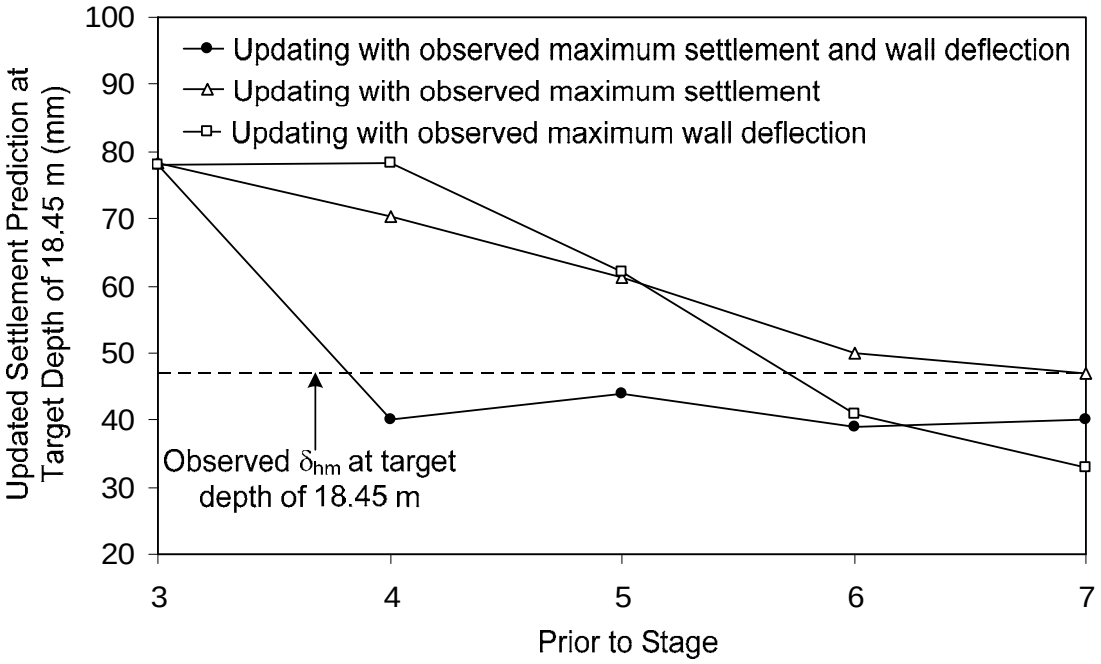

Figure 5.8 Comparison of the maximum settlement predictions with three different updating schemes

observed maximum wall deflection alone, and with both the observed maximum settlement and maximum wall deflection) are compared. As shown in Figure 5.7, the predictions of maximum wall deflection are most accurate when the soil parameters are updated based on the maximum wall deflection or both the maximum wall deflection and the maximum settlement. On the other hand, when the updated settlement predictions at the target depth of 18.45 m are compared in Figure 5.8, the updating scheme that is based on the observed maximum settlement alone yields the most accurate results, followed by the updating scheme based on both the maximum wall deflection and the maximum settlement, and the updating scheme based on the observed maximum wall deflection alone. Additionally, it is interesting to note that the updating scheme utilizing both maximum wall deflection and maximum settlement converges faster then the updating schemes utilizing only maximum wall deflection or maximum settlement.

In summary, all three updating schemes are effective in improving the predictions of both the maximum wall deflection and the maximum settlement, and the results are quite comparable. Overall though, updating the soil parameters based on both the observed maximum wall deflection and the maximum settlement yields slightly more accurate results in the predictions of both the maximum wall deflection and the maximum settlement in the subsequent excavation stages. This updating scheme also has the advantage of faster convergence to the maximum wall deflection and the maximum settlement that are observed at the final excavation depth, which is quite significant from the practitioners' viewpoint.

Updating the Prediction of Damage Potential Index (*DPI*)

Updating of soil parameters based on observations of maximum settlement and wall deflection can ultimately improve the prediction of the *DPI*. In addition to the input parameters that are related to soil conditions and the excavation design that has been previously defined, the prediction of *DPI* for an adjacent building requires extensive information about the properties of the adjacent building such as the location of the building [characterized in terms the distance from the excavation to two adjacent footings (d_1 and d_2) in the building where d_1 represents the distance from the excavation to the footing nearest to the excavation and d_2 represents the distance from the excavation to the footing furthest from the excavation], the embedment depth of the building, the soil-structure stiffness ratio [(E_sL^2/GHb) where E_s is the soil stiffness in the region of footing influence, L is the length of building portion subjected to ground movement, G is the elastic shear modulus of the building, H is the height of the building, and b is the building wall thickness as defined by Son and Cording (2005)], and the structure cracking strain ε_t. To investigate the effectiveness of any soil parameter updating scheme for improving the prediction of the *DPI*, case histories with various degrees of observed damage to buildings adjacent to excavation are essential. However, ideal cases are difficult to secure. In this study, a hypothetical case is created for the illustration of the proposed updating methodology.

The Taipei National Enterprise Center (TNEC) excavation case history, which is utilized in Chapters 3 and 4, is used as a basis for creating the hypothetical case. Basic details on the layout and design of the TNEC excavation can be found in Figures 4.3 and 4.4. It should be noted that Building *D* (Ou et al 1998, 2000) can be split up into 4 bays

when calculating the *DPI* using the procedure developed in Chapter 3. Based on a critical analysis of each bay shown in Chapter 3 as well as field observations by Liao (1996), the critical bay was identified and is utilized in this analysis. All of the relevant input parameters for computing *DPI* and necessary for updating of the soil parameters are listed in Table 5.2. To create a semi-hypothetical case for the present analysis, it is assumed that the soil parameters determined by Kung (2003) and Kung et al. (2007a) through extensive FEM analysis and laboratory testing can accurately predict the wall

Table 5.2 Mean values of excavation depths and system stiffness of TNEC case history

Factor	Excavation sequence (Stage No.)				
	3	4	5	6	7
Depth, H_e (m)	8.6	11.8	15.2	17.3	19.7
System stiffness, $EI/\gamma_w h_{avg}^4$	1023	966	1109	1115	1294
Observed Settlement (mm)	22	37	48	54	59
Observed DPI	0	1	18	20	18

- Mean of other input parameters for predicting ground movement profiles: $B/2$ = 20.6 m, s_u/σ'_v = 0.25 and E_i/σ'_v = 500, $\sum H_{clay}H_{wall}$ = 0.87, T = (46 - H_e) m, and embedment depth = 4 m.
- Characteristics of Critical Building Section: d_1 = 25.5 m and d_2 = 31.0 m from edge of excavation, embedment depth = 4 m, (E_sL^2/GHb)=15, and ε_t = 0.9.
- *COV*s of s_u/σ'_v and E_i/σ'_v = 0.16
- Coefficient of correlation of s_u/σ'_v and E_i/σ'_v = 0.3
- Mean and COV for Maximum Vertical Settlement: $BF_{\delta vm}$ = 1.00 and $COV_{\delta vm}$ = 0.35.
- Mean and COV for Maximum Lateral Settlement: $BF_{\delta lm}$ = 1.00 and $COV_{\delta lm}$ = 0.31.

deflection, ground settlement and lateral ground movements, and that the *DPI* can be accurately predicted. These *DPI* values calculated with the normalized soil parameters of $s_u / \sigma'_v = 0.31$ and $E_i / \sigma'_v = 650$, which represents the best estimates by Kung (2003), are assumed to be the "observed" values at the end of each target excavation stage as shown in Table 5.2. Thus, in terms of the *DPI* observations, this is a semi-hypothetical case; everything else is a real-world case as reported by Ou et al. (1998, 2000).

To demonstrate the updating of soil parameters based on the observed settlement and wall deflection and the subsequent analysis of all responses leading to the *DPI*, the initial estimates of the soil parameters are assumed to be $s_u / \sigma'_v = 0.28$ and $E_i / \sigma'_v = 575$. As discussed previously, the observed settlement and wall deflection are used as a basis for updating the soil parameters. Prior to Stage 4, the observed settlement and wall deflection at the end of Stage 3 are used to update the soil parameters, and then the analysis is repeated to calculate the wall deflection, ground settlement, lateral ground movement, and *DPI* of Building *D* at the target depths of 11.8 m, 15.2 m, 17.3 m and 19.7 m (these are the target depths for Stages 4, 5, 6, and 7, respectively). Similarly, based on the observed settlement and wall deflection at the end of Stage 4, the *DPI* values of Building *D* are updated at the target depths of 15.2 m (Stage 5), 17.3 m (Stage 6) and 19.7 m (Stage 7). This same process is repeated at the end of Stage 5 and then Stage 6. Figure 5.9 shows the prediction of the *DPI* at the target depth of 19.7 m (Stage 7) using the updated soil parameters prior to Stages 4, 5, 6, and 7. The results show that as the soil parameters are updated at each stage based on the observed settlement and wall deflection, the accuracy of the predicted *DPI* improves significantly.

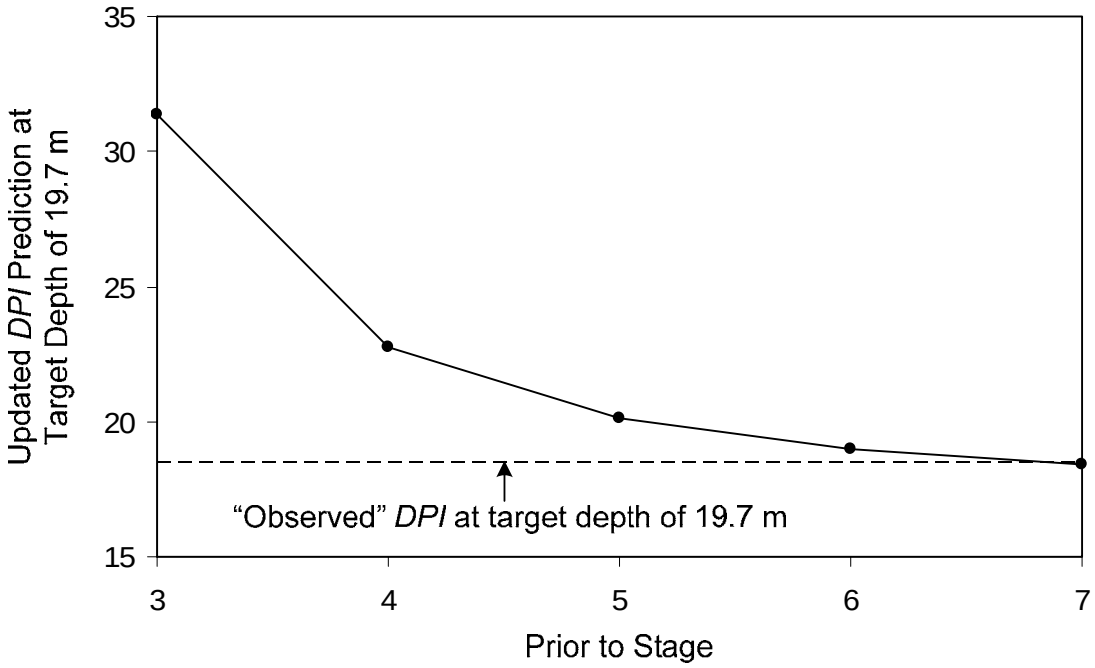

Figure 5.9 Predicted *DPI* with soil parameters updated based on the observed maximum settlement and wall deflection

Discussions: Simplified Approach for Updating Soil Parameters

In the algorithms for minimizing Equation 5.3 (or Equation 5.7), soil parameters are adjusted in the uncorrelated standard normal space and transformed back to the original space in order to maintain the correlation between the two soil parameters in the analysis. However, these algorithms may be simplified with an assumption that the ratio of the initial modulus of elasticity (E_i / σ'_v) over the normalized shear strength (s_u / σ'_v) is a constant for a given clay (Kung et al. 2007a). With this assumption, the minimization in Equation 5.3 (or Equation 5.7) can be carried out by adjusting only the parameter s_u / σ'_v, as the parameter E_i / σ'_v will change accordingly to keep the ratio constant. With this approach, the back-calculation of the soil parameters is greatly simplified since only one soil parameter has to be adjusted.

To demonstrate the validity of this approach, the Formosa case is again analyzed, and the soil parameters are updated by minimizing the RMSE in Equation 5.7. However, instead of adjusting both soil parameters, the ratio $\frac{E_i / \sigma'_v}{s_u / \sigma'_v}$ is assumed to be equal to 1700 with an initial estimate of $s_u / \sigma'_v = 0.30$ and $E_i / \sigma'_v = 510$, and the parameter s_u / σ'_v is adjusted in the analysis. Once the soil parameters are back-calculated, the relaxation technique is applied as described previously, and the soil parameters are updated for subsequent predictions of the wall and ground responses.

Figure 5.10 compares the results obtained using this simplified approach (i.e., adjusting only one soil parameter in the optimization process) with those obtained previously (through simultaneous adjustment of both soil parameters s_u / σ'_v and E_i / σ'_v). As shown in Figure 5.10, the simplified approach can achieve the same objective in improving the settlement prediction, and yields results comparable to those obtained by the "full" optimization approach. As shown in Figure 5.11, a similar trend is observed with the prediction of the maximum wall deflection as well. Thus, the simplified approach can be used with confidence when the ratio of the initial modulus of elasticity (E_i / σ'_v) over the normalized shear strength (s_u / σ'_v) is a constant.

Summary

In this chapter, an application of the observational method is presented in which soil parameters are *updated* using the ground settlement and wall deflection measured in a staged excavation for the purpose of improving excavation-induced building damage assessment. In this approach, the soil parameters are first back-calculated by minimizing

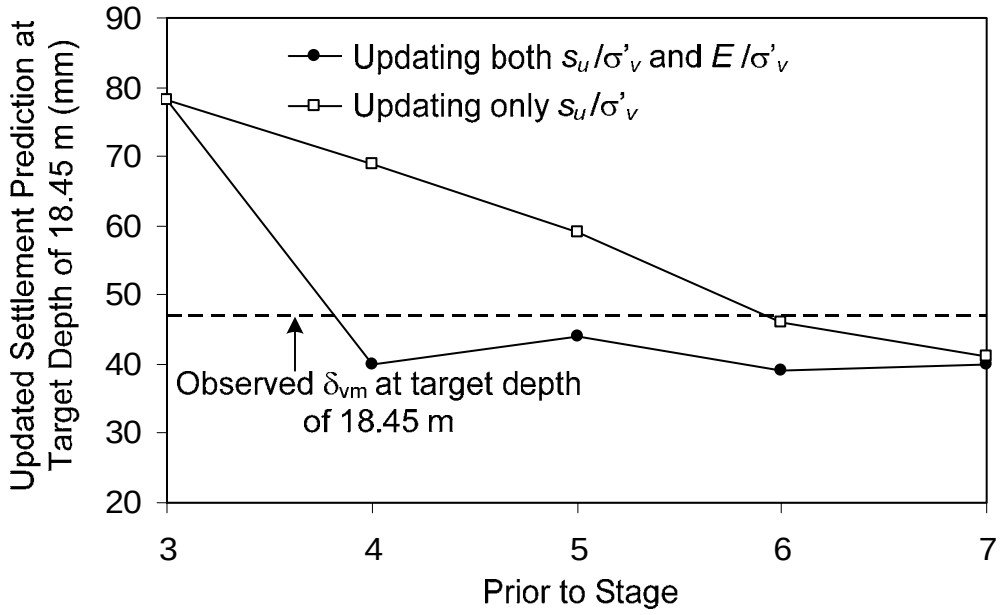

Figure 5.10 Comparison of Different Algorithms for Back-calculating Soil Parameters and Predicting Maximum Settlement

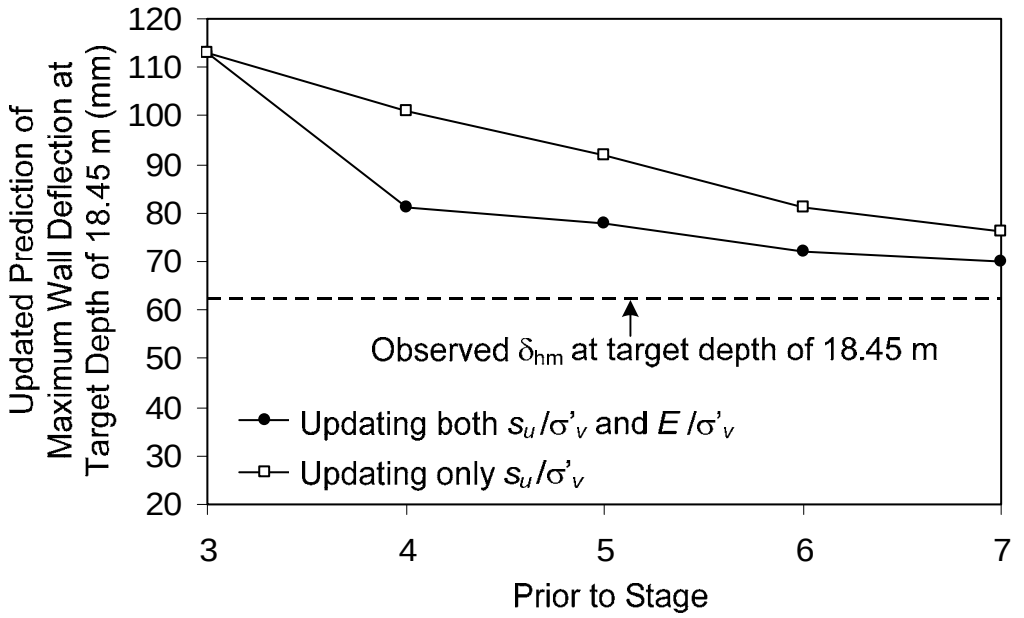

Figure 5.11 Comparison of Different Algorithms for Back-calculating Soil Parameters and Predicting Maximum Wall Deflection

the difference between the measured and predicted responses (settlement and wall deflection) at a given excavation stage. *Relaxation* is then applied to the back-calculated soil parameters to update these parameters, and the issue of selecting an appropriate weighting factor for convergence is explored. With the updated soil parameters, the ground settlement and wall deflection as well as the damage potential of buildings adjacent to the excavation in future stages of excavation are reanalyzed and updated.

The updating of soil parameters is shown to lead to improved predictions of the maximum wall deflection, the maximum settlement, and the *DPI*, and the developed approach is demonstrated to be a simplified yet effective means for applying an observational-based procedure to the problem of deep excavations. In particular, the updating scheme utilizing both the observed maximum settlement and the observed maximum wall deflection in the updating of the soil parameters is recommended, as it yields slightly better overall results in the predictions of the maximum wall deflection and ground settlement, and converges faster toward the observed responses.

CHAPTER SIX

SUMMARY, CONCLUSIONS, AND RECOMMENDATIONS

Summary

Within Chapters 2 through 5 of this dissertation, a framework for the fully-probabilistic analysis of the potential for excavation-induced building damage has been established. To this end, simplified empirical models have been developed to estimate the damage potential index (*DPI*) of a building affected by excavation-induced ground movements and assess the potential for serviceability damage to a building. However, there are several limitations to the established framework as stated below:

1. The KJHH and KSJH ground movement models have been developed for estimating the ground movements under the plane strain condition. However, due to the corner effects, the ground movements at the corner of an excavation are lesser than the ground movements near the midpoint of an excavation. Therefore, the established framework is more appropriate for application to buildings that are located near an excavation where the corner effect is less significant.
2. The KJHH and KSJH models were developed based on a database with a limited number of finite element (FEM) analysis and case histories. These FEM analysis and case histories consisted of excavations in predominately soft to medium clays with normal (or "good") workmanship. Consequently, the developed framework is limited in applicability to predominately soft to medium clays with normal (or "good") workmanship in the excavation.

3. The database collected by Son and Cording (2005) that was utilized in this dissertation study consisted mainly of brick-bearing buildings, which underwent hogging deformation. Therefore, although the established framework can be applied to cases with frame buildings or buildings experiencing sagging deformation, which is evident from reasonable results presented previously, it is most applicable to cases with brick-bearing buildings and hogging deformation.
4. In the established framework, the lateral ground movement profile as well the boundary for differentiating between hogging and sagging were both established based on limited case histories. While both the lateral ground movement profile and the general boundary for hogging and sagging are reasonable and adequate for analysis in the developed framework, the results should be viewed with caution.
5. Within this dissertation, serviceability damage is defined based on the crack width of a building. However, in some cases, the serviceability damage may be unrelated to crack width depending on the usage of the building. Therefore, the usage of the established framework requires the serviceability damage to be defined based on crack width.

Conclusions

Based on the results presented within this dissertation, particularly in Chapters 2 through 5, the following conclusions are drawn:

1. The results presented in Chapter 2 clearly demonstrate the importance of the calibration of model bias factor c_1. Proper calibration of the chosen serviceability limit state is as important as the selection of the serviceability limit state. The results also show that the model bias factor of a serviceability limit state model can be estimated with a sufficiently large set of the "observed" binary data (in this paper, tolerable and intolerable groups of excavation-induced building damage).
2. The mean and the coefficient of variation of the model bias factor (μ_{c1} and COV_{c1}) are both shown to be a function of the prior probability ratio. This finding along with the concept of the apparent model bias factor, which combines characteristics of both the "true" model bias factor and the "state" of information of the specific case, enables the development of an iterative procedure that is shown to be effective in tackling the issue of prior probability in the calibration of the model bias factor. The iterative procedure represents an innovative approach and allows for the simultaneous calibration of a model bias factor and probability of damage. The improvement in the "predictions" in the case histories examined can be attributed to the case-specific information gained during the iterative process.
3. The newly developed procedure utilizing the Damage Potential Index (*DPI*) offers a convenient approach for evaluating the damage potential of a building adjacent to an excavation. Using the empirical equations (Equations 3.1-3.8) presented in Chapter 3, the excavation-induced ground movements can be accurately predicted. Additionally, the developed models (Equations 3.9 and 3.10) for

estimating the angular distortion and maximum lateral strain in a building are simple, straightforward to apply, and allow for the incorporation of the soil-structure interaction into the estimation of angular distortion and lateral strain. Subsequently, the *DPI* can be calculated with Equation 3.11 and is demonstrated to be an effective and convenient index to capture the potential of building damage caused by an excavation. Additionally, this procedure can easily be implemented with simple engineering tools such as a spreadsheet and is demonstrated to be effective in the example applications.

4. The procedure developed in Chapter 3 can be easily adapted for a simplified probabilistic assessment of building damage if so desired. The component models and the entire evaluation process leading to the calculation of the "applied" *DPI* (or loading) are assessed and the uncertainty is characterized in terms of a standard deviation (σ_{DPI}). An example application presented in Chapter 3 demonstrates that a probabilistic assessment of the excavation-induced building damage potential can be easily carried out and satisfactory results can be obtained.
5. The serviceability limit state based on the Damage Potential Index (*DPI*) developed in Chapter 3 is shown to be an effective criterion for assessing the damage potential of a building adjacent to an excavation. The procedure for the probabilistic assessment of building damage potential based on this limit state is comprehensive and yet straightforward, and is founded on the well-established reliability theory. All uncertainties in both the resistance part and the loading part

of the reliability equation, including parameter uncertainty and model uncertainty, are explicitly considered in the reliability analysis. The entire procedure can be, and has been, implemented in an engineering tool such as an Excel spreadsheet.

6. The fully-probabilistic procedure is demonstrated to be feasible in the analysis of the TNEC case history. Since it can be efficiently implemented in a spreadsheet, this fully-probabilistic procedure has the potential to be indispensable tool for assessing the damage potential of a building that is induced by an excavation.
7. For a case analyzed with different parameter and/or model uncertainty scenarios, different probabilities can result even with the same *DPI* value. Thusly, it is vital for the engineer to perform a fully probabilistic assessment whenever possible. Even if the parameter uncertainty cannot be ascertained, it would be better off to perform some sensitivity analysis with different assumed COVs to gain additional insight for making better engineering decisions.
8. Reasonable and satisfactory results obtained from the sensitivity analysis supports indirectly the validity of the proposed fully-probabilistic framework. The sensitivity analysis also reveals the importance of the model uncertainties (c_1 and c_2) and the soil parameters, s_u/σ'_v and E_i/σ'_v in the computed probability of building damage. Other than the model uncertainties, the probability of building damage is most sensitive to these two soil parameters and much less sensitive to all other input parameters. The sensitivity analysis also found that when the COV of s_u/σ'_v or E_i/σ'_v reaches a certain level, the probability of damage becomes most sensitive to s_u/σ'_v or E_i/σ'_v, exceeding the importance of c_1 or c_2.

Therefore, it is vital to make a concerted effort to obtain the most accurate estimate of the soil parameters for the determination of the probability of building damage.

9. A simplified evaluation chart is developed based on the proposed probabilistic framework to further facilitate the application. The chart, which yields the probability of damage for a given *DPI*, is an efficient engineering tool. However, the chart is developed considering only model uncertainty and thus, the user must properly evaluate the case specific information to derive the input data.
10. The proposed methodology (updating through soil parameters) provides a simple and yet effective means for applying the observational method to the problem of deep excavation for monitoring the structural integrity of the buildings adjacent to the excavation. The proposed methodology is also shown to be superior to the previous approach of updating with the model bias factor. Additionally, the methodology is shown to be effective regardless of the initial estimate of the soil parameters.
11. The updating of soil parameters on the basis of the observed maximum settlement or maximum wall deflection *alone* yields comparable results with the updating that is based on both the observed maximum settlement and the observed maximum wall deflection. However, the latter updating scheme based on both types of observation converges faster, and is therefore recommended to use. In practice, the proposed methodology can still be applicable and satisfactory results can still be expected even if only one type of observation is available.

12. Use of the proposed procedures assumes normal (meaning "good") workmanship in the braced excavation. Because of the complex nature of braced excavations, the developed procedure should be used with sound engineering judgment. Updating the damage potential during the staged excavation with field observations and measurements should be conducted whenever possible using the procedure developed in Chapter 5. Additionally, continuous efforts should be made to secure additional case histories that have a complete set of measured data for further validation, and possible refinement, of the developed procedures.

Recommendations for Future Work

To further improve the framework established within this dissertation, a number of research steps can be undertaken, which include the following:

1. The KJHH and KSJH models should be further developed to be applicable to more situations. In particular, the corner effect should be incorporated into the KJHH and KSJH models through three-dimensional FEM analysis of the soil-wall systems so that the ground movement near the corner of an excavation can be predicted. With this development, the established framework will be applicable to buildings located anywhere near the excavation.
2. Additional case histories should be collected for validation of the established framework and models. In particular, the lateral ground movement profile as well as the distinction between hogging and sagging need to be validated with additional case histories or finite element analysis. Additionally, the performance of the established framework in analyzing sites with different characteristics (i.e.

sites with larger sandy layers, frame buildings, sagging deformation, or poor workmanship) must be assessed to determine the applicability of the established framework.

3. The issue of deformation type (hogging versus sagging) should be studied more extensively so that the effect is accurately incorporated into the established framework. The *DPI* values (Table 3.2) for different levels of damage presented within this dissertation could be improved. With the collection of additional data, the *DPI* ranges (Table 3.2) where different levels of damage occur can be more adequately characterized for both hogging and sagging deformation.
4. Alternative definitions of serviceability damage should be explored to possibly incorporate the usage of a building into the damage assessment since buildings with different usage requirements may have different serviceability requirements. With the alternative definitions of serviceability damage, the *DPI* ranges where levels of serviceability damage start to occur can be established accordingly.

REFERENCES

Ang, A. H.-S., and Tang, W. H. (2006). *Probability Concepts in Engineering: Emphasis on Applications to Civil and Environmental Engineering*, 2nd Edition, Wiley, New York.

Baecher, G.B., Christian, J.T. (2003), *Reliability and Statistics in Geotechnical Engineering*, John Wiley and Sons, London.

Bjerrum, L. (1963). "Discussion on: *Proceeding of Conference on Soil Mechanics and Foundation Engineering, Vol. III*." *Publication No 98*, Norwegian Geotechnical Institute, Oslo, Norway, 1-3.

Boone, S.J. (1996). "Ground-movement-related building damage." *Journal of Geotechnical Engineering*, Vol. 122, No. 11, pp. 886–896.

Boone, S.J. (2001). "Assessing construction and settlement-induced building damage: a return to fundamental principals." *Proc. of Underground Contruction*, Institution of Mining and Metalurgy, London, pp. 559-570.

Boscardin, M.D. and Cording, E.J. (1989). "Building response to excavation-induced settlement." *Journal of Geotechnical Engineering*, Vol. 115, No. 1, pp. 1–21.

Bowles, J.E. (1988). *Foundation analysis and design*. 4th Ed., McGraw-Hill, New York.

Burland, J.B. and Wroth, C.P. (1974). "Settlement of buildings and associated damage." *Proceeding of Conference on Settlement of Structures*, Pentech Press, London, pp. 611-654.

Burland, J.B., Broms, B.B., and DeMello, V.F.B. (1977). "Behaviour of foundations and structures: state-of-the-art report." *In Proceedings of the 9th International Conference on Soil Mechanics and Foundation Engineering*, Japanese Geotechnical Society, Tokyo, Japan, pp. 495–546.

Calvello, M., and Finno, R. J. (2004). "Selecting parameters to optimize in model calibration by inverse analysis." *Computers and Geotechnics*, 31(5), 411-425.

Christian, J.T. (2004). "Geotechnical Engineering Reliability: How Well Do We Know What We Are Doing?" *Journal of Geotechnical and Geoenvironmental Engineering,* ASCE, Vol. 130, No. 10, pp. 985-1003.

Clough, G.W., and O'Rourke, T.D. (1990), "Construction-induced movements of in-situ walls." Proc., *ASCE Conference on Design and Performance of Earth Retaining Structure, Geotechnical Special Publication No. 25*, New York, 439-470.

Cording, E.J., Long, J.H., Son, M., and Laefer, D.F. (2001). "Modeling and analysis of excavation-induced building distortion and damage using a strain-based damage criterion." *Proceeding of London Conference for Responses of Buildings to Excavation-Induced Ground Movements in London*, London. Eds., Geological Society, London, 79–92.

Der Kiureghian, A. and J. -B., Ke (1985), "Finite Element-Based Reliability Analysis of Framed Structures." *Proceedings of the 4th International Conference on Structural Safety and Reliability*, Vol. 1, New York: International Association for Structural Safety and Reliability, 395-404.

Duncan, J.M. (2000). "Factors of Safety and Reliability in Geotechnical Engineering." *J. of Geotech. and Geoenviron. Eng.*, Vol. 126, No. 4, pp. 307-316.

Finno, R. J. and Calvello, M. (2005). "Supported excavations: observational method and inverse modeling." *Journal of Geotechnical Geoenvironmental Engineering*, ASCE, 131(7), 826-836.

Finno, R.J. and Roboski, J.F. (2005). Three-dimensional response of a tied-back excavation through clay. *J. of Geotech. and Geoenviron. Eng.*, Vol. 131, No. 3, pp. 273-282.

Finno, R.J., Voss Jr., F.T., Edwin, R., and Blackburn, J.T. (2005). "Evaluating damage potential in buildings affected by excavations." *Journal of Geotechnical and Geoenvironmental Engineering*, 131(10), 1199-1210.

Grant, R., Christian, J.T., and Vanmarcke, E.H. (1974). "Differential settlement of buildings." *Journal of Geotechnical Engineering*, Vol. 100, No. 9, pp. 973-991.

Harr, M.E. (1987). *Reliability-Based Design in Civil Engineering*, McGraw-Hill, New York.

Hashash, Y. M. A., Jung, S., and Ghaboussi, J. (2004). "Numerical implementation of a neural network based material model in finite element analysis." *International Journal for Numerical Methods in Engineering*, 59(8), 989-1005.

Hasofer, A. M., and Lind, N. C. (1974), "Exact and Invariant Second-Moment Code Format." *Journal of the Engineering Mechanics Division*, ASCE, Vol. 100, No. 1, pp. 111-121.

Holman, T.P. (2005). "Small-strain behavior of compressible Chicago glacial clay." PhD thesis, Northwestern Univ., Evanston, Ill.

Hsiao, E.C.L., Schuster, M.J., Juang, C.H., and Kung, G.T.C. (2008). "Reliability Analysis and Updating of Excavation-Induced Ground Settlement for Building Serviceability Assessment." *Journal of Geoenvironmental and Geotechnical Engineering*, ASCE *(accepted)*.

Hsieh, P.G. and Ou, C.Y. (1997). "Use of the modified hyperbolic model in excavation analysis under undrained condition." *Geotechnical Engineering Journal*, SEAGS, Vol. 28, No. 2, pp. 123-150.

Hsieh, P.G. and Ou, C.Y. (1998). "Shape of ground surface settlement profiles caused by excavation." *Canadian Geotechnical Journal*, Vol. 35, pp. 1004-1017.

Hsieh, P.G., Kung, T.C., Ou, C.Y., and Tang, Y.G. (2003). "Deep excavation analysis with consideration of small strain modulus and its degradation behavior of clay." *In Proceedings of the 12th Asian Regional Conference on Soil Mechanics and Geotechnical Engineering*, Singapore, 1. pp. 785-733.

Jaynes, E.T. (1978). "Where do we stand on maximum entropy?" in *The Maximum Entropy Formalism*, R.D. Levine and M. Tribus, Eds., MIT Press, Cambridge, Mass.

Juang, C.H., Chen, C.J., Rosowsky, D.V., and Tang, W.H. (2000), "CPT-based liquefaction analysis, Part 2: Reliability for design." *Géotechnique*, Vol. 50, No. 5, pp. 593-599.

Juang, C.H., Yang, S.H., Yuan, H. and Khor, E.H. (2004), "Characterization of the uncertainty of the Robertson and Wride model for liquefaction potential." *Soil Dynamics and Earthquake Engineering*, Vol. 24, Nos. 9-10, 2004, pp. 771-780.

Juang, C.H., Fang, S.Y., and Khor, E.H. (2006), "First Order Reliability Method for Probabilistic Liquifaction Triggering Analysis Using CPT." *J. of Geotech. and Geoenvir. Engrg.,* ASCE, Vol. 132, No. 3, pp. 337-350.

Kung, T. C. (2003). "*Surface Settlement Induced by Excavation with Consideration of Small Strain Behavior of Taipei Silty Clay*." Ph.D. Dissertation, Department of Construction Engineering, National Taiwan University of Science and Technology, Taipei, Taiwan.

Kung, G.T.C., Hsiao, E.C.L. and Juang, C.H. (2007a). "Evaluation of a simplified small-strain soil model for estimation of excavation-induced movements." *Canadian Geotechnical Journal*, Vol. 44, No. 6, pp. 726-736.

Kung, G.T.C., Juang, C.H., Hsiao, E.C.L., and Hashash, Y.M.A. (2007b). "A simplified model for wall deflection and ground surface settlement caused by braced excavation in clays." *J. of Geotech. and Geoenviron. Eng.*, ASCE, Vol. 133, No. 6, pp. 731-747.

Low, B.K. and Tang, W.H. (1997). "Efficient reliability evaluation using spreadsheet." *Journal of Engineering Mechanics, ASCE*, 123(7), pp. 749-752

Liao, J. T. (1996). *Performance of a top down deep excavation*. Ph.D. Dissertation, Department of Construction Engineering, National Taiwan University of Science and Technology, Taipei, Taiwan.

O'Rourke, T.D., Cording, E.J., and Boscardin, M. (1976). "The ground movements related to braced excavation and their influence on adjacent buildings." Univ. of Illinois Rep. No. DOT-TST-76T-22, Prepared for U.S. Dept. of Transportation, Washington, D. C.

Ou, C.Y., Hsieh, P.G., and Chiou, D.C. (1993). "Characteristics of ground surface settlement during excavation." *Canadian Geotechnical Journal*, Vol. 30, No. 5, pp. 758-767.

Ou, C. Y., and Tang, Y. G. (1994). "Soil parameter determination for deep excavation analysis by optimization." *Journal of the Chinese Institute of Engineers*, 17(5), 671-688.

Ou, C.Y., Liao, J.T., and Lin, H.D. (1998). "Performance of diaphragm wall using Top-down method." *J. of Geotech. and Geoenviron. Eng.*, ASCE, Vol. 124, No. 9, pp. 798-808.

Ou, C.Y., Liao, J.T., and Cheng, W.L. (2000). "Building response and ground movements induced by a deep excavation." *Geotechnique*, Vol. 50, No. 3, pp. 209-220.

Peck, R.B. (1969). "Deep excavations and tunneling in soft ground." *Proc., 7th Int. Conf. on Soil Mechanics and Foundation Engineering*, State-of-the-Art Volume, 225-290.

Phoon, K.K. (2004). General Non-Gaussian Probability Models for First Order Reliability Method (FORM): A State-of-the Art Report. *ICG Report 2004-2-4 (NGI Report 20031091-4)*, International Center for Geohazards, Oslo, Norway.

Phoon, K. K., and Kulhawy, F. H. (1999). "Characterization of geotechnical variabilities." *Canadian Geotechnical Journal*, 36(4), 612-624.

Phoon, K.K. and Kulhawy, F.H. (2005). "Characterization of model uncertainties for laterally loaded rigid drilled shafts," *Géotechnique*, Vol. 55, No. 1, pp. 45-54.

Polshin, D.E. and Tokar, R.A. (1957). "Maximum allowable nonuniform settlement of structures." *Proceeding of 4th Int. Conf. on Soil Mechanics and Foundation Engineering*, Vol. 1, Butterworth, England, pp. 402–405.

Skempton, A.W. and MacDonald, D.H. (1956). "The allowable settlements of buildings." *Proceeding of Institution of Civil Engineers*, London, Part 3, Vol. 6, pp. 727–768.

Son, M. (2003). *The response of buildings to excavation-induced ground movements*. PhD thesis, Univ. of Illinois at Urbana-Champaign, Urbana, Ill.

Son, M. and Cording, E.J. (2005). "Estimation of building damage due to excavation-induced ground movements." *J. of Geotech. and Geoenviron. Eng.*, Vol. 131, No. 2, pp. 162-177.

Son, M. and Cording, E.J. (2007). "Evaluation of building stiffness for building response analysis to excavation-induced ground movements." *J. of Geotech. and Geoenviron. Eng.*, Vol. 133, No. 8, pp. 995-1002.

Whittle, A.J, and Hashash, Y.M.A., and Whitman, R.V. (1993). "Analysis of deep excavations in Boston." J. Geotech. Engrg. 119(1), 69-90.

Wu, T.H. (2008), "Case history of an embankment on soft ground." the Peck Lecture, March 9, 2008, New Orleans, Louisiana.

Zhang, J., Andrus, R.D, and Juang, C.H. (2008). "Model Uncertainty in Normalized Shear Modulus and Damping Relationships." *J. of Geotech. and Geoenviron. Eng.*, Vol. 134, No. 1, pp. 24-36.

Zhang, L.M. and Ng A.M.Y. (2005). "Probabilistic limiting tolerable displacements for serviceability limit state design of foundations." *Geotechnique*, Vol. 55, No. 2, pp. 151-161.